THE UNIVERSITY OF ALBERTA

Physics of the Marine Ice Accretion Process
i) Spreading and Freezing of Saltwater drops
ii) Mass Loss due to Splashing on a Wet Accretion

by

© Eric Obreiter

A THESIS

SUBMITTED TO THE FACULTY OF GRADUATE STUDIES AND RESEARCH

IN PARTIAL FULFILMENT OF THE REQUIREMENTS FOR THE DEGREE

OF MASTER OF SCIENCE

DEPARTMENT OF MECHANICAL ENGINEERING

EDMONTON, ALBERTA
Fall, 1987

Permission has been granted to the National Library of Canada to microfilm this thesis and to lend or sell copies of the film.

The author (copyright owner) has reserved other publication rights, and neither the thesis nor extensive extracts from it may be printed or otherwise reproduced without his/her written permission.

L'autorisation a été accordée à la Bibliothèque nationale du Canada de microfilmer cette thèse et de prêter ou de vendre des exemplaires du film.

L'auteur (titulaire du droit d'auteur) se réserve les autres droits de publication; ni la thèse ni de longs extraits de celle-ci ne doivent être imprimés ou autrement reproduits sans son autorisation écrite.

ISBN 0-315-41176-7

THE UNIVERSITY OF ALBERTA

RELEASE FORM

NAME OF AUTHOR: Eric Obreiter

TITLE OF THESIS: Physics of the Marine Ice Accretion Process i) Spreading and Freezing of Saltwater Drops ii) Mass Loss due to Splashing on a Wet Accretion.

DEGREE: Master of Science
YEAR THIS DEGREE GRANTED: Fall, 1987

Permission is hereby granted to THE UNIVERSITY OF ALBERTA LIBRARY to reproduce single copies of this thesis and to lend or sell such copies for private, scholarly or scientific research purposes only.

The author reserves other publication rights, and neither the thesis nor extensive extracts from it may be printed or otherwise reproduced without the author's written permission.

(SIGNED) Eric Obreiter

PERMANENT ADDRESS:

1716 - 111th Ave. S.W.
Calgary, Alberta
CANADA T2W-1R5

DATE: June 19 1987

THE UNIVERSITY OF ALBERTA
FACULTY OF GRADUATE STUDIES AND RESEARCH

The undersigned certify that they have read, and recommend to the Faculty of Graduate Studies and Research for acceptance, a thesis entitled

Physics of the Marine Ice Accretion Process
i) Spreading and Freezing of Saltwater drops
ii) Mass Loss due to Splashing on a Wet Accretion

submitted by Eric Obreiter in partial fulfilment of the requirements for the degree of Master of Science.

E M Gates
(Supervisor)

Joni Piyest

Edward Lozowski

Date: June 19 1987

ABSTRACT

The purpose of this study was to examine several physical phenomenona applicable to the modelling of marine ice accretions. Of particular interest were the effects of the water loss associated with the splashing of drops on a wet accretion and the influence of salinity, surface temperature, drop diameter and impact velocity on the spreading and freezing of drops on cold dry surfaces.

In order to examine the latter phenomenon, an experimental investigation of the impact, spreading and freezing of large drops was undertaken. The investigation utilized large fresh and saltwater drops with diameters ranging from 1.1 to 2.4 mm, impacting at 4.0 to 4.8 m/s on copper, stainless steel, glass, plexiglass and ice surfaces maintained at -10 and -20°C.

To study the effect of water loss, resulting from the splashing of drops on a wet accretion, a computer model was used to look at the mechanics of droplet motion, in particular the trajectories of the small droplets generated by the splashing. The primary purpose was to quantify the mass (i.e. droplets) that can be permanently lost from the surface of a wet accretion as a result of the splashing phenomenon.

ACKNOWLEDGEMENT

The author would like to thank Dr. E.M. Gates for his supervision and guidance in the preparation of this thesis. The author would also like to thank Dr. E.P. Lozowski (Division of Meteorology) for his assistance with the present study.

Special thanks to all the Technical staff in the Department of Mechanical Engineering for their cooperation and assistance in the development and fabrication of the numerous experimental protypes and components. As well, thanks are due to Mr. R. Haley and Dr. P. Smy (Department of Electrical Engineering, University of Alberta) for their assistance in the production of the high speed videos.

The author would also like to express his gratitude for the financial support provided by a N.S.E.R.C. Postgraduate Scholarship (1984-1986) and a Department of National Defense Grant (Contract No. 2SU82-0034).

Finally, I would like to direct the biggest thanks of all to my wife Sandy, for bearing with me.

TABLE OF CONTENTS

CHAPTER PAGE

1. INTRODUCTION 1
    - 1.1 Background Information 1
    - 1.2 Modelling 3
    - 1.3 Empirical Models 3
    - 1.4 Analytical Models 4
    - 1.5 Present Investigation 6
2. EXPERIMENTAL APPARATUS AND TEST PROCEDURES 8
    - 2.1 The Cold Room 8
    - 2.2 Drop Production 10
        - 2.2.1 Drop Generation 11
        - 2.2.2 Methods of Drop Production 12
        - 2.2.3 High Voltage Drop Production Method . 16
    - 2.3 Impact Surfaces 19
    - 2.4 Salt Water 21
    - 2.5 Drop Velocity and Temperature 22
        - 2.5.1 Drop Impact Velocity 24
        - 2.5.2 Drop Timing Circuits 26
        - 2.5.3 Drop Temperature 27
    - 2.6 Spreading Test Procedures 30
        - 2.6.1 Photographic Techniques 30
        - 2.6.2 High Speed Video Techniques 37
    - 2.7 Freezing-Time Test Procedure 40
3. Presentation of Results 43
    - 3.1 Introduction 43

CHAPTER PAGE

3.2.1 Spreading of Drops on a Warm Surface 43

3.2.2 Spreading of Drops on a Cold Surface 49

3.3 Spreading Results 52

3.3.1 Spreading Factor verses Time 52

3.3.2 Spreading Factor - Maximum 57

3.3.3 Spreading Speed - Initial 57

3.3.4 Spreading Factor - Final Size 59

3.4 Freezing and Cooling 64

3.4.1 Freezing and Cooling Times 64

3.4.2 Total Time 68

4. DISCUSSION OF RESULTS 70

4.1 Spreading 71

4.2 Discussion of Spreading Results 71

4.2.1 Maximum Spreading Factor 74

4.2.2 Initial Spreading Speed 80

4.2.3 Final Size 82

4.3 Freezing and Cooling Times 89

4.3.1 Introduction 89

4.3.2 Measurement of the Freezing and Cooling Time 90

4.3.3 Drops Freezing on Plexiglass 93

4.3.4 Freezing Time 97

4.3.4.1 Freezing Time - Semi-Infinite Solid Solution 98

4.3.4.2 Freezing Time - Kinetic Growth 101

4.4 Discussion of Results - Freezing Time 103

CHAPTER PAGE

4.5 Total Time 108

4.6 Summary 111

5. SPLASHED DROPS 114

5.1 Introduction 114

5.2 Computer Trajectory Model 115

5.3 Presentation of Results 118

5.4 Discussion of Results 120

5.4.1 Drop Trajectories 120

5.4.2 Re-Impact Angle 127

5.4.3 Impinging Mass Loss 131

6. SUMMARY and CONCLUSIONS 137

REFERENCES 140

APPENDIX A. Drop Impact Velocity 147

APPENDIX B. Drop Temperature at Impact 153

APPENDIX C. Trajectories of Drops "Shed" During a Splash on a Water Coated Cylinder 158

Appendix D. Velocity Program Listing 162

LIST OF TABLES

TABLE **PAGE**

2.1 Physical Properties of Impact Surface Materials and Water.............................. 20

2.2 Typical analysis of the salt water produced from the Rila synthetic seawater mix (Salinity = 33 ± 0.6 g/kg)................... 23

2.3 A comparison of the drop temperature at impact for drops falling in the cold room or in room temperature air.................................. 31

3.1 Effect of impact surface temperature and salinity on the maximum Spreading Factor ($S.F._{max}$) and the corresponding time required to reach $S.F._{max}$................................ 58

3.2 The effect of salinity and impact surface on the initial spreading rate* of water drops on cold dry surfaces (*- average rate until time $t = D_d/V_{im}$)... 60

3.3 Experimentally determined freezing times for salt and distilled waterdrops on cold dry surfaces (T_{air}= T_s= temp. of surface)......... 67

3.4 Total time t_T ($t_i + t_f + t_c$) required to freeze 2.4 mm diameter waterdrops, impacting at 4.8 m/s then cool the impact surface to its initial temperature (i.e. t_c = time required to cool impact surface to 99% of $T_m - T_s$)............. 69

4.1 Maximum spreading factor based on surface energy of a disk of uniform thickness, as calculated from Equation 4.4................... 77

4.2 Thickness of spread out drops (i.e. disk of uniform thickness)..............................100

4.3 Comparison of Freezing time t_f including the effect of convective heat transfer from the spread out drop surface as determined from Equation 4.10................................. 104

4.4 Calculated and measured freezing times for salt and distilled water drops spreading on cold dry surfaces.............................. 105

LIST OF FIGURES

FIGURE PAGE

2.1 Schematic of the cold room set-up and equipment used in the photographing of spreading drops on cold surfaces.............. 9

2.2 Dropping Tip used in conjunction with a high voltage source to produce a range of single, uniformly sized water drops (all dimensions in millimeters)............................ 13

2.3 Schematic of a "Concentric Air" drop generator.................................... 15

2.4 The diameter of distilled water drops as a function of applied voltage, obtained from the tip illustrated in Figure 2.2............ 18

2.5 Effect of the initial velocity of the charged drops on the drop's impact velocity (initial velocity results from coulomb attraction of the high voltage set-up)..................... 25

2.6 Drop velocity as a function of distance fallen for drops produced by the high voltage set-up (Figure 2.2). Note that the 2.4 mm drops are not produced using this set-up.............. 28

2.7 Drop timing circuit used to determine the time required for the drop to fall the distance H2 as shown in Figure 2.1....................... 29

2.8 Schematic of the cooling reservoir used to control the initial drop temperature......... 32

2.9 Schematic of the Hewlett Packard data acquisition system used in recording the impact surface temperature during the freezing of a drop on the surface............ 42

3.1 The definition of Spreading Factor (S.F.) as used to specify the size of a spreading drop... 44

3.2 The spreading factor of distilled water drops spreading on a warm (20°C) copper surface.... 54

3.3 The effect of salinity on the spreading of 2.4 mm diameter waterdrops on a -20°C copper surface (V_{im} = 4.8 m/s)..................... 56

FIGURE **PAGE**

3.4 The effect of impact surface temperature on the spreading of 2.4 mm diameter waterdrops on a stainless steel surface ($V_{im}=4.8$ m/s)... 56

3.5 Final size (S.F.) verses Impact Weber # for distilled and salt waterdrops spreading on -20 and -10^{o}C ice surfaces ($T_{air}=T_{s}$=temp. of ice surface and $T_{drop}=1^{o}$C)................ 61

3.6 Final size (S.F.) verses Impact Weber # for distilled and salt waterdrops spreading on 20, -20 and -10^{o}C copper surfaces ($T_{air}=T_{s}$= temp. of copper surface and $T_{drop}=1^{o}$C)....... 62

3.7 Final size (S.F.) verses Impact Weber # for distilled and salt waterdrops spreading on -20 and -10^{o}C stainless steel 304 surface ($T_{air}=T_{s}$= temp. of surface and $T_{drop}= 1^{o}$C)... 63

3.8 Freezing of a spread out (S.F.=4.5) fresh water drop on a -10^{o}C plexiglass plate (temperature recorded from a surface mounted thermocouple).......................... 65

4.1 Temperature of a drop (liquid layer) during freezing on a cold dry surface (theoretical). 91

4.2 The surface temperature of the impact plate as a function of time, during the freezing and cooling of a layer of water on the plate's surface (assummed profile)........... 94

5.1 A description of the parameters used to define the trajectories of "splashed" drops.................................... 117

5.2 The effect of the initial "splashed" drop position, measured from the stagnation line on the drop trajectories (D_{c}=1 m, V_{a}=10 m/s, $T_{a}=-15^{o}$C, D_{d}=100 μm, $Ang_{d}=90^{o}$C, V_{d}=2 m/s)... 121

5.3 The effect of the initial "splashed" drop position vector (Ang_{d}) on the drop trajectory (D_{c}=1 m, V_{a}=10 m/s, $T_{a}=-15^{o}$C, D_{d}=100 μm, $Ang_{c}=20^{o}$, V_{d}=2 m/s)......................... 121

FIGURE PAGE

5.4 The effect of the "splashed" drop diameter (D_d) on the resulting drop trajectories (D_c=1 m, V_a=10 m/s, T_a=-15^{o}C, Ang_d=90^{o}, Ang_c=20^{o}, V_d=2 m/s) 123

5.5 The effect of the initial "splashed" drop velocity (V_d) on the drop trajectories (D_c= 1 m, V_a= 10 m/s, T_a=-15^{o}C, Ang_d=90^{o}, Ang_c=20^{o}, D_d=100 μm) 123

5.6 The effect of impact cylinder diameter (D_c) on the trajectories of "splashed" drops (V_d=2 m/s, V_a=10 m/s, T_a=-15^{o}C, Ang_d=90^{o}, Ang_c=20^{o}, D_d=100 μm) 125

5.7 The effect of freestream air velocity (V_a) on the trajectories of "splashed" drops (V_d=2 m/s, D_c=1 m, T_a=-15^{o}C, Ang_d=90^{o}, Ang_c=20^{o}, D_d=100 μm) 125

5.8 Predicted drop trajectories based on the theory of potential flow around a cylinder (V_d=0 m/s, D_c=1 m, T_a=-15^{o}C, D_d=1 mm) 126

5.9 The effect of initial drop velocity (V_d), freestream air velocity (V_a) and drop diameter (D_d), on the Re-Impact Angle, of drops splashed from a water coated cylinder (D_c=1 m, T_a=-15^{o}C, Ang_d=90^{o}) 129

5.10 The effect of initial drop velocity (V_d), cylinder diameter (D_c) and drop diameter (D_d), on the Re-Impact Angle of the drops splashed from a water coated cylinder (V_a=10 m/s, T_a=-15^{o}C, Ang_d=90^{o}) 130

5.11 The percentage of the drops splashed from the surface of a water coated cylinder that re-impact on the cylinder as a function of initial drop velocity (V_d), drop diameter (D_d) and cylinder diameter (D_c) (V_a=10 m/s, T_a=-15^{o}C, Ang_d=90^{o}) 133

C.1 Forces acting on a drop 158

LIST OF PLATES

PLATE		PAGE
1.1	Ice accumulation on a small Dutch Tanker, the "Anna Broere", which ran aground near Cape Rozewie (Poland southern Baltic sea) Jan.1, 1979. Photo: Paul Zakrzewski	2
1.2	Removal of ice accretion from a ship using a wooden hammer	2
1.3	A photograph of the small drops "shed" from the crown of water as a result of the splashing of a 2.4 mm diameter water drop on a layer of water (V_{im} = 4.8 m/s)	7
2.1	Sequence of photographs illustrating the spreading of a 2.4 mm diameter drop on a -20^{o}C smooth glass plate (V_{im} = 4.8 m/s)	35
2.2	The image produced by the Kodak high speed video system for a 2.4 mm diameter distilled water drop spreading on a -10^{o}C copper plate.	39
2.3	An illustration of the cursors used to measure spreading drop dimensions directly from the Kodak high speed video image	39
3.1	Photographic sequence illustrating the spreading of a 2.55 mm diameter waterdrop on a room temperature glass surface (V_{im}= 4.23 m/s)	46
3.2	Photographic sequence illustrating the spreading of a 2.55 mm diameter waterdrop on a -10^{o}C glass surface (V_{im}=4.23 m/s)	51
3.3	Final size and shape of 2.4 mm diameter salt water drops freezing on a -20^{o}C copper surface (V_{im}= 4.8 m/s)	53
3.4	Final size and shape of 2.4 mm diameter drops freezing on a -20^{o}C ice surface (V_{im}=4.8 m/s)	53

NOMENCLATURE

Symobol		Units
a	acceleration	[m^2/s]
A	area	[m^2]
Ang_c	drop velocity vector from cylinder surface	[deg]
Ang_d	drop position from stagnation line	[deg]
Ang_{re}	Re-Impact Angle	[deg]
c	specific heat capacity of water	[J/kg·°C]
c_p	constant pressure specific heat capacity	[J/kg·°C]
c_v	constant volume specific heat capacity	[J/kg·°C]
C_{drag}	coefficient of drag	
D	diameter	[m]
DIF	diffusivity of water vapor in air	[m^2/s]
E	emissivity	dimensionless
f	Sherwood number	dimensionless
F	force	[N]
G_i	rate of growth of an ice layer	[W]
h	convective heat transfer coefficient	[W/m^2·°C]
H	distance	[m]
K or k	thermal conductivity	[W/m·°C]
KE	kinetic energy	[J]
l_f	latent heat of fusion	[J/kg]
l_v	latent heat of vaporization	[J/kg]
m	mass	[kg]
Nu	Nusselt number	dimensionless
P	pressure	[Pa]

Symobol		**Units**
Pr	Prandtl number	dimensionless
R	specific gas constant	[J/kg·k]
Re	Reynolds number	dimensionless
S	salinity	[g/kg]
Sc	Schmidt number	dimensionless
SE	surface energy	[J]
S.F.	spreading factor	dimensionless
t	time	[s or ms]
T	temperature	[^{o}C or k]
V	velocity	[m/s]
We #	Impact Weber Number	dimensionless
y(t)	thickness of ice layer	[μm]
X,Y	position of drop	[m]
σ	Stefan-Boltzman constant	[$J/m^2 \cdot s \cdot k$]
ρ	density	[kg/m^3]
μ	dynamic viscosity of air	[kg/m·s]
δR	thickness of spread out drop	[μm]
α	thermal diffusivity	[m^2/s]
γ	surface tension coefficient	[dyne/cm]
Ψ	stream function	[m^2/s]

Subscripts

a	air
c	cylinder or cooling
d	drop
f	freezing
final	final value
i	ice or initial
im	impact
max	maximum value
PT	constant pressure: moist air
s	surface or spreading
T	total
v	vapor
w	water
a/w	air-water interface

CHAPTER 1

INTRODUCTION

1.1 Background Information

With the recent upswing in offshore activities in northern waters has come an increased emphasis on the marine icing phenomenon. The accretion of ice on marine structures (i.e. ships and drilling rigs) produces increased static and wind generated loads on the structures, that can result in potentially hazardous situations. The primary concerns are the instability of floating structures and the possibility of structural damage to stationary and floating structures.

The most dangerous and primary cause of marine ice accretions is the freezing of the sea spray generated by impacting waves. Over a period of several days during a storm in 1979, the semi-submersible drilling rig Ocean Bounty accumulated an estimated 500 tons of ice (Minsk, 1984). Although this load did not damage the structure, it was potentially hazardous and it became necessary to jettison drilling mud as a precaution to maintain stability. Plate 1.1 illustrates the ice accumulation on a small Dutch tanker, "Anna Broere" which ran aground near Cape Rozewie (Poland) in the southern Baltic Sea, January 1, 1979.

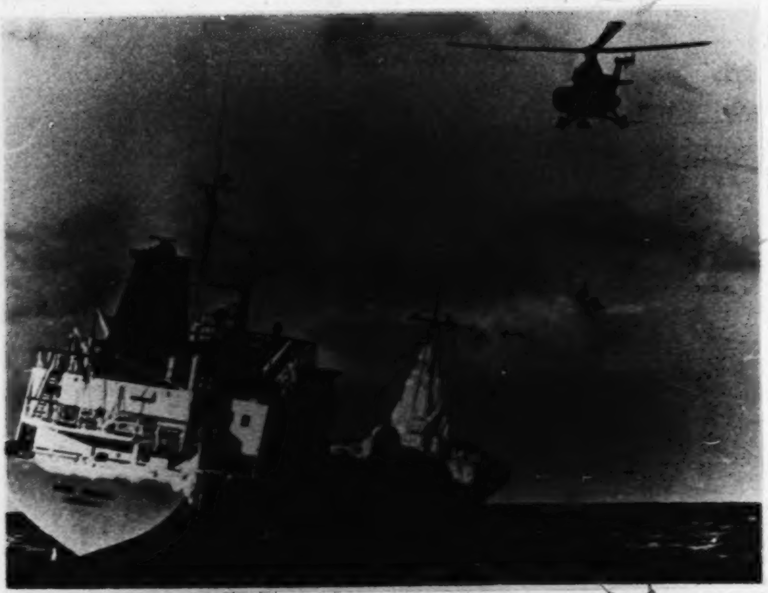

PLATE 1.1 Ice accumulation on a small Dutch Tanker, the "Anna Broere", which ran aground near Cape Rozewie (Poland southern Baltic sea), Jan.1, 1979. Photo: Paul Zakrzewski.

PLATE 1.2 Removal of ice accretion from a ship using a wooden hammer.

1.2 Modelling

Of particular interest to the marine icing phenomenon has been the development of marine icing "models" that can be used to predict or forecast ice accretion rates for a given set of meteorological, accretion and physical parameters. Such models could aid in the design of marine structures by predicting the mass of accreted ice, which in turn is needed to determine any increased static and/or wind-generated loads. The operator of a marine structure could also use the models to forecast potentially hazardous conditions, and take preventive action if possible. The marine icing models currently available have been developed primarily from two different perspectives, those based on observations (i.e. empirical) and those that are analytical in nature, although the distinction is not always clear.

1.3 Empirical Models

Mertins (1968) developed a series of marine forecasting nomograms to forecast ice accretion rates on ships in the North Atlantic. These nomograms were developed through comparison of environmental parameters with ship icing reports and included the effect of the most important environmental factors, namely air temperature, wind speed and sea temperature. Wise and Comiskey (1980) and Comiskey et. al. (1984) developed nomograms, based on Mertins' original work, to forecast superstructure icing in Alaskan waters. Pease and Comiskey (1985), using data from ship icing incidents in Alaskan waters, also developed marine nomograms to forecast the most severe cases of marine icing.

The major shortcoming of these empirical models, is that since they are based on specific icing data, generalization to different marine structures and meteorological conditions has met with limited success. As well, the majority of the observations correspond to the icing of ships, primarily smaller vessels and the applicability to large stationary structures (e.g. drilling platforms) is not obvious. As a result, increased emphasis has been placed on the development of analytical models which ideally could be used to predict ice accretion mass and possible shape, for arbitrarily shaped accretion surfaces and a wide range of environmental conditions.

1.4 Analytical Models

Analytical models attempt to model the physics of the icing process. The basic algorithm involves determining the mass flux that is accreted (i.e. collision efficiency) and how much of the accreted mass freezes or if it all freezes, the accretion surface temperature via the steady state heat balance at surface of the accretion. The collision efficiency is defined as the fractional mass in a swept out volume that is accreted on a surface.

Horjen, et. al. (1984), Stallabrass (1980) and Kachurin, et. al. (1974) have all developed analytical marine icing model using the same "basic" algorithm, although the details of their formulations are somewhat different. Previously, analytical models have been developed that predict the accumulation of ice under "atmospheric" icing conditions. In developing these analytical models the authors must make simplifying assumptions to keep the models practical. These simplifying assumptions are generally derived from an understanding of the basic physics of the appropriate accretion process.

Since the basic physics of the marine icing process are presently not well understood, the authors take a "black box" approach, ignoring the details of the kinematic and thermodynamic processes of the single drops in terms of the overall accretion process. Although it might be possible to develop a marine icing algorithm along the same lines as an atmospheric icing model, the conditions typically associated with the marine icing situation would prevent the use of the simplifing assumptions based on atmospheric icing conditions. The major differences between marine and atmospheric icing conditions are large drops generally not in kinematic or thermodynamic equilibrium with the air, intermittent periods of no icing and salinity. In order to improve analytical marine icing models, the modellers must develop a better understanding of the basic physics of the marine ice accretion process.

1.5 Present Investigation

The present investigation was undertaken in order to examine some of the basic physics of the marine ice accretion process, with particular interest in the spreading and freezing of large saline drops on cold dry surfaces and the splashing of drops on a liquid layer. Towards this end an experimental investigation was under taken to determine the importance of salinity, surface temperature, drop size and velocity on the spreading of single drops on cold dry surfaces. In addition the effect of heat transfer and freezing on this spreading process was also examined. Of primary importance was the relationship between the spreading and freezing of the single drops to the overall marine ice accretion process.

A further analytical investigation was undertaken in order to examine the kinematics of the splashing process in relationship to the splashing of drops on a liquid surface in a wet accretion. Plate 1.3 illustrates the "splash" produced when a 2.4 mm diameter drop impacts with a velocity of 4.8 m/s (V_{im}) on a layer of water. The primary purpose of this investigation was to quantify the mass loss associated with the splashing of drops on a "wet" (i.e. partially unfrozen) accretion, typical of the marine icing situation.

PLATE 1.3 A photograph of the small drops "shed" from the crown of water as a result of the splashing of a 2.4 mm diameter drop on a layer of water (V_{im} = 4.8 m/s).

CHAPTER 2

EXPERIMENTAL APPARATUS AND TEST PROCEDURES

In order to examine the spreading and freezing of large drops on cold dry surfaces, an experimental set-up was developed to maintain the surface temperature and record the spreading process. This was accomplished through the use of high speed photographic and video techniques which effectively "slowed" the motion of the spreading drop. Additional tests were also performed to determine the "freezing time" of the drops.

2.1 The Cold Room

The majority of the experimental tests were conducted in a Foster refrigerated cold room. The cold room is one of three cold rooms located in the Mechanical Engineering Building at the University of Alberta. The cold room has a floor area of 4 m^2 and an interior height of 2.15 meters. The forced air cooling unit is capable of maintaining the temperature in the cold room between -5 and -23 ± 1°C.

Figure 2.1 is a schematic of the equipment and experimental set-up located in this cold room. The major components of the set-up are the drop source (single drop generator), the drop timing circuit, a 35 mm Nikon camera and a strobotac. The drop source was used to produce single drops, ranging from 1.1 to 2.4 mm in diameter. A detailed description of the drop source can be found in

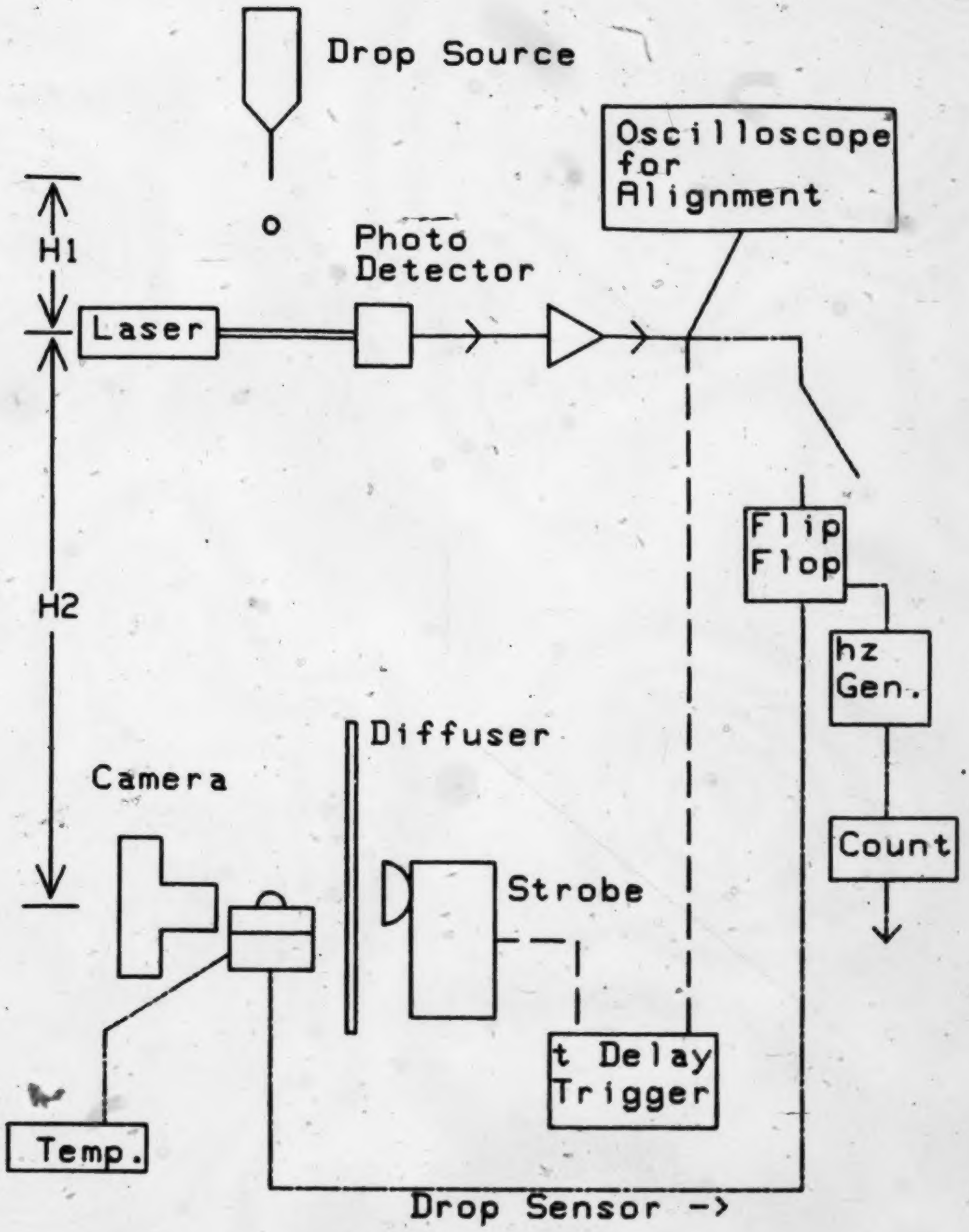
Drop Source
Oscilloscope for Alignment
H1
Photo Detector
Laser
H2
Flip Flop
hz Gen.
Diffuser
Camera
Count
Strobe
t Delay Trigger
Temp.
Drop Sensor ->

FIGURE 2.1 Schematic of the cold room set-up and equipment used in the photographing of spreading drops on cold surfaces.

Section 2.2.3. The drops fell a total of 168.5 cm before impacting on the cold test surfaces. Located 70 cm (H1) below the drop source was a Laser (Hughes, Model 3221H-C) and a Photo Detector. The Photo Detector was used to detect the drops at the instant they had fallen the 70 cm from the drop source. The electrical signal from the Photo Detector could then be used in the drop timing circuit to determine the time required for the drop to fall the additional 98.5 cm (H2). In order to record the spreading of the drops a 35 mm single lens reflex camera complete with a 55 mm macro lens and a 68 mm extension tube was focused on the impact surface. This combination of the lens and extension tube produces an image to subject size ratio of 1.24. Located directly opposite the camera was a light diffuser (Lexan Sheet) and a General Radio Type 1531A Strobotac (Light source). The photo detector output was used to initiate a timing circuit which caused a single flash of light to be emitted from the strobotac. The duration of the flash was on the order of several microseconds.

2.2 Drop Production

One of the main thrusts of the experimental study was to determine if salinity produced any significant differences, in terms of the spreading and freezing of water drops on cold dry surfaces. This difference was to be determined through the size (diameter) and the appropriate times required for the drops to spread and freeze on the cold dry surfaces. Of particular interest in this study were the drops representative of the sea spray generated by wave impacts. This sea spray generally consists of relatively large drops up to several millimeters in diameter. A method of producing consistently sized "single" drops with predictable trajectories had to be developed before any meaningful experimental results could be obtained. The required method shall be referred to as Drop Generation.

2.2.1 Drop Generation

Besides the need for repeatable drop sizes, the photographic techniques employed in this study necessitated two additional drop production requirements. First, the drops had to fall with a controllable and consistent trajectory and second, the rate of drop production had to be no greater than approximately 1 drop/second. These requirements were based strictly on the need to obtain detailed photographs of single drops as they spread on a cold dry surface. The consistent trajectories ensured that the drops fell on the impact surface, at the position corresponding to the focal point of the camera. The maximum drop production rate of 1 drop/sec was needed to prevent multiple photo detector signals or equivalently, multiple film exposures.

The problems associated with producing repeatable drop diameters have been investigated for many years. As early as 1882, Rayleigh used vibrations to break up a jet of liquid into a stream of regularly spaced drops (Magarvey and Taylor, 1956). To meet all of the special drop production requirements of this present study, several drop production methods were investigated before a suitable method was found.

2.2.2 Methods of Drop Production

Initially, water was allowed to flow through a small stainless steel tube with inner and outer diameters of 0.69 and 1.07 mm, respectively. This method consistently produced drops 2.55 mm in diameter. The theory behind this method of drop production is that the drop will grow at the tip of the tube until its weight is great enough to overcome the surface tension forces, "adhering" the drop to the tip. Lane (1946) showed that to obtain a 1.0 mm diameter drop requires a tube with an outer diameter of 0.02 mm. From a practical point of view, it is not possible to construct and successfully use a 0.02 mm tube to produce 1.0 mm drops.

Several authors (Lane 1946, Reil and Hallett 1969, Samuels and Sparks, 1973 and Cheng and Cross, 1975) have shown that it is possible to obtain uniformly sized drops, by allowing a concentric stream of air to "blow" suspended drops from the tip of a hypodermic needle (Figure 2.2). Changes in the air flow velocity and the flow rate of the

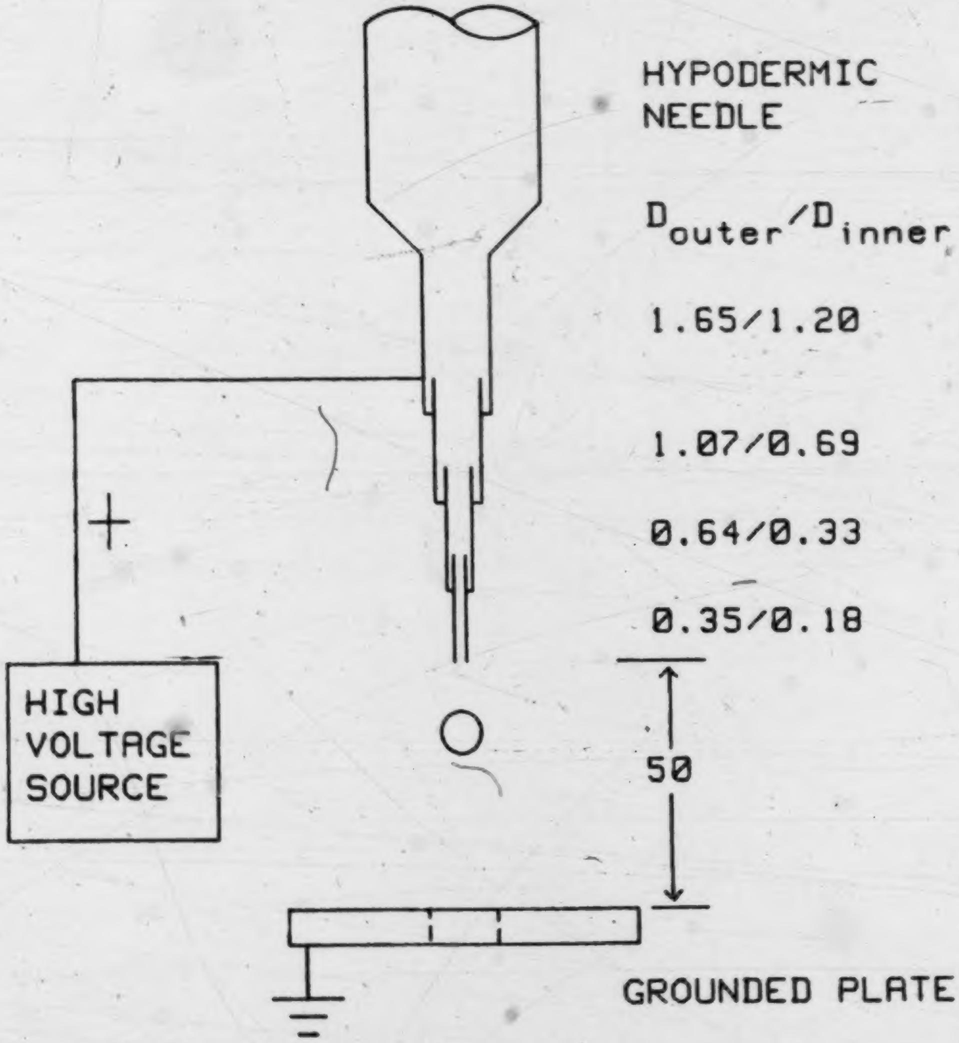
HYPODERMIC NEEDLE
D_{outer}/D_{inner}
1.65/1.20
1.07/0.69
0.64/0.33
0.35/0.18
+
HIGH VOLTAGE SOURCE
50
GROUNDED PLATE

FIGURE 2. Dropping Tip used in conjunction with a high voltage source to produce a range of single, uniformly sized water drops (all dimensions are in millimeters).

dropping liquid vary the size and frequency of drop production. However, the range of drop sizes is limited by the tube or tip diameter.

In order to effectively decrease the diameter of the hypodermic needle (dropping tip), a series of stainless steel tubes were "telescoped" down to the final smallest tip diameter (Figure 2.2). This telescoping design served several useful purposes. First the smallest diameter provides an upper limit for the drop size (no airflow to blow the drop from tip). As well, in comparison to a single tube with the smallest diameter, the telescoping reduces the resistance to the flow of water through the tip and provides greater rigidity to the dropping tip.

An actual working model of the concentric air device (Figure 2.3) was constructed, and testing showed it was capable of producing drops ranging from 0.5 to 2.5 mm in diameter using the tip specified in Figure 2.2. The major drawbacks of the device included the difficulties associated with producing repeatable drop trajectories and controlling drop production frequencies. Both of these difficulties had to be overcome to ensure the success of this study. Further work on the device by others, Samuels and Sparks (1973) and Cheng and Cross (1975), indicated that pulsing the air flow could help alleviate the trajectory problems. Although it may have been possible to modify the concentric air device, the complications and sophistication could not be justified for this study. It

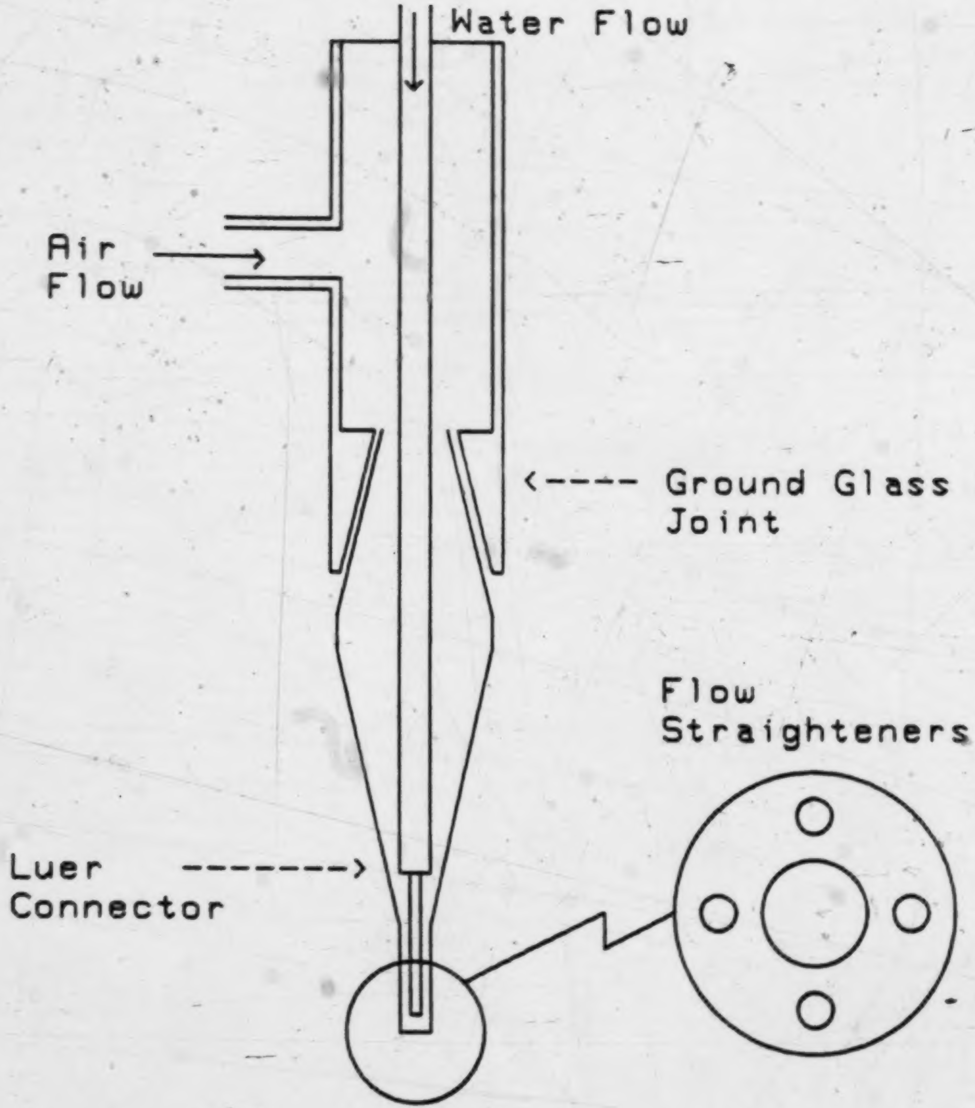
Water Flow
Air
Flow
<---- Ground Glass
Joint
Flow
Straighteners
Luer
Connector
------>

FIGURE 2.3. Schematic of a "Concentric Air" drop generator.

was therefore determined that an alternate method be employed to produce the single drops.

Several other devices were investigated before a suitable drop producing device was choosen. One such device is that described by Magarvey and Taylor (1956) and Wolf (1961), in which a vibrating reed is used to break up a jet of fluid into smaller drops. The drops produced by this method are generally very small (<1 mm) and are produced at a rate much too large to be successfully used in this study. Abbott and Cannon (1972) and later Cannon and Grotewold (1980) claimed to be able to produce small drops one at a time, ranging in diameter from 4 to 130 μm and 6 μm to 1 mm respectively, using the wire eggression principle. Simply put, the wire egression principle involves pulling a fine wire from the meniscus of a fluid film at rest. The wire draws a "stream" of fluid from the surface which breaks off and contracts into a drop. However, the complexity of this device made it impractical for use in this study.

2.2.3 High Voltage Drop Production Method

The method finally choosen to produce the desired range of drop sizes uses the electrostatic force between a charged drop and a fixed ground to "pull" the drops from the dropping tip. Raghupathy and Sample (1970) and Ahire and Kamra (1984) have investigated the production of drops using high voltage sources and Russo, Withnell and Hieftje

(1981) used the method successfully to produce isolated drops for use in the study of atomization in flames.

The basic set-up for the method is shown in Figure 2.2 and involves charging the drops by applying a high voltage potential to the dropping tip. A ground plate, with a centered hole, is placed at fixed distance below the tip. The dropping liquid being positively charged is "attracted" to the grounded plate. If the water in the tip were uncharged, the water would flow from the tip and a drop would grow on the tip until the weight of the drop was large enough to overcome the surface tension force. If however, the drop is now charged by some known voltage, the "Coulomb" attraction will prevent the drop from growing to its maximum size. Figure 2.4 shows the drop diameter as a function of applied voltage for the particular set-up shown in Figure 2.2. It is of interest to note that once the charged drop has been produced, it is possible to vary its trajectory by allowing the drop to pass through an electric field applied between two parallel plates. However, for this study the resulting drop trajectories produced by the high voltage system were repeatable and did not require the application of an electric field. The minimum size of single discernible drops that can be produced by the high voltage system is a function of the dropping tip and grounded plate dimensions, as well as tip to plate spacing. In the particular set-up used for this study (Figure 2.2), the

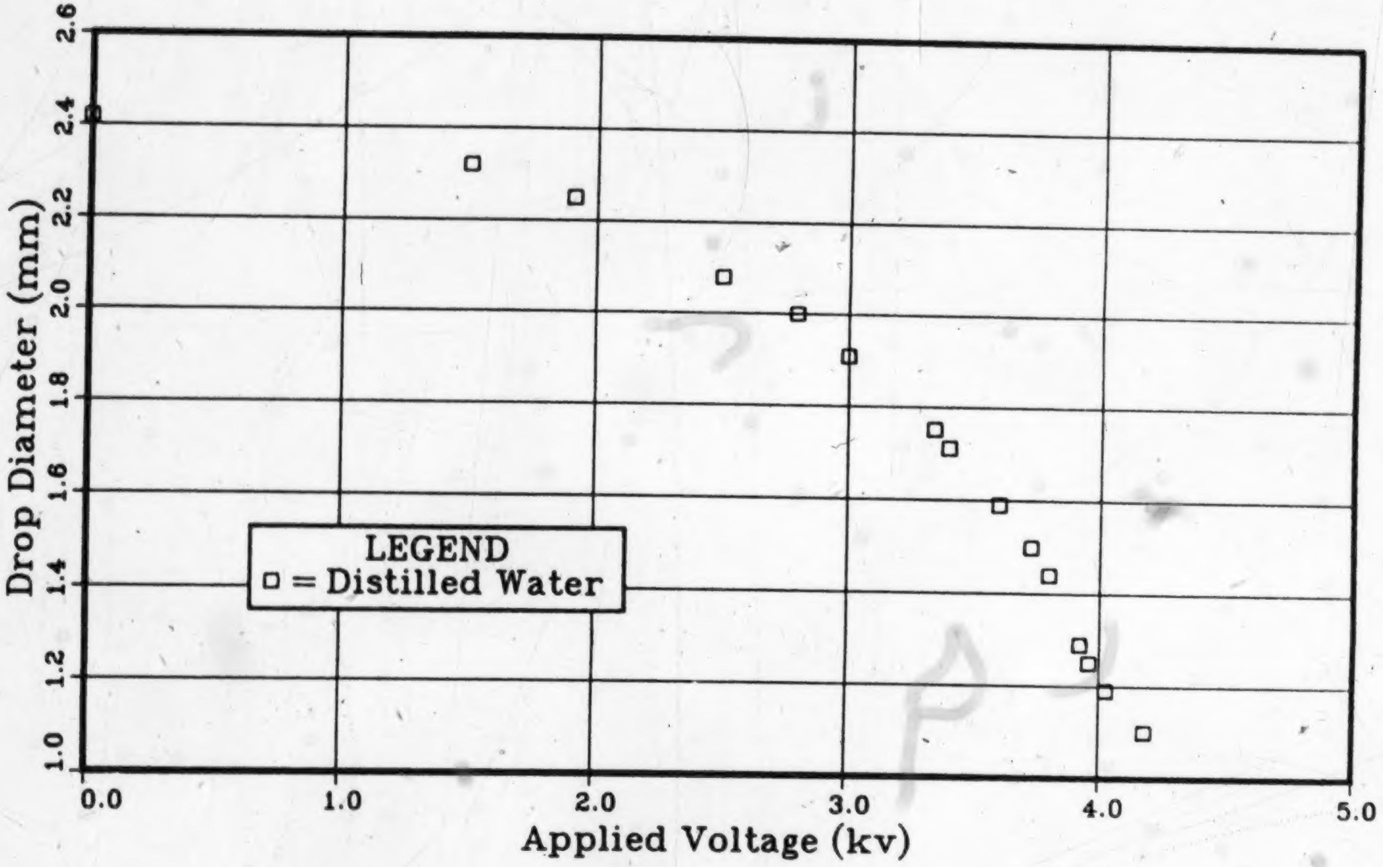

FIGURE 2.4 The diameter of distilled water drops as a function of applied voltage, obtained from the tip illustrated in Figure 2.2.

range of drop diameters obtainable was 1.1 to 2.4 mm. If the applied voltage is increased beyond that required to produce the smallest drops, the drop production mode changes from a "dripping" mode (single drops) to a "spraying" mode, in which numerous randomly sized and very small drops are produced (Ahire and Kamra, 1984).

2.3 Impact Surfaces

In order to ensure a variation in the heat transfer and spreading processes of a drop impacting on a cold dry solid surface, several different impact surfaces were chosen. These included copper, stainless steel, plexiglass, ice and glass. These materials would provide a large range of thermal properties (Table 2.1) and some variation in surface roughness.

The surface of the copper plates was prepared by polishing with 0.05 μm gamma alumina grit. The maximum surface roughness 1.0 μm and centerline average (CLA) roughness 0.1 μm, were measured using a Talysurf Surface Measuring Instrument (The CLA measurement is based on the ASA B46: 1955 standard). The glass, plexiglass and stainless steel plates were utilized with their originally manufactured surfaces intact. The glass and plexiglass surfaces were assummed to be smooth and were replaced if any surface flaws appeared. The surface of the stainless steel plates was protected by removable plastic film. The protected surface was used for all of the experimental

TABLE 2.1 Physical Properties of Impact Surface Materials and Water.

Surface Material	ρ Density (kg/m^3)	c - Specific Heat Capacity (J/kg·°C)	k - Thermal Conductivity (W/m·°C)
Copper[1] ASTM B152	8941	385	339
Ice[2] @ 0°C	890	2106	2.44
Stainless[1] Steel-304	8027	502	159
Plexiglass[3]	1190	1465	0.376
Water[4] Distilled	1000	4218	0.552
Salt	1025	4070	0.552

[1] Metals Handbook, American Society for Metals
[2] Pruppacher and Klett (1978)
[3] Johnson's Industrial Plastics
[4] Mark's Standard, Handbook for Mechanical Engineers

tests and had maximum and centerline roughnesses of 2.5 μm and 0.5 μm, respectively. The ice surfaces were prepared to ensure a high density ice substrate and a smooth impact surface. This was accomplished by slowly freezing samples of warm distilled water and choosing only the samples with minimal quantities of trapped air. The surfaces of the samples were further prepared by melting them on a clean hotplate before refreezing.

The temperature of the surfaces was monitored by thermocouples implanted flush with or just below the surface. Since the method of implanting the thermocouples introduced a local roughness to the impact surface the drops were not allowed to impact at the thermocouple location during any spreading tests. The impact plates (surfaces) were held in place by a small vise mounted on a solid base. The angle of the impact surface could be varied 15° from the horizontal position by pivoting the jaws of the vise.

2.4 Salt Water

In order to examine the influence of salinity on the freezing and spreading of water drops as they impact on cold dry surfaces, it was necessary that a consistent salinity salt water be available. For this reason a synthetic seawater mix under the brand name Rila Marine Mix was choosen to produce the required salt water samples. The mix has the advantage of providing a chemically defined medium which can be consistently reproduced. A typical chemical analysis of the samples produced from the Rila Marine Mix can be found in Table 2.2. The mix should produce a sample with a salinity close to that of seawater (34.325 g/kg, Assur, 1960) and a specific gravity ranging from 1.020 to 1.025.

The sample solution is prepared by adding 39.943 grams of the dry Rila Marine Mix to each liter of distilled water. The sample was allowed to sit in a closed plastic container for a week to ensure all the salts were dissolved. The sample used for this study had a specific gravity of 1.023 and a salinity of 33 g/kg. Tsurikov (1974) showed that based on the above salinity the corresponding freezing point depression may vary from -1.895 to -1.917°C, depending on the choice of the semi-empirical formulation. For this study a value of -1.9°C was used.

2.5 Drop Velocity and Temperature

As mentioned previously, the large drops in sea spray may not be in thermodynamic or kinematic equilibrium with the surrounding air. In terms of modelling ice accretions under these conditions, it is necessary to calculate the drop temperature and velocity at the instant that the drops impact with an icing surface. Similarly, the temperature and impact velocity of the test drops must be determined to ensure consistency of the experimental

TABLE 2.2 Typical analysis of the salt water produced from the Rila synthetic seawater mix (Salinity = 33 ± 0.6 g/kg).

RILA PRODUCTS

P. O. BOX 114 • TEANECK, N. J. 07666 • 201/836-0855

1-lb. of RILA MARINE MIX when dissolved in 3 gallons of tap water will produce a solution having the following typical analysis:

	mg/100 ml	ppm
Cl^-	1913	19130
Na^+	1046	10460
$SO_4^=$	260	2600
Mg^{++}	126	1260
Ca^{++}	49	490
K^+	34.8	348
Tris Amino	3.2	32
Br^-	2.7	27
$BO_3^{\equiv}$	1.2	12
I^-	.897	8.97
Sr^{++}	.350	3.50
Mn^{++}	.050	.50
F^-	.040	.40
Zn^{++}	.020	.20
Fe^{+++}	.010	.10
Co^{++}	.007	.07
Al^{+++}	.003	.03
$MoO_4^=$	.002	.02
Rb^+	.0006	.006
Li^+	.0006	.006
Cu^{++}	.0001	.001

Specific Gravity:	approx. 1.025
pH:	8.0 - 8.3
Solubility:	complete

measurements.

2.5.1 Drop Impact Velocity

The impact velocity refers to the velocity at which the drops strike the impact surface. To determine the velocity of a water drop falling under the influence of gravity, the gravitional force and the appropriate drag forces must be taken into account. For this reason a "Velocity" program was developed utilizing experimentally and analytically obtained expressions for the drag on a freely falling water drop. A detailed analysis of the development of the program can be found in Appendix A. The program was capable of determining the "instantaneous" drop velocity, as a function of distance fallen or time, by using a stepwise iterative scheme. Since time and distance are both measurable experimental quantities, they may be used in conjunction with the "Velocity" program to ensure an accurate determination of the drop's impact velocity.

Figure 2.5 is a plot of the drop velocity as a function of distance fallen (drop position), as calculated from the "Velocity" program. Given that the initial drop velocity at the dropping tip is known, the impact velocity can be readily determined. However, for the smaller drops produced by the high voltage system, the coulomb attraction results in an "unknown" initial velocity.

Consider two 1.1 mm drops, one with an initial velocity of 1.9 m/s and the other without any initial

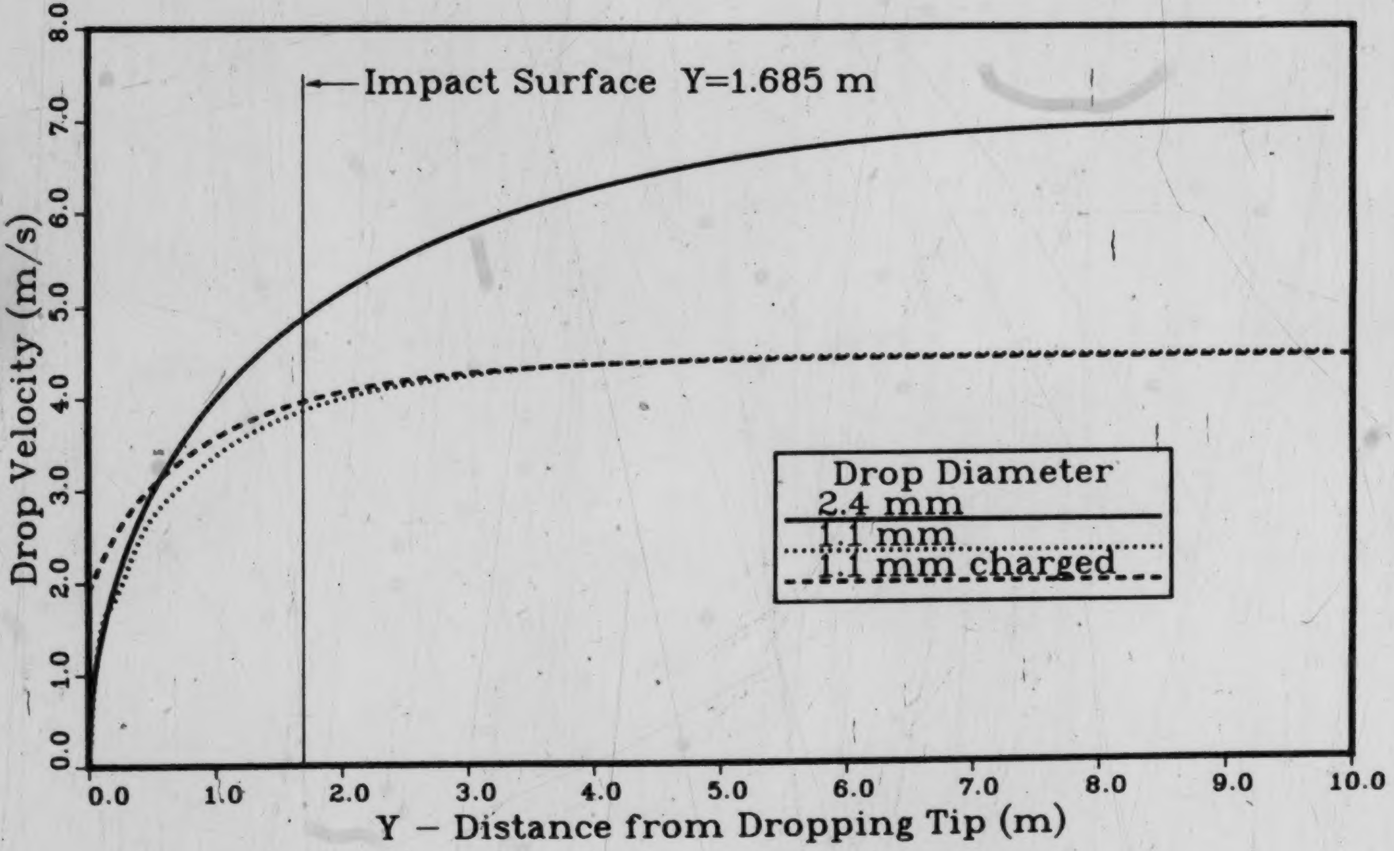

FIGURE 2.5 Effect of the initial velocity of the charged drops on the drop's impact velocity (initial velocity results from coulomb attraction of the high voltage set-up).

velocity. As shown in Figure 2.5 both drops would reach terminal velocity (4.2 m/s) after falling approximately 3 meters. However, at the position of the impact surface, the drop velocities are 4.0 and 3.9 m/s respectively. This illustrates the need to account for the "unknown" initial velocity to ensure the correct impact velocity. This was accomplished through the use of the Drop Timing Circuits.

2.5.2 Drop Timing Circuits

The drop timing circuit, consisting of the laser and photo detector, the time delay generator and the strobotac (Figure 2.1), served two primary purposes. First the circuit was utilized in the photographic technique, as explained in Section 2.6.1, to control the precise triggering of the strobotac used to "freeze" a spreading drop's motion. An appropriate "delay time" was choosen so as to cause the strobotac to flash at the precise moment that the drop touches the impact surface.

Second the circuit provided the time for the drop to fall the distance H2 (98.5 cm) as illustrated in Figure 2.1. This time referred to as the "delay time" was used in conjunction with the "Velocity" program to obtain the impact velocity of the drops produced by the high voltage system, which as a result of the electrostatic force have an unknown initial velocity. The first step in the procedure is to use the "Velocity" program to calculate the position and corresponding velocity of a freely falling drop as a function of time. Since the drops produced by the high voltage system are "free falling" during the time that they travel the distance H2, it is simply a matter of finding a calculated interval, from the velocity program, in which the drop travels 98.5 cm (H2) in the measured time delay. Since the drops used in this study travel at less than terminal velocity the chosen interval is unique and the endpoint of the interval gives the corresponding impact velocity. Figure 2.6 shows the impact velocities for the 1.1, 1.5 and 2.4 mm diameter drops used in this study. The impact velocities as indicated by the "impact position" were 4.0, 4.4 and 4.8 m/s respectively.

In order to determine this "delay time" for the drops produced by the high voltage source the photo detector output was channeled to a separate timing circuit (Figure 2.7). The signal from the photo detector starts the timing circuit, while a "sensing" plate, placed at the location of the impact surface and responsive to charged drops, stops the circuit. Since the circuit is "counting" the cycles of a 1000 hz signal, the count represents the "delay time" directly in milliseconds.

2.5.3 Drop Temperature

The temperature of the impacting drop was obtained by equating the change in the drop's internal energy to the conductive, radiant and mass transfer modes appropriate to

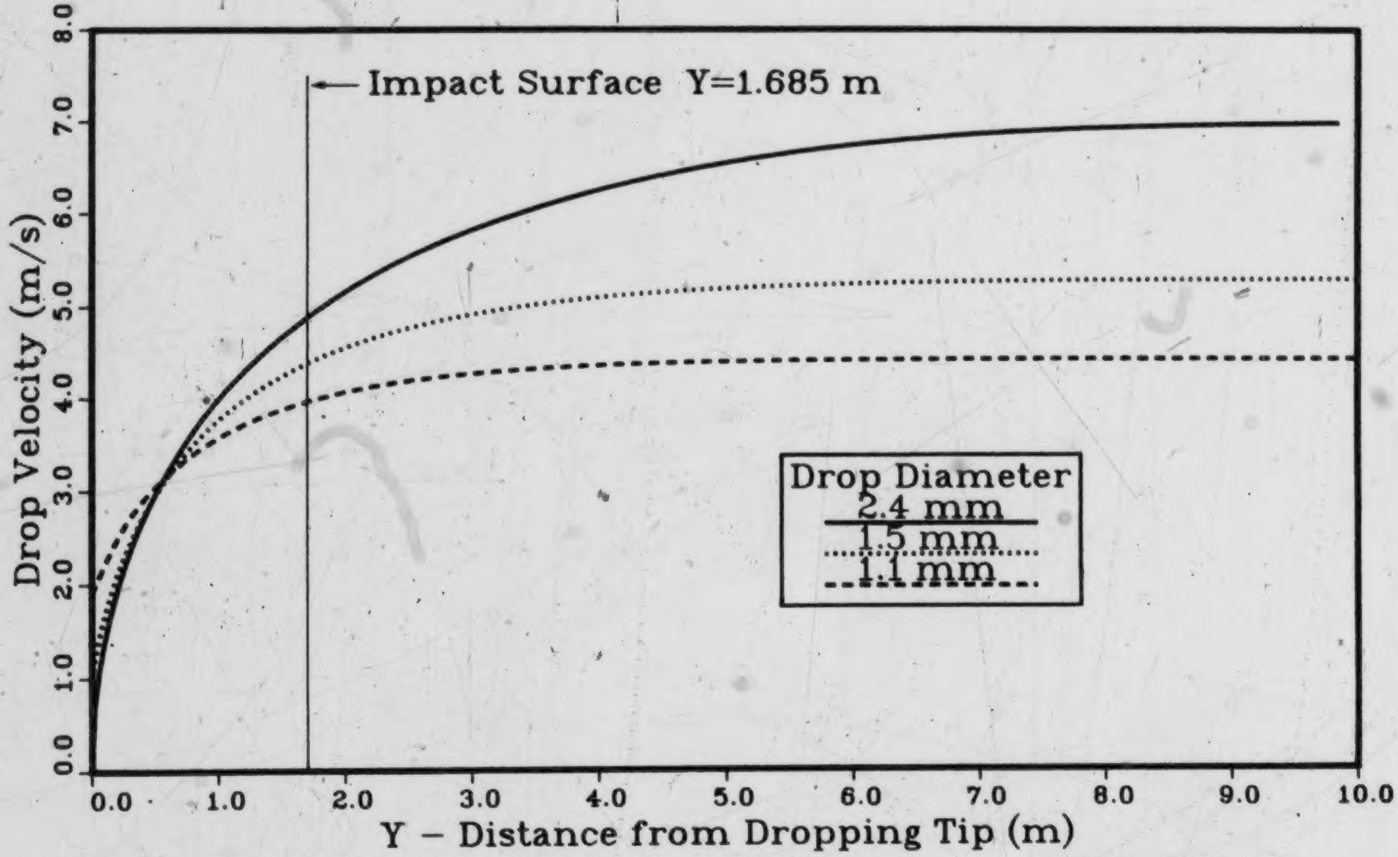

FIGURE 2.6 Drop velocity as a function of distance fallen for drops produced by the high voltage set-up (Figure 2.2). Note that the 2.4 mm drops are not produced using this set-up.

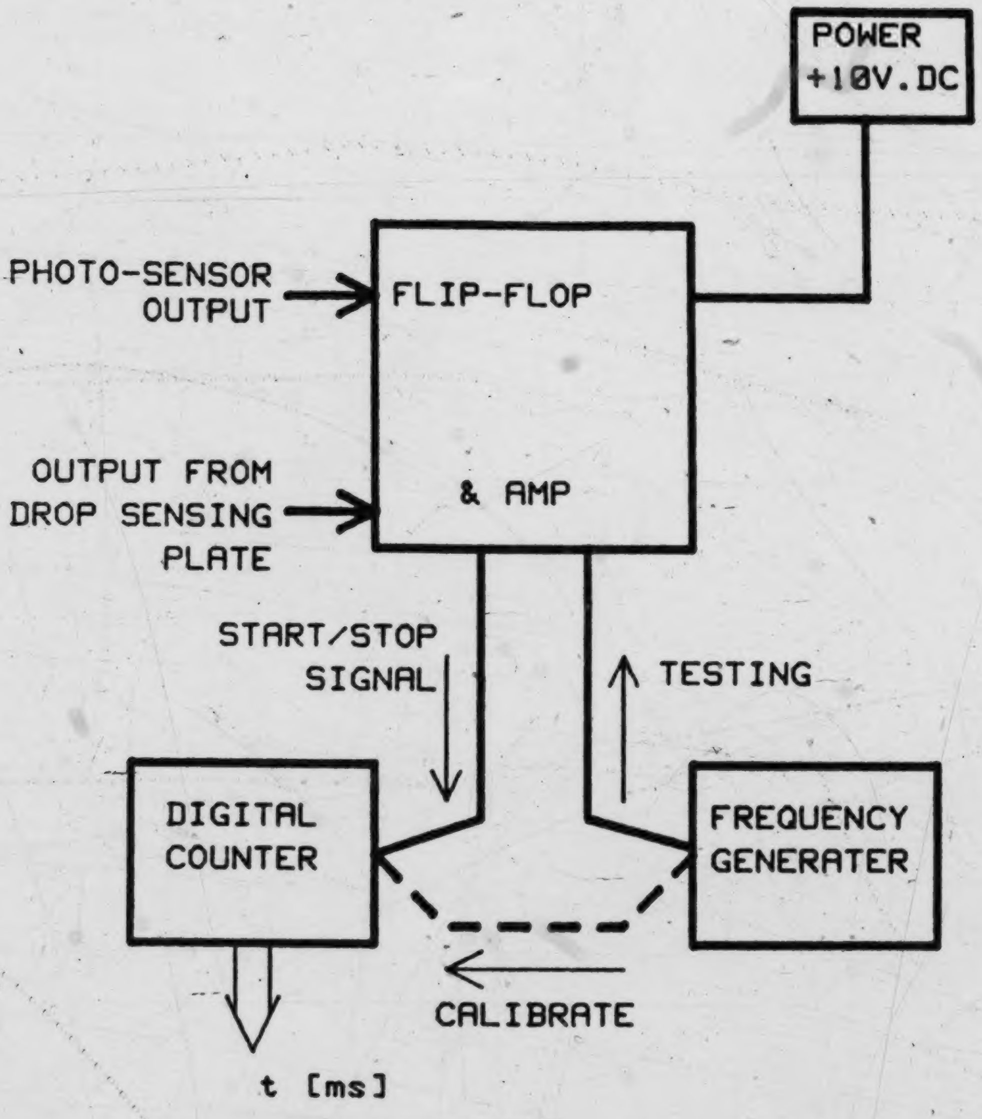
POWER
+10V.DC
PHOTO-SENSOR OUTPUT
FLIP-FLOP
& AMP
OUTPUT FROM DROP SENSING PLATE
START/STOP SIGNAL
TESTING
DIGITAL COUNTER
FREQUENCY GENERATER
CALIBRATE
t [ms]

FIGURE 2.7 Drop timing circuit used to determine the time required for the drop to fall the distance H2 as shown in Figure 2.1.

a freely falling water drop (Auld, 1980 and Pruppacher and Klett, 1978). To account for the fact that the drops are moving relative to the air, the drop temperature was calculated simultaneously with its velocity in the iterative "Velocity" program. The appropriate equations and the development of the iterative scheme can be found in Appendix B. Table 2.3 summarizes the drop temperature at impact for 2.4, 2.0, 1.5 and 1.1 mm diameter drops falling in either room temperature (20°C) or -20°C air (the drop temperature was initially 1°C). The table illustrates that none of the drops used in this experimental study would be supercooled (<0°C) at the time of impact.

In order to determine the temperature of the drops at the moment of contact with the impact surfaces, it is required that the drop's initial temperature upon leaving the dropping tip be known. This temperature was obtained by placing a thermocouple inside the reservoir which supplied the drop production water near to the dropping tip, as illustrated in Figure 2.8. The reservoir temperature was held constant by the continuous circulation of a glycol cooling bath.

2.6 Spreading Test Procedures

2.6.1 Photographic Techniques

As stated previously the majority of the experimental

TABLE 2.3 A comparison of the drop temperature at impact for drops falling in the cold room or in room temperature air.

Drop Diameter D_d (mm)	Drop Temperature[1] at Impact T_d ($^{\circ}$C)	
	Falling in Cold Room[2] $T_a = -20^{\circ}$C	Falling at room temp. $T_a = 20^{\circ}$C
2.4	1.16	1.30
2.0	1.19	1.42
1.5	1.16	2.16
1.1	0.15	2.94

[1] Initial drop temperature = 1°C.

[2] Drops fall 0.5 m in room temperature air before falling an additional 1.185 m in the cold room.

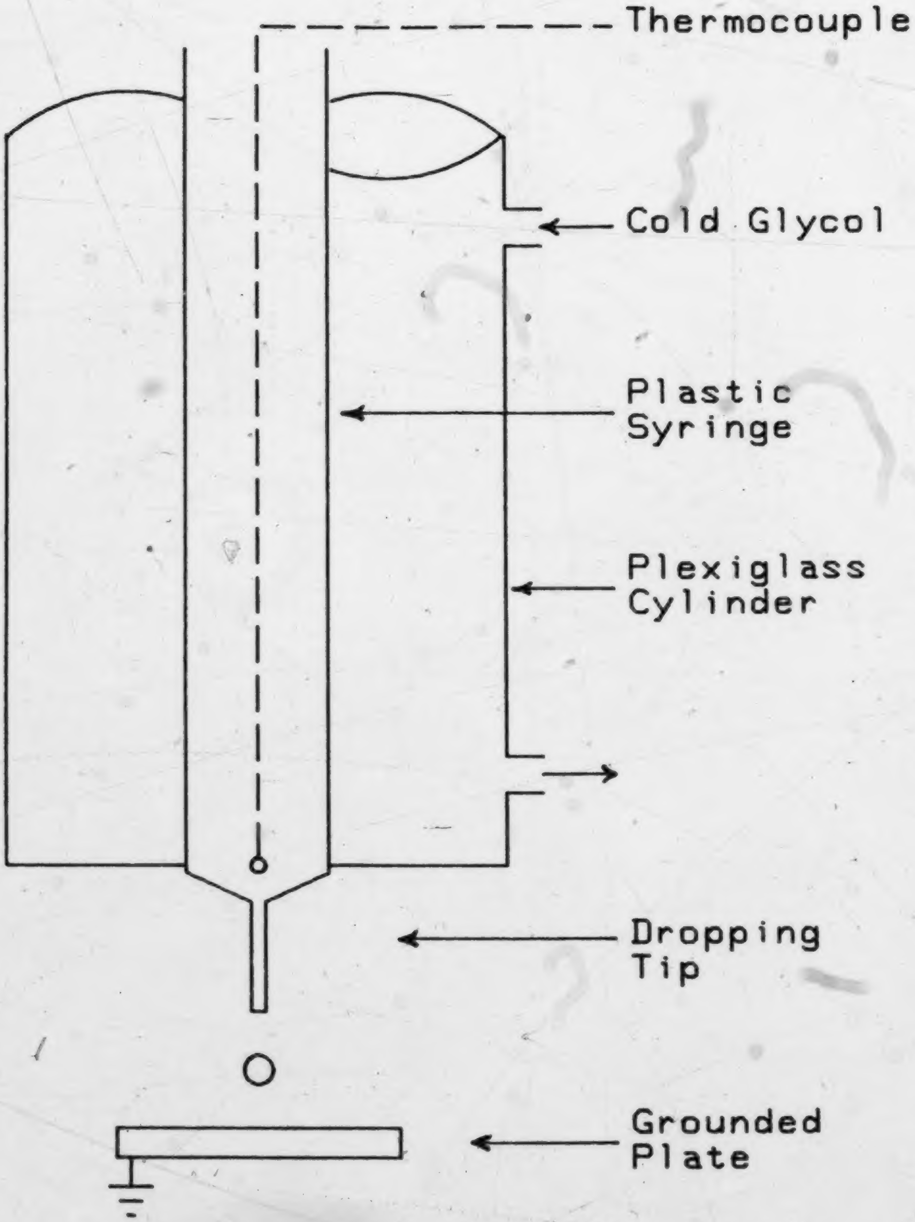
Thermocouple
Cold Glycol
Plastic Syringe
Plexiglass Cylinder
Dropping Tip
Grounded Plate

FIGURE 2.8 Schematic of the cooling reservoir used to control the initial drop temperature.

tests utilized a 35 mm single lens reflex camera to record the spreading of drop on cold dry surfaces. In order to produce a "motion picture" like sequence of photographs (Plate 2.1) required consistently sized drops and a measurable time delay.

This method was selected over high speed photography for a number of reasons. One of the major pitfalls of high speed photography is the possibility that the event may not be captured on the film. Whether it be lighting or focus problems or simply the event occurring outside the field of view of the camera. Needless to say the results are not known until the film has been developed. Another problem associated with high speed photography is the waste of a large portion of the film while the camera reaches its operating speed.

The basic procedure used in this study was to photograph a sequence of drops having the same impact velocity and diameter but at different times during the spreading process. Note that for each of the times several photographs were taken to ensure the repeatability of the results. Figure 2.1 shows a schematic of the set-up used to photograph the impacting drops. As illustrated in the figure, a laser beam and a photo detector were placed at a known distance (H2 = 98.5 cm) above the impact surface. The photo detector was used to generate an electrical signal when the drop fell through the beam. The signal was used in conjunction with the time delay generator to

PLATE 2.1 Sequence of photographs illustrating the spreading of a 2.4 mm diameter water drop on a -20^{o}C smooth glass plate (V_{im} = 4.8 m/s).

t=time S.F.=spreading factor

t = 0.15 ms S.F. = 1.75

t = 0.3 ms S.F. = 2.67

t = 0.5 ms S.F. = 2.98

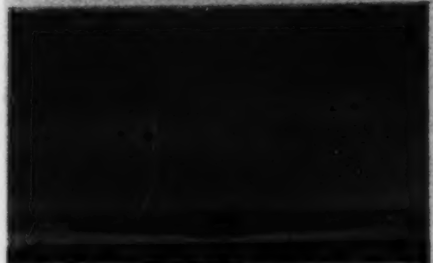
t = 1.0 ms S.F. = 3.75

t = 1.5 ms S.F. = 4.46

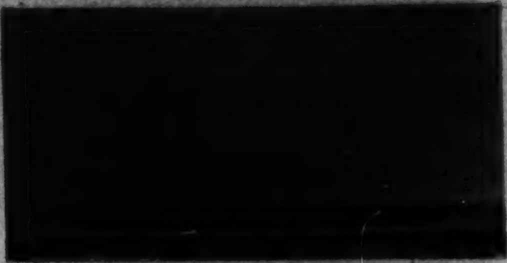
t = 2.0 ms S.F. = 4.75

t = 3.2 ms S.F. = 5.21

t = 6.25 ms S.F. = 5.08

t = 9.25 ms S.F. = 4.88

produce a single short (< 5 μs) duration flash from the strobotac. The time delay generator was capable of delaying the signal (flash) by 1 μs to 100 seconds. For the first drop in the "movie-like" sequence, the appropriate time delay was the time required for the drop to travel the distance H2. Once this time was known, the cold room was darkened, the camera's shutter opened and the motion of the drop was effectively "stopped" by the relatively short flash and captured on the film. The drop was removed from the surface and the procedure was repeated several times.

The subsequent drops were photographed with a correspondingly longer delay time, resulting in the "movie-like" sequence (Plate 2.1). This method, although very time consuming, did prove to have certain advantages. The photographs were very detailed and sharp and could be used to obtain the spreading sizes and shapes of the impacting drops, as functions of time. The method also reduced the need to process and sort the huge amounts of film and data that would be produced using a high speed camera.

Dimensional quantities were obtained from the photographs by simply including a scale in the photograph. The photographs were also be used to obtain an independent value of the drop diameter to compare with that calculated from the mass of 100 collected drops. The comparison indicated that the two methods agreed to within approximately 2% with respect to the drop diameters.

2.6.2 High Speed Video Techniques

Part way through the completion of the experimental portion of this study, the use of a Kodak High Speed Video "Camera" was made available by the Department of Electrical Engineering. The camera is one of only two presently operating in Canada. The camera was capable of framing rates ranging from 60 to 2000 frames/second. In addition, it was possible to produce 6 images per frame thus providing a maximum equivalent framing rate of 12,000 frames/second. This corresponds to 0.083 ms per image making the video ideally suited to record the spreading of the drops considered in this study.

The principle behind the video camera's operation is to record the image using a grid of pixels (i.e. light sensitive diodes). The electronic circuitry converts the image from the diodes into a black and white image recorded on a video tape. The major advantage of the high speed video system is its ability to instantly reproduce the recorded sequence. This ability can be greatly appreciated by anyone who has worked with a high speed camera. Other advantages of the high speed video system are the capability of explicitly displaying the time between frames and the ease at which linear measurements can be obtained from the images.

After recording the sequence of interest the video tape could be simply rewound and viewed on a video screen, frame by frame (Plate 2.2). In addition to the recorded image, the system overlayed an "informative" frame around the perimeter of the image. The frame provided the framing rate, the time of day and the date, the particular frame number and a test identification number. As mentioned previously, the images are representative of a grid of pixels. As illustrated in Plate 2.3, horizontal and vertical cursors could be superimposed on top of the image. The cursors could be moved manually and their position in terms of pixels displayed in the "informative" frame. The insertion of a scale in the image provides the conversion to actual dimensions. The image on the screen can be transferred to a standard video recorder for future use.

The actual test procedure and equipment was the same as that described in 2.6.1 Photographic Techniques, with the exclusion of the elaborate timing circuits. An additional problem arose since the tests had to be performed in the Electrical Engineering building without the aid of a cold room. To accomplish the freezing of the drops on cold dry surfaces, a portable cooling plate was used. The cooling plate consisted of a copper plate, 6 inches square (15 cm) and 1/8 of an inch (0.3 cm) thick. Soldered to the bottom of the plate was a helically wound coil of 5/16 inch (0.7 cm) copper tubing. The entire plate was enclosed in an insulated box. The cooling was provided

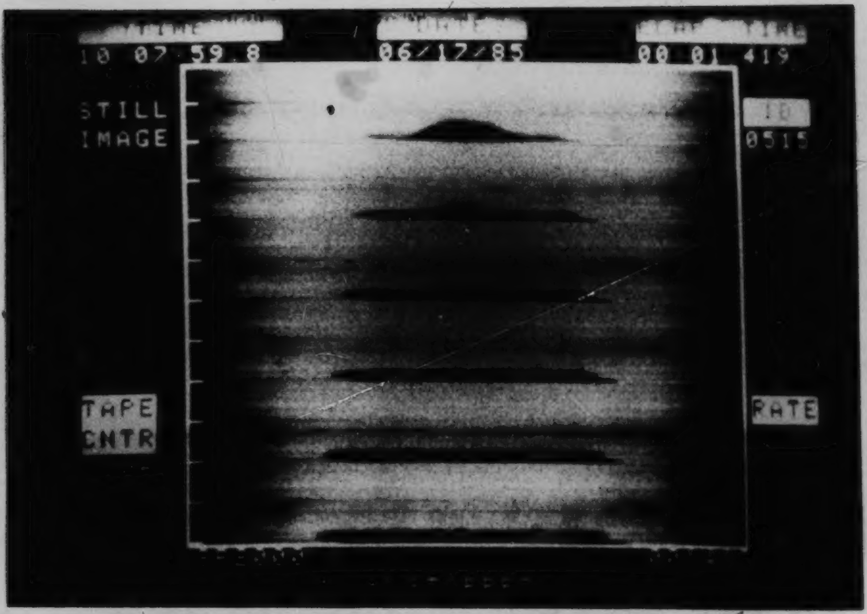
10 07 59.8
06/17/85
00 01 419
STILL
IMAGE
ID
0515
TAPE
CNTR
RATE

PLATE 2.2 The image produced by the Kodak high speed video system for a 2.4 mm diameter distilled water drop spreading on a -10°C copper plate.

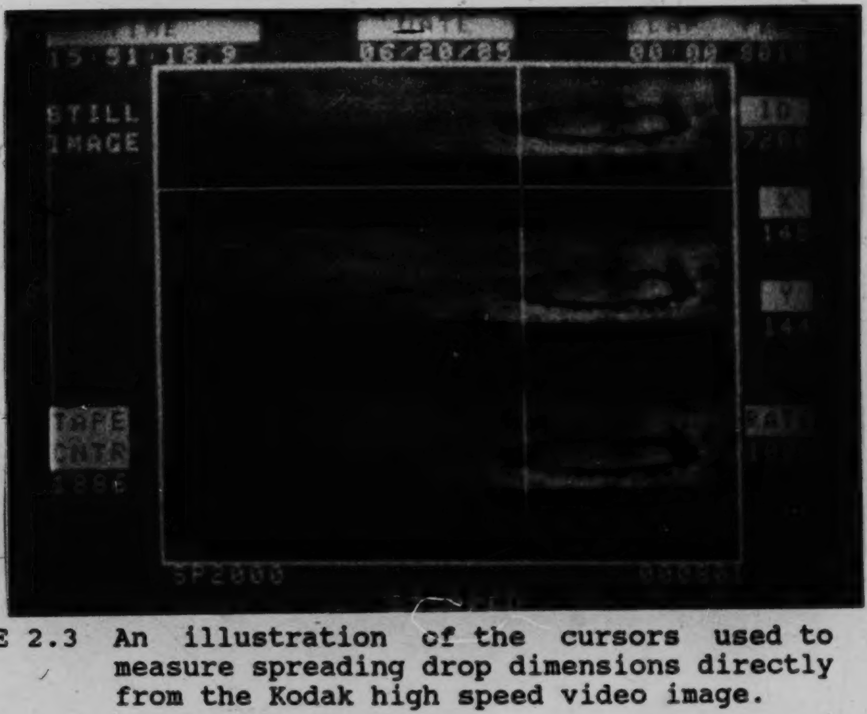
15 51 18.9
06/20/85
STILL
IMAGE
ID
X
Y
TAPE
CNTR
SP2000

PLATE 2.3 An illustration of the cursors used to measure spreading drop dimensions directly from the Kodak high speed video image.

by circulating glycol from a large temperature-controlled bath. The temperature of the plate was recorded by a surface-mounted thermocouple and the temperature of the bath adjusted accordingly. The actual impact plates were placed directly on top of the cooling plate and allowed to cool to the test temperature.

2.7 FREEZING TIME TEST PROCEDURE

In addition to photographing the spreading of the drops, separate tests were performed to quantify the time required for the single drops to freeze on the cold surfaces. The tests were performed in the cold room utilizing the portable cooling plate because it provided better control of the impact surface temperature. The basic procedure was to allow the single drops to impact, spread and freeze on the impact surface at the location where a thermocouple was mounted flush with the surface.

The surface mounted thermocouple was prepared as follows, to minimize any affect on the spreading process. First a small groove large enough to accommodate a 36 gauge thermocouple wire was machined into the top of the impact surface. Then two holes were drilled perpendicular to the groove through to the bottom of the plate. The copper and constantan wires were inserted through these holes before being butt welded and epoxied into position (i.e. into the groove). The plate was polished using 0.05 μm gamma alumina grit to the surface roughness given in Section 2.3. This special care was taken to ensure a rapid response time for the thermocouple.

A Hewlett Packard data acquisition unit (Figure 2.9) was used to record the thermocouple output. The data acquisition was limited to 100 readings per second.

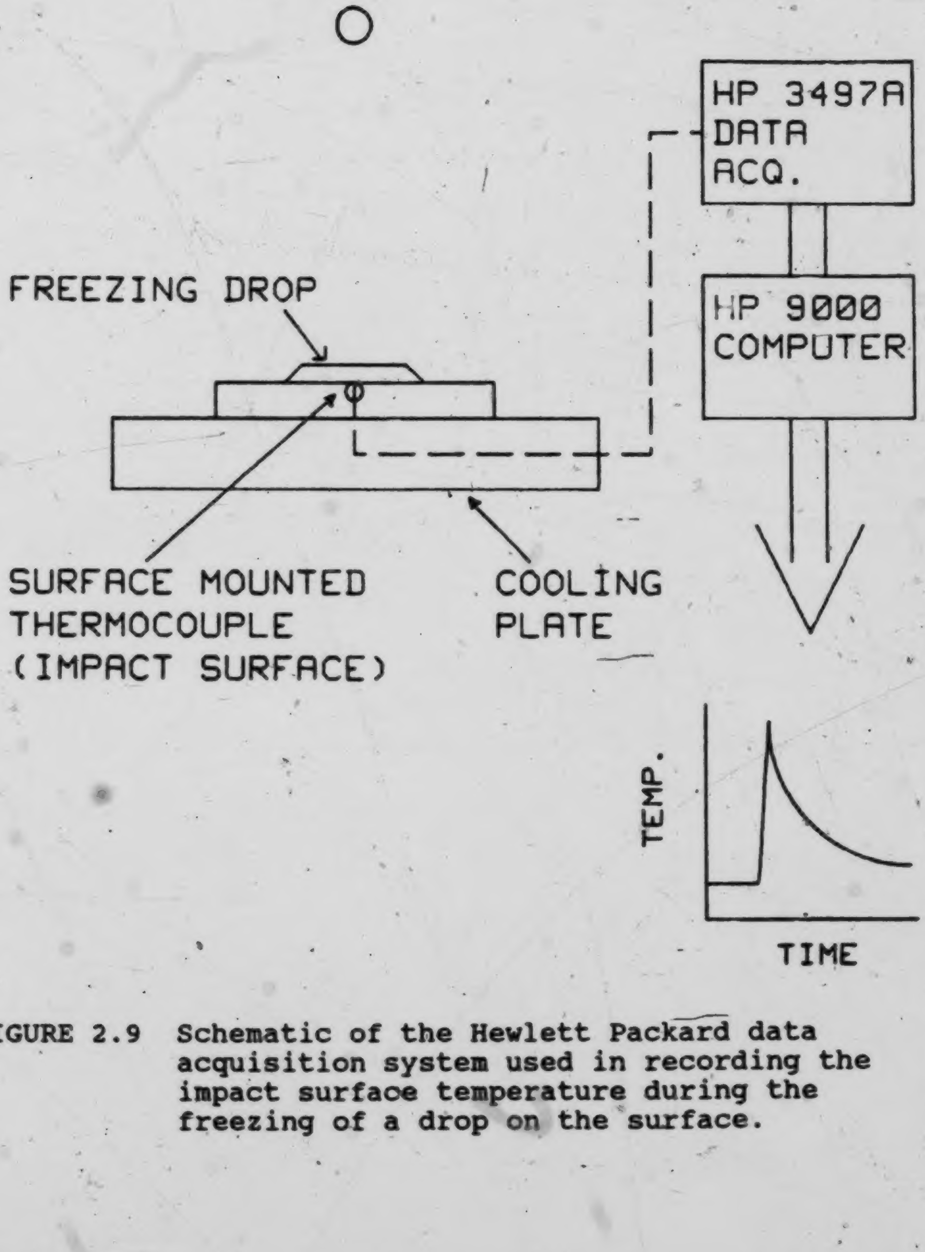
HP 3497A
DATA
ACQ.
HP 9000
COMPUTER
FREEZING DROP
SURFACE MOUNTED
THERMOCOUPLE
(IMPACT SURFACE)
COOLING
PLATE
TEMP.
TIME

FIGURE 2.9 Schematic of the Hewlett Packard data acquisition system used in recording the impact surface temperature during the freezing of a drop on the surface.

CHAPTER 3

PRESENTATION OF RESULTS

3.1 Introduction

The purpose of the experimental portion of this study was to examine the physical processes that occur during the impacting, spreading and freezing of single drops on cold dry surfaces. These physical processes include the heat flux to the icing surface, the viscous dissipation during spreading, and the effects of the surface tension forces. Of particular interest to the present study was the determination the effects of salinity, drop diameter and velocity, impact surface temperature and roughness on the spreading process. This was accomplished by measuring the size of the spreading drop (i.e. spreading factor Figure 3.1) as a function of time. The ranges of the parameters were choosen to correspond to a "typical" marine icing situation, characterized by large saline drops, that are generally not in thermodynamic or kinematic equilibrium with the surrounding environment (Lozowski and Gates, 1985).

3.2.1 Spreading of Drops on a Warm Surface

Plate 3.1 shows a 2.55 mm distilled water drop impacting with a speed of 4.23 m/s on a smooth glass surface. The sequence of 10 photographs illustrates the spreading of the drop on the glass surface from the time

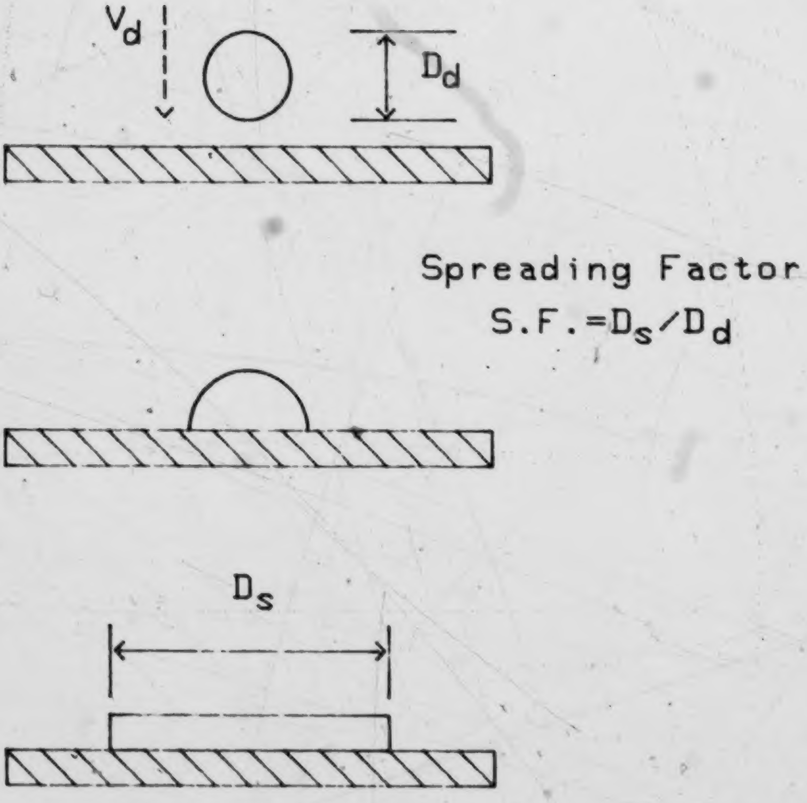
V_d
D_d
Spreading Factor
S.F.=D_s/D_d
D_s

FIGURE 3.1 The definition of Spreading Factor (S.F.) as used to specify the size of a spreading drop.

PLATE 3.1 Photographic sequence illustrating the spreading of a 2.55 mm diameter waterdrop on a room temperature glass surface (V_{im}=4.23 m/s).

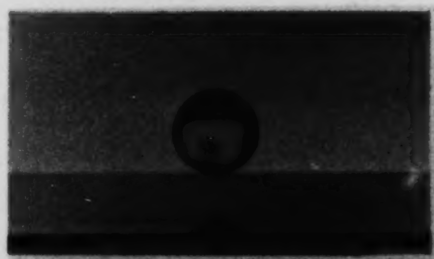

t=time S.F.=spreading factor

t = 0.05 ms S.F. = 1.00

t = 0.25 ms S.F. = 2.33

t = 0.55 ms S.F. = 3.08

t = 0.75 ms S.F. = 3.33

t = 1.0 ms S.F. = 3.75

t = 1.2 ms S.F. = 4.17

t = 1.6 ms S.F. = 4.67

t = 2.2 ms S.F. = 4.96

t = 3.2 ms S.F. = 5.33

it impacts until the drop reaches its maximum spread-out size ($S.F._{max}$). Thus plate provides an illustrated perspective of the spreading process on a warm surface for comparison with the spreading and freezing of a drop on a cold surface.

The first photograph in the sequence shows the initially spherical drop an instant (≈.1 ms) before it impacts on the surface. Just after the drop impacts it remains essentially spherical with the exception of a small portion in contact with the surface. Even at this initial stage of the spreading the drop has begun to spread radially outward, from the point of impact on the surface. This is illustrated by the thin "band" or "ring" of water with a circumference slightly larger than the circumference of the section of the drop in contact with the surface, as visible in the 2nd photograph in the sequence. As the apex of the drop moves closer to the impact surface, the drop begins to flatten and deform as the circumferential "ring" enlarges (3rd photograph in the sequence). At this point there is a smooth transition between the remaining portion of the drop (i.e. remaining portion of the initially spherical drop) and the circumferential "ring".

The apex of the drop continues to move toward the surface while mass from the drop "flows" into the "ring" increasing it's circumference. As the spreading continues the leading edge of the "ring" begins to thicken as illustrated in the 5th photograph in the sequence. This thickening of the leading edge becomes well-defined by the time the apex of the drop has completely dissappeared (7th photograph). At this point, the initially spherical "drop" is comprised of what appears to be a "disk" of water with a somewhat thicker and bumpier circumferential "ring".

The "disk" continues to increase in diameter while the leading edge (ring) thickens and the bumps or ripples become more evident (8th and 9th photographs in the sequence). This ripply or wavy appearance of the leading edge corresponds to the formation of a gravity wave. The disk continues to spread until it reaches its maximum spread out size referred to as $S.F._{max}$. As illustrated in the 10th photograph in the sequence where the drop has reached $S.F._{max}$, the gravity wave is now well defined in the relatively thick leading edge of the spread-out drop.

The shape of the spread-out drop illustrated in the 10th photograph of the sequence does not represent the final shape of the drop on a warm surface. As a result of being "spread out" on the surface, the surface tension forces cause the drop to "contract" and take on the shape of a somewhat flattened "hemisphere" of water, with a diameter of approximately twice its initial spherical diameter. This final shape is obtained when the gravitional potential and surface tension forces are in equilibrium. The above description only holds true if the water "wets" the surface (i.e. the contact angle is less than 90°), as is the case with water on glass.

3.2.2 Spreading of Drops on a Cold Surface

For comparison with the spreading of a drop on a warm surface, Plate 3.2 shows the spreading of a 2.55 mm diameter distilled water drop on a -10°C glass surface. The drop arrived at the surface with an impact velocity of 4.23 m/s and a temperature of 1°C. With the exception of the -10°C glass surface the conditions under which the spreading occurs are identical to those used to illustrate the spreading of a drop on a warm surface (Plate 3.1). A comparison of these plates illustrates two of the obvious affects that freezing (heat transfer) has on the spreading process.

On the warm surface, after the apex of the drop is no longer apparent (7th photograph, Plate 3.1), the "ring" of water at the leading edge of the spreading drop begins to form a gravity wave. This gravity wave is well defined by the time the drop reaches $S.F._{max}$ (10th photograph, Plate 3.1). However on the cold surface, although there are indications that the gravity wave is beginning to develop (7th photograph, Plate 3.2), by the time the drop reaches $S.F._{max}$ the gravity wave is no longer apparent (9th photograph, Plate 3.2).

The second effect of the freezing (i.e. heat transfer) on the spreading process is obvious from the 10th

PLATE 3.2 Photographic sequence illustrating the spreading of a 2.55 mm diameter waterdrop on a -10°C glass surface (V_{im}=4.23 m/s).

t=time S.F.=spreading factor

t = 0.2 ms S.F. = 2.15

t = 0.3 ms S.F. = 2.67

t = 0.5 ms S.F. = 3.11

t = 1.0 ms S.F. = 3.48

t = 1.2 ms S.F. = 3.63

t = 2.0 ms S.F. = 4.59

t = 2.25 ms S.F. = 4.96

t = 3.25 ms S.F. = 5.26

t = 8.25 ms S.F. = 5.19

photograph in Plate 3.2. This photograph shows the final shape of the drop as a relatively flat layer of ice, in comparison with a drop on a warm surface where the equilibrium (i.e. final) shape has a somewhat "hemispherical" profile. However, it is the large difference in the final spread out size (S.F.) which is of particular importance. It is also interesting to note that for the drop spreading on the cold surface the width of the "ring" at the leading edge of the spreading drop is larger for the equilibrium shape (10th photograph) than for the shape corresponding to $S.F._{max}$ (9th photograph, Plate 3.2). This gives the frozen drop a flat "donut" like appearance (i.e. a depression in the central portion of the spread out drop).

Plates 3.3 and 3.4 show the final size and shape of 2.4 mm drops frozen on -20°C copper and ice surfaces after impacting on the surfaces at 4.8 m/s. Both Plates indicate the depression in the center of the "donut" like shape; however, the diameter of the depression is smaller for the ice surface.

3.3 Spreading Results

3.3.1 Spreading Factor verses Time

For illustrative purposes Figure 3.2 plots the spreading factor of drops spreading on a warm (>20°C) copper surface, as a function of time, for Impact Weber

PLATE 3.3 Final size and shape of 2.4 mm diameter salt water drops freezing on a -20°C copper surface (V_{im} = 4.8 m/s).

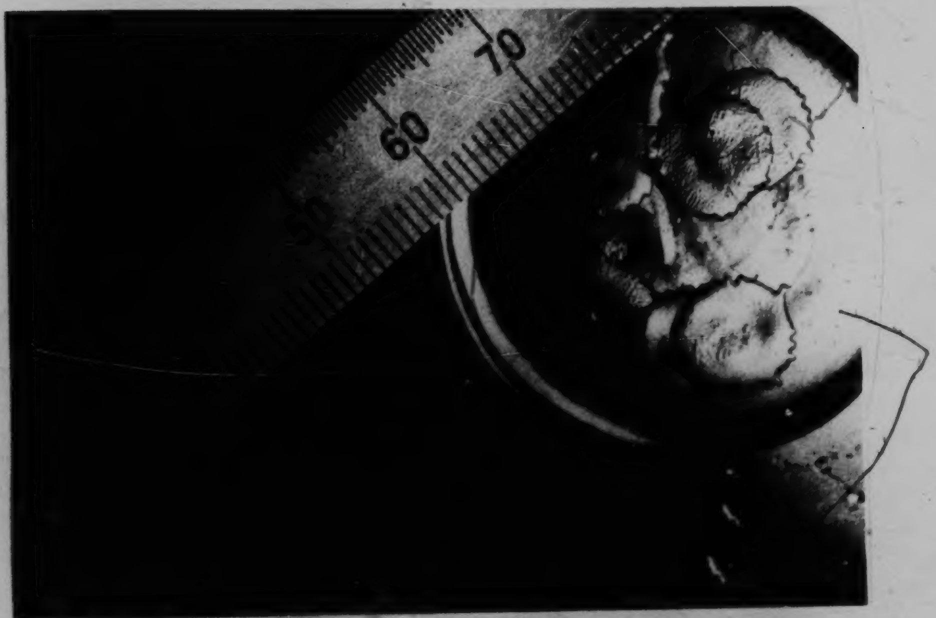

PLATE 3.4 Final size and shape of 2.4 mm diameter drops freezing on a -20°C ice surface (V_{im}=4.8 m/s).

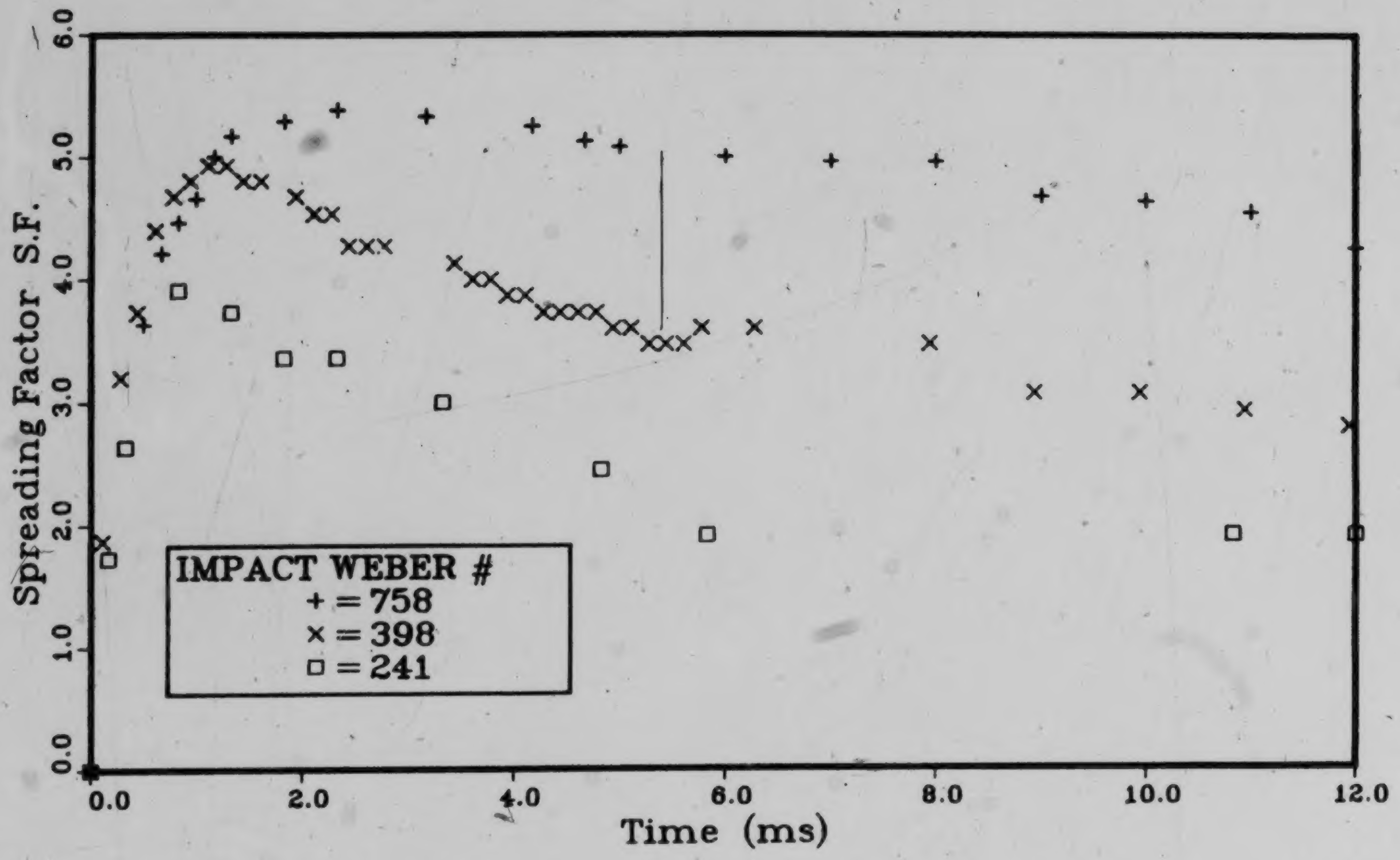

FIGURE 3.2 The spreading factor of distilled water drops spreading on a warm (20°C) copper surface.

Numbers of 758, 398 and 241. The Impact Weber Number (We #) is defined as 12 times the ratio of the kinetic to surface energy of the impacting drop and is given by:

$$\text{We \#} = \rho_w V_{im}^2 D_d / \gamma_{a/w} \qquad (3.1)$$

where

$\gamma_{a/w}$ = surface tension coefficient for air-water interface
= 73 dyne/cm = .073 nt/m

The Impact Weber Numbers of 758, 398 and 241 referred to in Figure 3.2 represent 2.4, 1.5 and 1.1 mm diameter distilled water drops impacting at 4.8, 4.4 and 4.0 m/s respectively. A simple dimensional analysis suggests that the spreading factor (D_s/D_d) is a function of the Reynolds number and Weber number. Since the Weber number represents the two most important components of the drop energy, namely the kinetic and surface energy, which are of particular importance especially during the initial stages of spreading, the Impact Weber number was choosen to nondimensionalize the impacting drop parameters. In addition, due to limitations of the experimental set-up the drop velocities were not varied independently of the drop diameters. The Weber number conveniently allowed the drop diameter and the corresponding velocity to be represented by a single non-dimensional variable.

Figures 3.3 and 3.4 are also plots of the spreading factor as a function of time, except that the spreading is

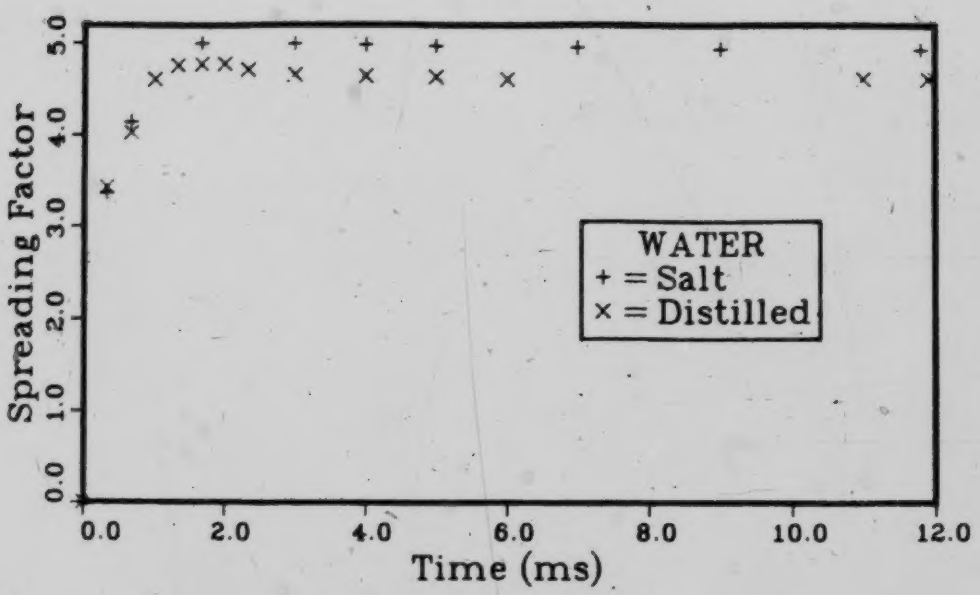

FIGURE 3.3 The effect of salinity on the spreading of 2.4 mm diameter waterdrops on a $-20^{\circ}C$ copper surface (V_{im} = 4.8 m/s).

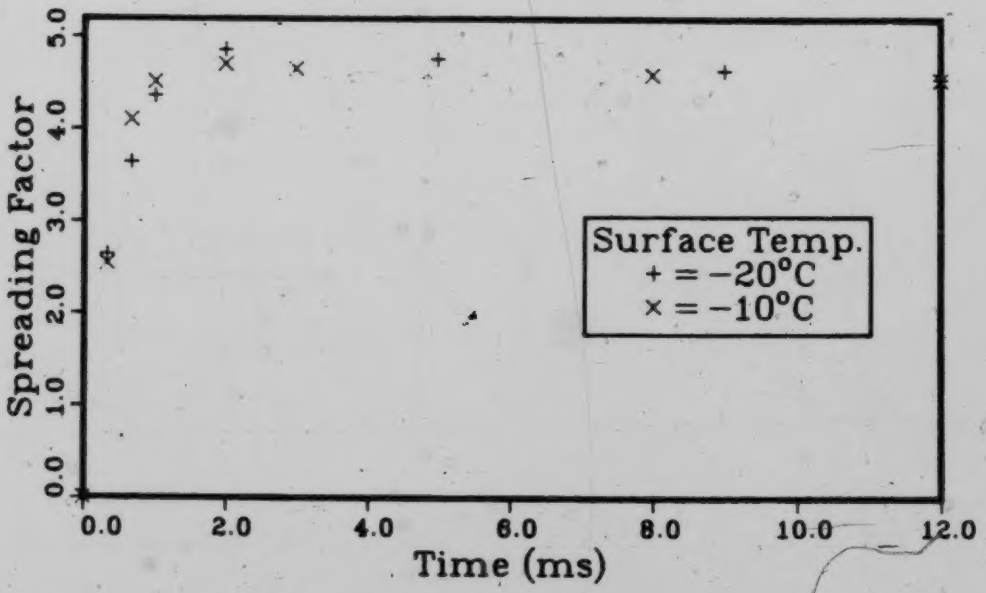

FIGURE 3.4 The effect of impact surface temperature on the spreading of 2.4 mm diameter waterdrops on a stainless steel surface (V_{im}=4.8 m/s).

occurring on a cold surface. Figure 3.3 shows the effect of salinity on spreading of a 2.4 mm drop (V_{im} = 4.8 m/s) on a smooth -20°C copper surface, while Figure 3.4 shows the effect of the impact surface temperature (-10, -20°C) on the spreading of 2.4 mm diameter water drops on a cold stainless steel surface (V_{im} = 4.8 m/s).

3.3.2 Spreading Factor - Maximum

Table 3.1 summarizes $S.F._{max}$ and the time required to reach $S.F._{max}$ for drops spreading and freezing on copper, stainless steel and ice surfaces. The table shows the effect of the impact surface temperature (20, -10 and -20°C), We # (241, 398 and 751) and salinity (S=33 g/kg) on $S.F._{max}$ and the time to $S.F._{max}$. The values in this table were summarized from a single video or photographic test and due to time limitations were not repeated.

3.3.3 Spreading Speed - Initial

The initial spreading speed (V_s) or radial spreading velocity was said to be the average radial spreading speed from the time of impact until the time t_s, where t_s is equal to D_d/V_{im}, the time required for the impacting drop to move the distance equal to its initial (spherical) diameter. Had the drop's motion not been impeded by the impact with the solid surface, t_s would correspond to the time at which the apex of the impacting drop would no longer be apparent (Plate 3.1, 7th photograph in sequence).

TABLE 3.1 Effect of impact surface temperature and salinity on the maximum Spreading Factor (S.F.$_{max}$) and the corresponding time required to reach S.F.$_{max}$.

SURFACE		DROP		S.F.$_{max}$		Time to S.F.$_{max}$	
Material	Temp. (°C)	Diameter (mm)	Impact Velocity (m/s)	Distilled	Salt	Distilled (ms)	Salt (ms)
Copper	20	2.4	4.8	5.38	5.38	2.33	2.33
	-10	2.4	4.8	4.85	5.13	2.00	2.00
	-20	2.4	4.8	4.76	5.00	1.33	1.67
	20	1.5	4.4	4.93	4.93	1.20	1.20
	-10	1.5	4.4	4.85	4.69	1.33	1.00
	-20	1.5	4.4	4.12	4.57	0.91	1.00
	20	1.1	4.0	3.91	3.91	0.83	0.83
	-10	1.1	4.0	3.80	—	1.50	—
S.S. 304	-10	2.4	4.8	4.85	4.86	1.55	2.00
	-20	2.4	4.8	4.31	4.86	1.33	2.00
	-10	1.5	4.4	4.49	4.42	1.17	2.00
	-20	1.5	4.4	4.37	4.11	1.16	1.17
Ice	-10	2.4	4.8	5.00	5.40	2.33	2.44
	-20	2.4	4.8	5.15	5.60	1.67	2.33

Table 3.2 summarizes the effect of salinity and impact surface temperature on the initial spreading rate of the drops. The surface temperatures used for these tests were 20, -10 and -20°C for the copper plates and -10 and -20°C for the stainless steel plates. The effect of We # (241, 378 and 751) on this spreading rate is also illustrated in this table.

3.3.4 Spreading Factor - Final Size

Figures 3.5 through 3.7 show the final size, in terms of spreading factor, as a function of the Impact Weber number (non-dimensional ratio of inertial to surface tension forces). Final size refers to the spreading factor after the spreading and/or freezing have been completed (i.e. equilibrium shape and size). The figures show $S.F._{final}$ for variations in surface temperature and salinity (S =0 or 33 g/kg) for the drops spreading and freezing on ice, copper and stainless steel surfaces.

Figure 3.5 shows the variation in final size for impact surface temperatures of -10 and -20°C, as well as the effect of salinity for drops spreading and freezing on an ice layer. Figures 3.6 and 3.7 show the variation in $S.F._{final}$ under the same conditions, except the drops are frozen on copper and stainless steel surfaces. In Figures 3.5 through 3.7 the air temperature was the same as the impact surface temperature and the drops arrived at the

TABLE 3.2 The effect of salinity and impact surface temperature on the initial spreading rate* of water drops on cold dry surfaces (* - average rate until time $t = D_d/V_{im}$).

SURFACE		DROP		Initial Spreading rate/ Impact Velocity	
Material	Temp. (°C)	Diameter (mm)	Impact Velocity (m/s)	Distilled	Salt
Copper	20	2.4	4.8	1.81	——
	20	1.5	4.4	1.71	——
	20	1.1	4.0	1.16	——
	-10	2.4	4.8	1.78	1.77
	-10	1.5	4.4	1.22	1.70
	-10	1.1	4.0	0.89	——
	-20	2.4	4.8	1.86	1.87
	-20	1.5	4.4	1.19	1.47
S.S. 304	-10	2.4	4.8	1.75	1.66
	-20	2.4	4.8	1.65	1.57
	-20	1.5	4.4	1.46	1.71

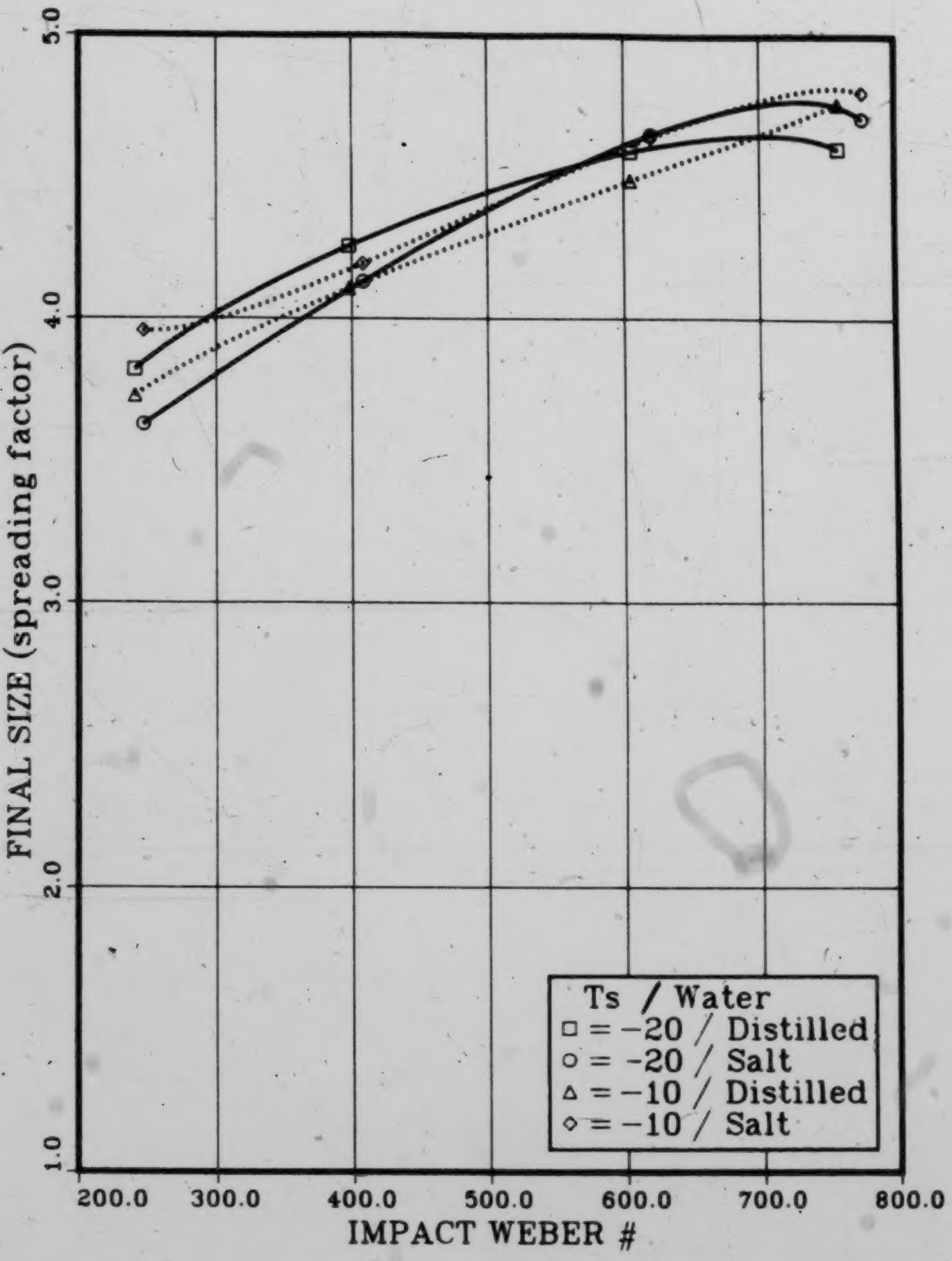

FIGURE 3.5 Final size (S.F.) verses Impact Weber # for distilled and salt waterdrops spreading on -20 and -10°C ice surfaces ($T_{air}=T_s$=temp. of ice surface and $T_{drop}=1^{o}C$).

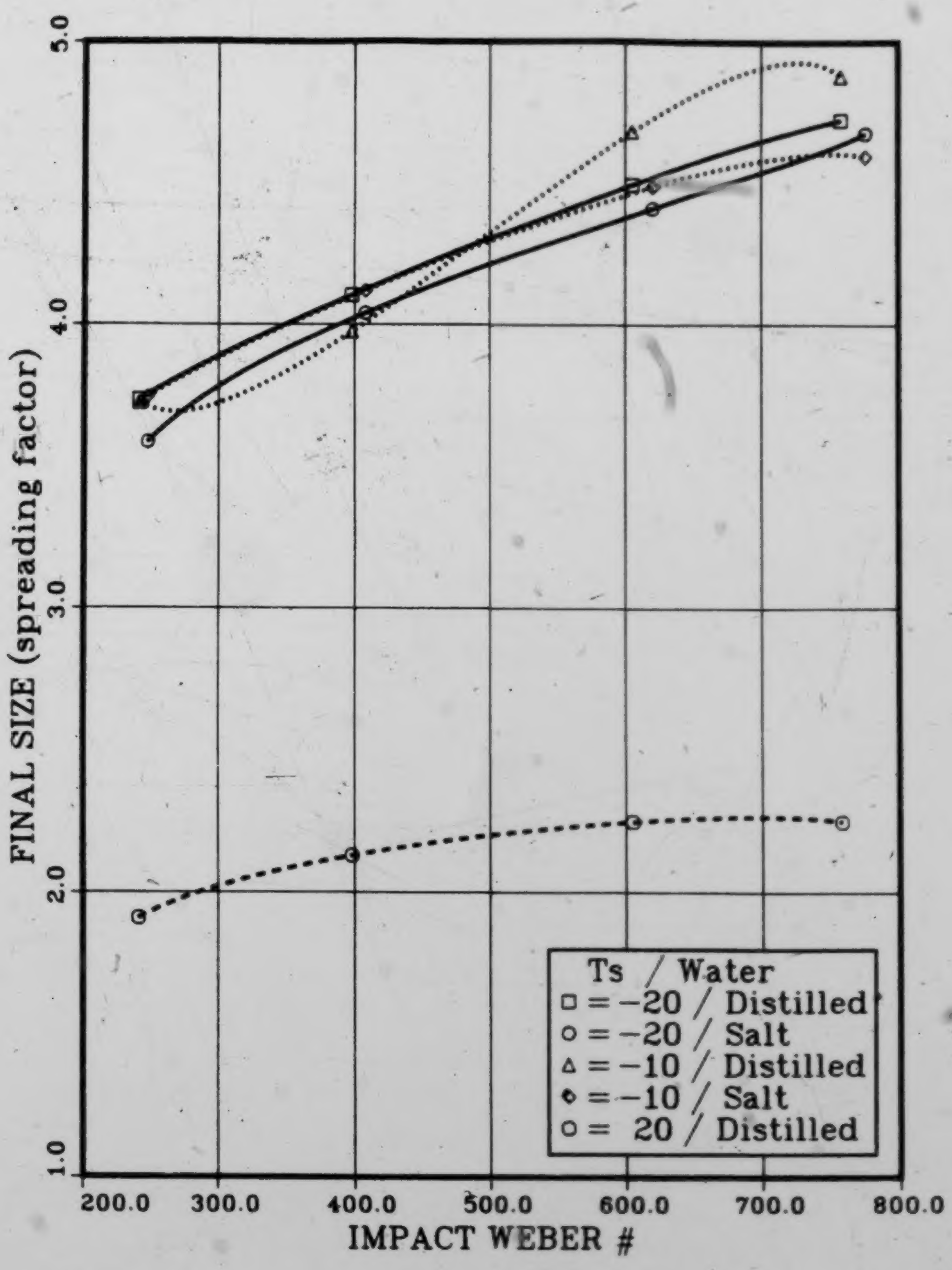

FIGURE 3.6 Final size (S.F.) verses Impact Weber # for distilled and salt waterdrops spreading on 20, -10 and -20^{o}C copper surfaces ($T_{air}=T_s=$ temp. of copper surface and $T_{drop}=1^{o}C$).

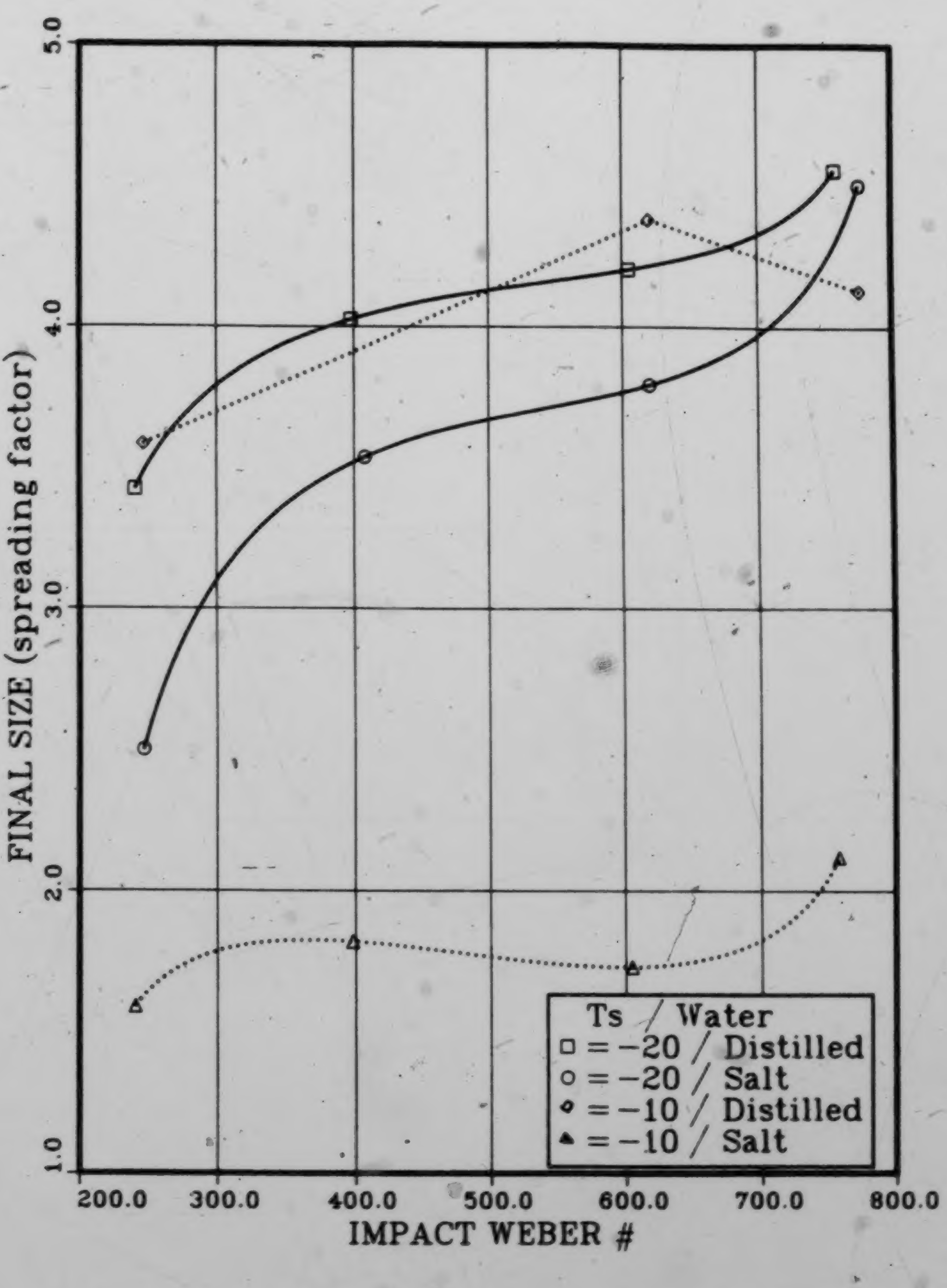

FIGURE 3.7 Final size (S.F.) verses Impact Weber # for distilled and salt waterdrops spreading on -20 and -10°C stainless steel 304 surfaces (T_{air}=T_s= temp. of surface and T_{drop}=1°C).

surface with a temperature of approximately 1^{o}C.

Note that the experimental tests used to determine the final size of the spread-out drops (i.e. S.F.$_{final}$) were performed independently of the high speed video and photographic sequences. Since only a single photograph of the drops was required to determine the final size, several tests could be performed to insure the results were statistically valid.

3.4 Freezing and Cooling

In addition to determining the size of the spread-out drops, it is important in terms of modelling ice accretions to determine the temperature of the freezing drops as a function of time. Since it was not possible to measure the drop temperature, the impact surface temperature was measured and correlated to the drop temperature.

3.4.1 Freezing and Cooling Times

Figure 3.8 plots the surface temperature of a plexiglass plate as a function of time, recorded during the spreading of a 2.55 mm diameter distilled water drop on the plate. The drop arrived at the surface with an impact speed of 4.3 m/s and a temperature of 4^{o}C and froze as a "disk" of water with a spreading factor of 4.5. The initial surface temperature was -10^{o}C and the air temperature was maintained at -12^{o}C. The figure

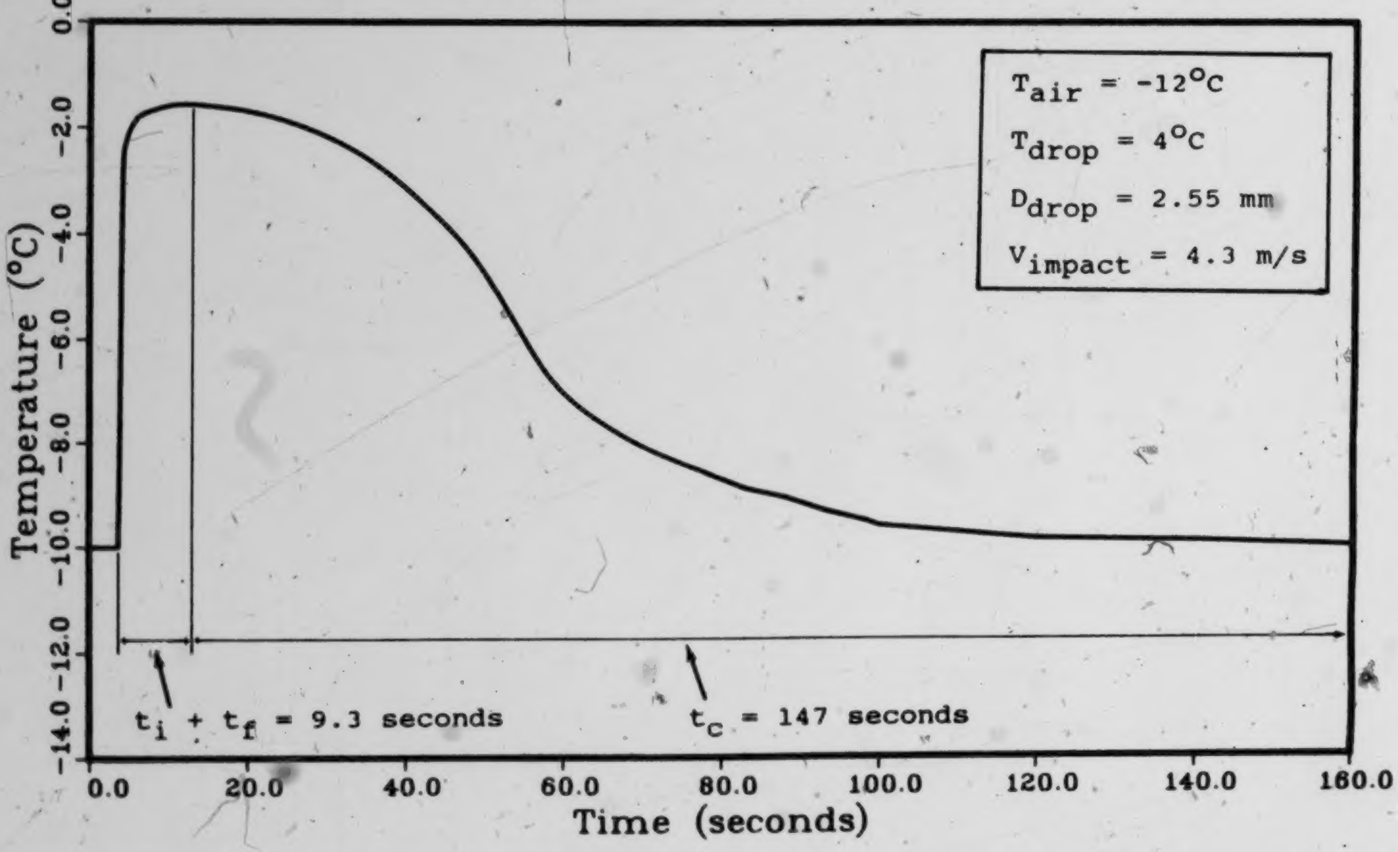

FIGURE 3.8 Freezing of a spread out (S.F. = 4.5) fresh water drop on a -10°C plexiglass plate (temperature recorded from a surface mounted thermocouple).

illustrates the three time periods or stages appropriate to the freezing of the drop and the cooling of the drop and the surface to the initial surface temperature (i.e. temperature of surface prior to the arrival of the drop).

It is the sum of these three times (t_i, t_f and t_c) which is referred to as the total time. The time t_i was equal to zero in this particular case since the impacting drop was not supercooled. This time t_i corresponds to the time required for ice to grow in a "portion" of the drop if the drop is supercooled. This "portion" of the drop is equal to the degree of supercooling times the drop's specific heat capacity divided by the latent heat of fusion. The time t_f corresponds to the time required to freeze the drop (i.e. cool the drop to 0°C and remove the latent of fusion). The time t_c corresponds to the time required to return the impact surface and the drop to the initial temperature of the surface.

Table 3.3 summarizes the experimentally determined freezing times for single distilled and saline water drops freezing on -10 and -20°C copper and stainless steel surfaces. The table includes the freezing times for 2.4, 1.5 and 1.1 mm drops impacting with velocities of 4.8, 4.4 and 4.0 m/s respectively. These times were estimated from the high speed video results by assuming that the drop was frozen when the spreading factor did not change (i.e. time corresponding to $S.F._{final}$). Since the drops arrived at the surface at approximately 1°C, t_i was taken to be equal

TABLE 3.3 Experimentally determined freezing times for salt and distilled waterdrops on cold dry surfaces ($T_{air} = T_s =$ temp. of surface).

SURFACE		DROP		FREEZING TIME t_f (ms)	
Material	Temp. (^oC)	Diameter (mm)	Impact Velocity (m/s)	Distilled	Salt
Copper	-10	2.4	4.8	16.0	14.0
	-10	1.5	4.4	8.0	6.0
	-20	2.4	4.8	14.0	13.0
	-20	1.5	4.4	6.0	4.0
S.S. 304	-10	2.4	4.8	17.0	13.0
	-10	1.5	4.4	13.0	11.0
	-20	2.4	4.8	10.0	12.0
	-20	1.5	4.4	6.0	6.0
Plexiglass	-10	2.55	4.23	9300	——

to zero.

3.4.2 Total Time

Table 3.4 summmarizes the experimentally determined total time ($t_i + t_f + t_c$) measured using a surface mounted thermocouple and the H.P. data acquisition unit (Section 2.6). The table includes the total time for 2.4 mm drops impacting at 4.8 m/s on -20°C copper and stainless steel surfaces. The table also includes the effect of salinity and the initial drop temperature on t_T.

TABLE 3.4 Total time t_T ($t_i + t_f + t_c$) required to freeze 2.4 mm diameter waterdrops, impacting at 4.8 m/s, then cool the impact surface to its initial temperature (i.e. t_c = time required to cool impact surface to 99% of $T_m - T_s$).

SURFACE		Drop Temp. at Impact (^oC)	Salt or Distilled Waterdrop	Total time t_T (ms)	Standard Deviation σ	Sample Size N
Material	Initial Temp-T_s (^oC)					
Copper	-20	1	d	1730	——	1
	-20	1	s	1890	150	7
	-20	20	d	1900	100	4
	-20	20	s	1990	30	2
S.S.304	-20	1	d	1840	90	3
	-20	1	s	1900	190	2
	-20	20	d	1890	130	2
	-20	20	s	2110	130	3

CHAPTER 4

DISCUSSION OF RESULTS

As a result of the increased activity in offshore operations in northern waters, there has been increased emphasis placed on marine icing research. Of particular interest is the development of analytical models which can be used to predict ice accretion rates and possibly shapes, under typical marine icing conditions. Typical marine icing conditions are characterized by large saline drops which are generally in neither kinematic nor thermodynamic equilibrium with the air (Lozowski and Gates, 1985). The primary source of these drops is the sea spray generated by impacting waves.

Of particular interest in the present study is the effect of salinity, impact surface temperature, and drop diameter and impact velocity (Impact Weber Number) on the spreading of large drops on cold dry surfaces. Towards this end an experimental study was undertaken to examine the physical processes involved with the impacting, spreading and freezing of single drops on cold dry surfaces. These physical processes include the heat transfer to the icing surface, and the effects of surface tension forces and heat transfer on the spreading. This spreading and freezing of drops on cold dry surfaces corresponds to the initial stage of the ice accretion process (i.e. no previously accreted water or ice).

4.1 Spreading

Engel (1955) used high speed photography and chemical tracing techniques to examine the collision of large water drops (3 mm in diameter) with a solid surface, at speeds up to terminal velocity. Engel's investigation led to the development of empirical relationships defining the time dependence of the impact force and the radial flow velocity. Savic and Boult (1955) also examined the spreading of large drops on warm surfaces. More recently Macklin and Payne (1969) examined the spreading of accreted drops on an ice coated metal cylinder; however, they were primarily concerned with conditions typical to atmospheric icing, in particular drops with diameters on the order of 50 μm.

For this study the primary interest was with the marine icing situation, in particular the spreading and freezing of large saline drops. At the present time this author is unaware of any research directed primarily at this marine icing situation. However spreading of large drops on warm surfaces provides a basis of comparison for similar drops spreading and freezing on cold dry surfaces.

4.2 Discussion of Spreading Results

As explained previously (Section 2.6.1), the majority of the results related to the spreading of drops on cold dry surfaces were obtained through the use of high speed video or photographic techniques. These experimental results provided a means of determining the parameters that best describe the spreading of drops on dry surfaces, namely the spreading rate as a function of time, the initial spreading speed, $S.F._{max}$ and final size ($S.F._{final}$). These parameters were then used as a basis to determine the effects of salinity (S=0 or 33 g/kg), impact surface temperature, drop impact velocity and drop diameter on the spreading process.

The "initial" spreading velocity (V_s) was taken to be the average radial spreading velocity, from the instant of impact until the time t_s. Time t_s is equal to D_d/V_{im}, the time required for the impacting drop to move the distance equal to its diameter. Had there not been resistance to the spreading of the drop, t_s would correspond to the time at which the impact momentum of the spherical drop had been converted into radial momentum of the spreading drop (i.e. complete flattening of the spherical portion of the drop).

Figure 3.3 illustrates graphically the effect of salinity (S=0 or 33 g/kg) on the freezing of drops on a -20°C copper surface. The points on the figure correspond to the spreading of 2.4 mm diameters distilled and saline water drops, with impact velocities of 4.8 m/s on the copper surface. The curves on this figure suggest that as a function of time, the spreading size is not strongly dependent on the salinity. Although the lower freezing point of the saline drops allowed the salt water drops to

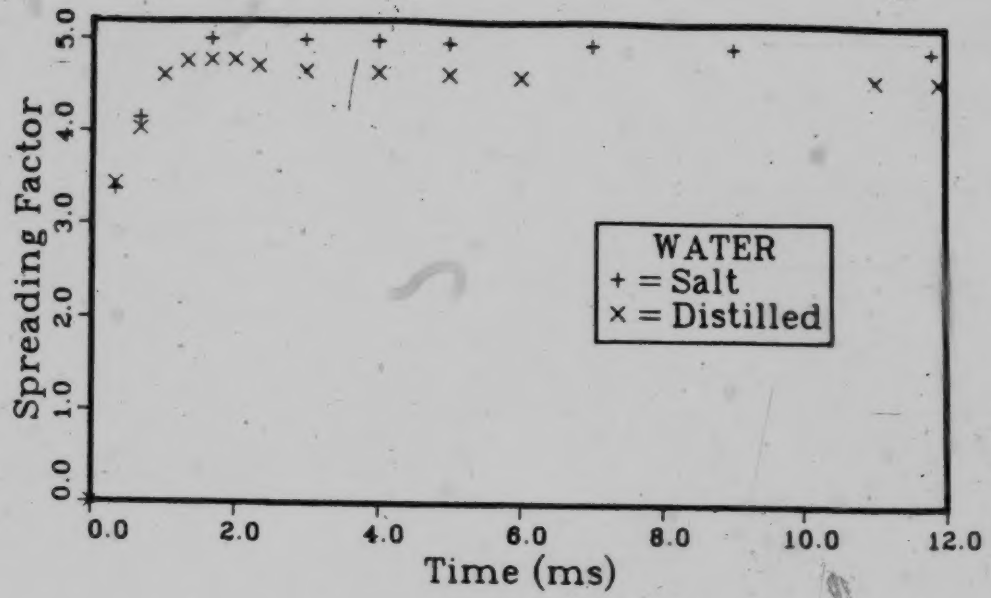

FIGURE 3.3 The effect of salinity on the spreading of 2.4 mm diameter waterdrops on a $-20^{\circ}C$ copper surface (V_{im} = 4.8 m/s).

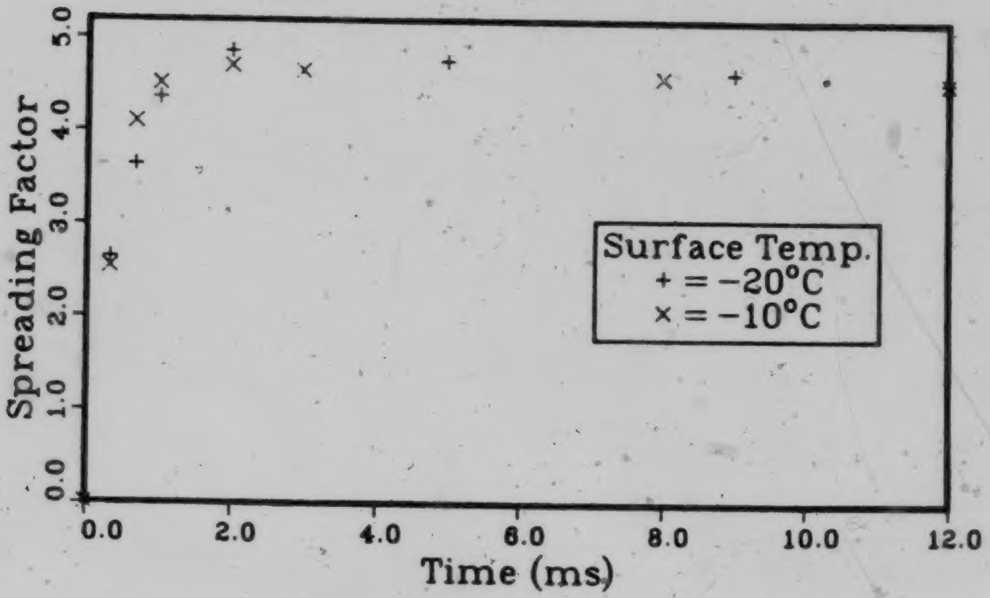

FIGURE 3.4 The effect of impact surface temperature on the spreading of 2.4 mm diameter waterdrops on a stainless steel surface (V_{im}=4.8 m/s).

attain a slightly larger $S.F._{max}$ (≈4%), the curves for the distilled and saline drops are esssentially the same, in terms of spreading rate (i.e. slope) and the final size.

Figure 3.4 illustrates the effect of impact surface temperature on the freezing of 2.4 mm diameter saline water drops on a stainless steel (S.S. 304) plate (V_{im} = 4.8 m/s). For impact surface temperatures of -10 or -20°C, $S.F._{max}$ was essentially the same (4.86). This would tend to suggest that very little freezing occurs during this initial spreading (up to $S.F._{max}$). Another indication of this apparent lack of freezing, which can be deduced from both Figures 3.3 and 3.4, is the time required to reached $S.F._{max}$. For all the drops freezing and spreading on the cold surfaces this time was on the order of 2 ms which is comparable to the corresponding time (2.33 ms) on warm surfaces, as indicated in Figure 3.2.

4.2.1 Maximum Spreading Factor

Calculation of the maximum spreading factor requires a knowledge of the velocity distribution in the spreading drop so as to quantify the energy dissipated by the viscous forces during spreading. Given the complexity of such a calculation and the experimental nature of the present study, such a calculation was not warranted. However, an estimate of an upper limit to the maximum spreading factor can be obtained by considering only the surface energy of the spread-out drop. To calculate this surface energy the drop was assumed to spread out as a disk of uniform thickness and only the energy of the surface exposed to the air was considered. An estimate of the $S.F._{max}$ can then be obtained by equating this surface energy to the energy of the drop at impact.

The falling drop's energy consists of its kinetic (KE_d), surface (SE_d) and gravitional potential energy, which was excluded since it represented less than 0.1% of the drop's total energy at impact. The kinetic energy (KE_d) is given by:

$$KE_d = \pi D_d^3 \rho_w V_{im}^2/12 \qquad (4.1)$$

and the spherical drop's surface energy SE_d by:

$$SE_d = \pi D_d^2 \sigma_{a/w} \qquad (4.2)$$

where

D_d = drop diameter (mm)

ρ_w = density of water (kg/m^3)

V_{im} = drop impact velocity (m/s)

$\sigma_{a/w}$ = surface tension - air/water (dynes/cm)

The surface energy of a disk of uniform thickness SE_{disk} is given by:

$$SE_{disk} = A_s \sigma_{a/w} = \pi(D_s^2 + D_s \delta R) \sigma_{a/w} \qquad (4.3)$$

where

δR = thickness of disk (μm)

D_s = diameter of spread out drop (mm)

A_s = drop surface area exposed to air (mm^2)

Equating 4.3 to 4.1 + 4.2 and simplifing:

$$\frac{D_d^3 \rho_w V_{im}^2}{12 \sigma_{a/w}} + D_d^2 = D_s^2 + \frac{D_d^3}{6 D_s} \qquad (4.4)$$

Solving equation 4.4 iteratively for D_s gives the results shown in Table 4.1. For 2.4, 1.5 and 1.1 mm drops impacting at 4.8, 4.4 and 4.0 m/s on a warm surface the estimated S.F.$_{max}$ were 8.0, 5.84 and 4.59 as compared to experimental values of 5.38, 4.93 and 4.59 (Table 3.1). These differences indicate the importance of the viscous dissapation in the spreading process. However, this is beyond the scope of the present study; therefore, the subject has been left for future consideration.

Table 3.1 summmarizes the effects of surface temperature and salinity (S=0 or 33 g/kg) on the experimentally determined S.F.$_{max}$ and the time to S.F.$_{max}$. For 2.4 mm diameter distilled drops impacting at 4.8 m/s on a copper surface, the maximum spreading factors were 5.38, 4.85, and 4.76 for copper surfaces maintained at 20, -10 and -20°C, respectively. This trend of decreasing S.F.$_{max}$ with decreases in impact surface temperature was observed for all of the remaining tests using distilled water. For 1.5 mm drops on copper the S.F.$_{max}$ decreased

TABLE 4.1 Maximum spreading factor based on surface energy of a disk of uniform thickness, as calculated from Equation 4.4.

Drop Diameter D_d (mm)	Impact Velocity V_{im} (m/s)	Spreading Diameter D_s (mm)	Maximum Spreading Factor $S.F._{max}$
2.4	4.8	19.2	8.0
2.0	4.7	14.64	7.32
1.5	4.4	8.76	5.84
1.1	4.0	5.05	4.59

TABLE 3.1 Effect of impact surface temperature and salinity on the maximum Spreading Factor (S.F.$_{max}$) and the corresponding time required to reach S.F.$_{max}$.

SURFACE		DROP		S.F.$_{max}$		Time to S.F.$_{max}$	
Material	Temp. (^{o}C)	Diameter (mm)	Impact Velocity (m/s)	Distilled	Salt	Distilled (ms)	Salt (ms)
Copper	20	2.4	4.8	5.38	5.38	2.33	2.33
	-10	2.4	4.8	4.85	5.13	2.00	2.00
	-20	2.4	4.8	4.76	5.00	1.33	1.67
	20	1.5	4.4	4.93	4.93	1.20	1.20
	-10	1.5	4.4	4.85	4.69	1.33	1.00
	-20	1.5	4.4	4.12	4.57	0.91	1.00
	20	1.1	4.0	3.91	3.91	0.83	0.83
	-10	1.1	4.0	3.80	—	1.50	—
S.S. 304	-10	2.4	4.8	4.85	4.86	1.55	2.00
	-20	2.4	4.8	4.31	4.86	1.33	2.00
	-10	1.5	4.4	4.49	4.42	1.17	2.00
	-20	1.5	4.4	4.37	4.11	1.16	1.17
Ice	-10	2.4	4.8	5.00	5.40	2.33	2.44
	-20	2.4	4.8	5.15	5.60	1.67	2.33

from 4.93 to 4.85 to 4.12 as the surface temperature was lowered from 20 to -10 to -20^{o}C respectively. Similarly for the 1.1 mm drops the S.F.$_{max}$ decreased from 3.91 to 3.80 as the temperature went from 20 to -10^{o}C. For the saline water drops this trend was still evident; however, the reduction in S.F.$_{max}$ was in general not as large. For the 2.4 mm drops (V_{im} =4.8 m/s) S.F.$_{max}$ decreased from 5.38 to 5.13 to 5.00 and 4.93 to 4.69 to 4.57 for 1.5 mm drops. This may be explained by a simple freezing point depression which allows the drops to attain a slightly larger size before "freezing" becomes a factor.

The effect of surface roughness on S.F.$_{max}$ is illustrated in Table 3.1 through the comparison of the results for the stainless steel surface (e = 2.5 μm) to the copper surface (e = 1.0 μm). For all the drops frozen on the copper plates the S.F.$_{max}$ was always greater than or equal to those freezing on stainless steel. For S.S. 304 the surface roughness resulted in a decrease of 10% in S.F.$_{max}$. Based on the thermal conductivities of the surfaces, if the surfaces had the same roughness the drops would have "frozen" more quickly on the copper surface (i.e. S.F.$_{max}$). Thus the actual decrease in S.F.$_{max}$ due solely to roughness is slightly larger.

The largest S.F.$_{max}$ was obtained for drops freezing on ice surfaces. For a -10^{o}C surface the S.F.$_{max}$ was 5.0 for distilled and 5.4 for 2.4 mm diameter salt water drops and at -20^{o}C, 5.15 and 5.60 respectively. There is some doubt as to the reliability of these results since it was difficult to distinguish the "edge" of a freezing disk of water on an ice surface from the "images" produced by a high speed video system. Another difficulty with the ice surfaces was ensuring that they maintained the same "roughness" for all tests.

In summary, $S.F._{max}$ decreased as temperature decreased, increased with salinity, and decreased with increased roughness. However, in general a decrease in $S.F._{max}$ implied a decrease in the time required to reach $S.F._{max}$. This suggests most of the spreading up to $S.F._{max}$ had occurred prior to any "freezing" (i.e. freezing and spreading processes occur under different time scales).

4.2.2 Initial Spreading Speed

The effect of salinity (S=0 for distilled water) and surface temperature on the initial spreading rate is summarized in Table 3.2. The initial spreading rate is defined as the average spreading speed from the time of impact to the time t_{drop}; where t_{drop} is defined as the drop diameter divided by the impact velocity. Lowering the surface temperature from -10 to -20°C appears to have little effect on this initial spreading rate. For a 2.4 mm distilled water drop freezing on a copper surface the ratio of the spreading to the impact speed (V_s/V_{im}) was 1.78 on the -10°C surface and 1.86 for a -20°C surface, and 1.77 and 1.87 respectively for salt water drops. The

TABLE 3.2 The effect of salinity and impact surface temperature on the initial spreading rate* of water drops on cold dry surfaces (* - average rate until time $t = D_d/V_{im}$).

SURFACE		DROP		Initial Spreading rate/ Impact Velocity	
Material	Temp. (°C)	Diameter (mm)	Impact Velocity (m/s)	Distilled	Salt
Copper	20	2.4	4.8	1.81	——
	20	1.5	4.4	1.71	——
	20	1.1	4.0	1.16	——
	-10	2.4	4.8	1.78	1.77
	-10	1.5	4.4	1.22	1.70
	-10	1.1	4.0	0.89	——
	-20	2.4	4.8	1.86	1.87
	-20	1.5	4.4	1.19	1.47
S.S. 304	-10	2.4	4.8	1.75	1.66
	-20	2.4	4.8	1.65	1.57
	-20	1.5	4.4	1.46	1.71

remaining results verify this trend, suggesting that very little heat transfer (freezing) occurs during the initial spreading of either salt or distilled water drops.

An understanding of this initial rate of spreading can help put the reduction in $S.F._{max}$, as a result of heat transfer (freezing), into perspective. When the drop first impacts on the surface the initial spreading speed will be greater than the impact speed (Table 3.2). However, this initial spreading is followed by a sharp decline in the spreading rate up to $S.F._{max}$. This is illustrated in Figures 3.3 and 3.4 by the initially large slope of S.F. verses time curves follow by a much smaller slope. It is during this "slower" portion of the spreading that the freezing begins to affect the spreading drop.

4.2.3 Final Size

In terms of modelling ice accretions the final size of the spread-out drop is of more significance than the maximum size ($S.F._{max}$), although they may not be much different. It is ultimately the size of the spread-out drop that is going to determine the heat transfer rate from the drop (i.e. "freeze" the drop and cool it to the impact surface temperature). Figures 3.5 through 3.7 show the final size ($S.F._{final}$) for drops freezing on cold dry surfaces as a function of Impact Weber number (12 times the non-dimensional ratio of inertial to surface tension forces). The figures plot the spreading factor as a

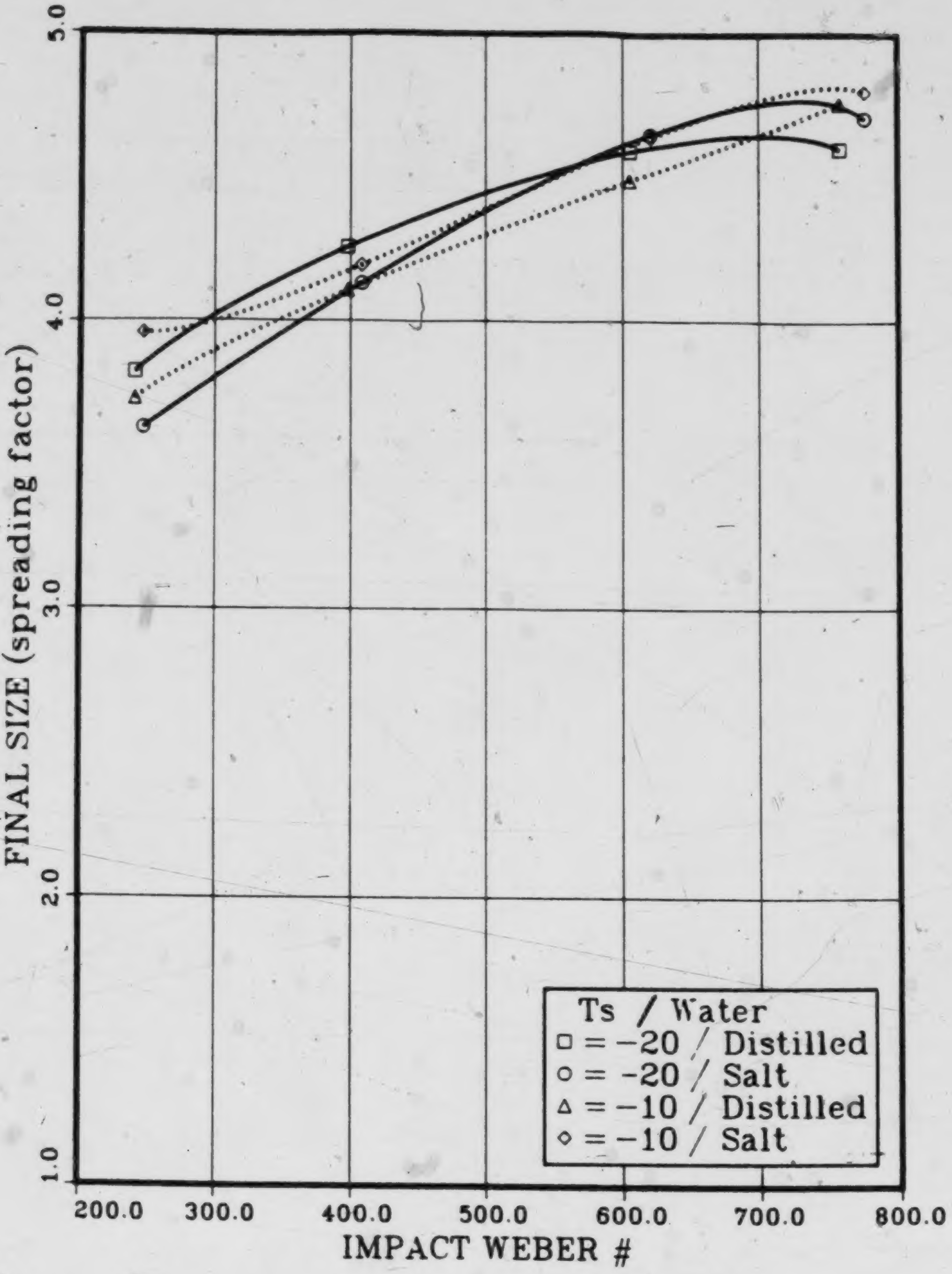

FIGURE 3.5 Final size (S.F.) verses Impact Weber # for distilled and salt waterdrops spreading on -20 and -10°C ice surfaces (T_{air}=T_s=temp. of ice surface and T_{drop}=1°C).

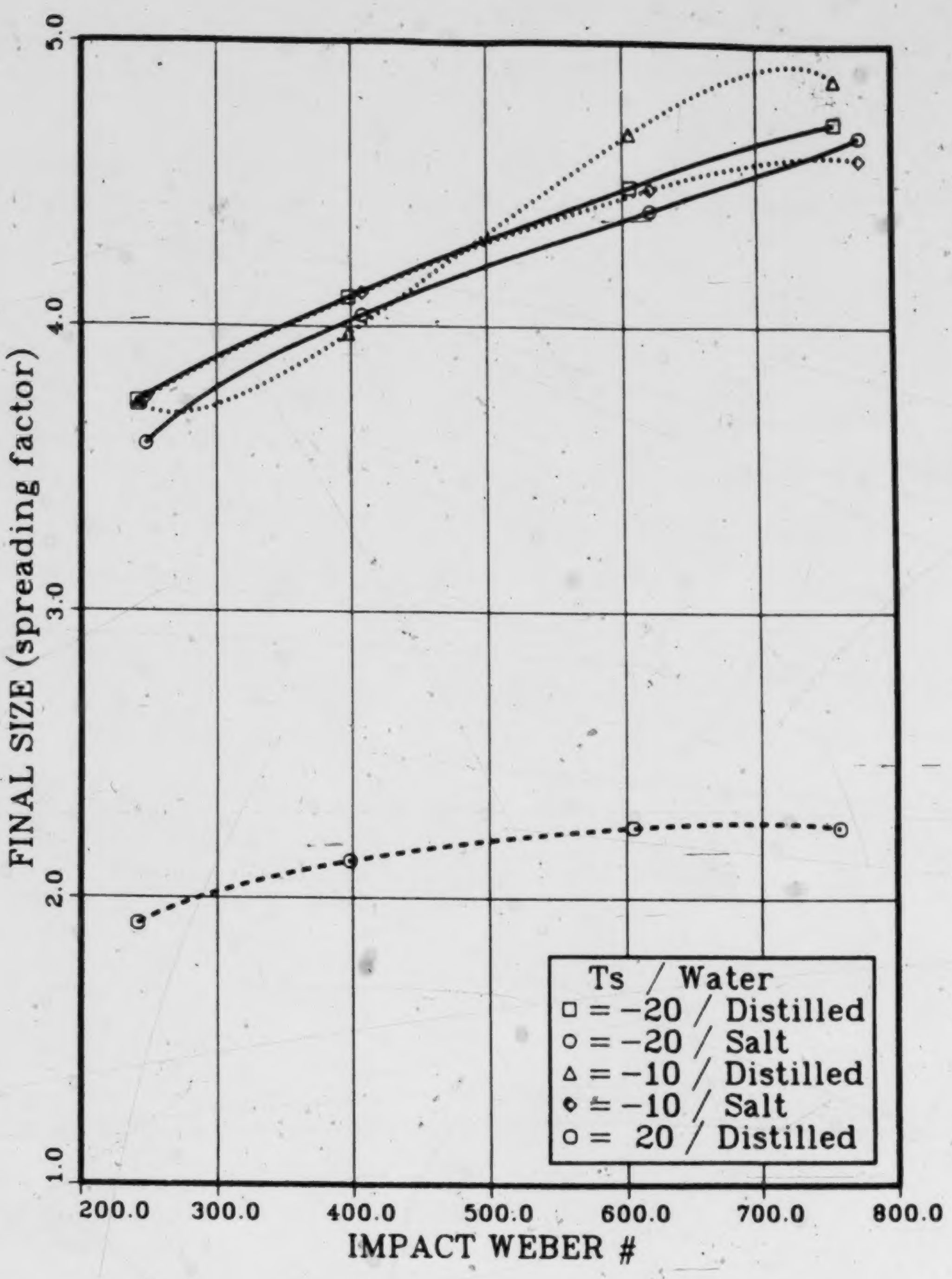

FIGURE 3.6 Final size (S.F.) verses Impact Weber # for distilled and salt waterdrops spreading on 20, -10 and -20°C copper surfaces ($T_{air}=T_s=$ temp. of copper surface and $T_{drop}=1^{\circ}C$).

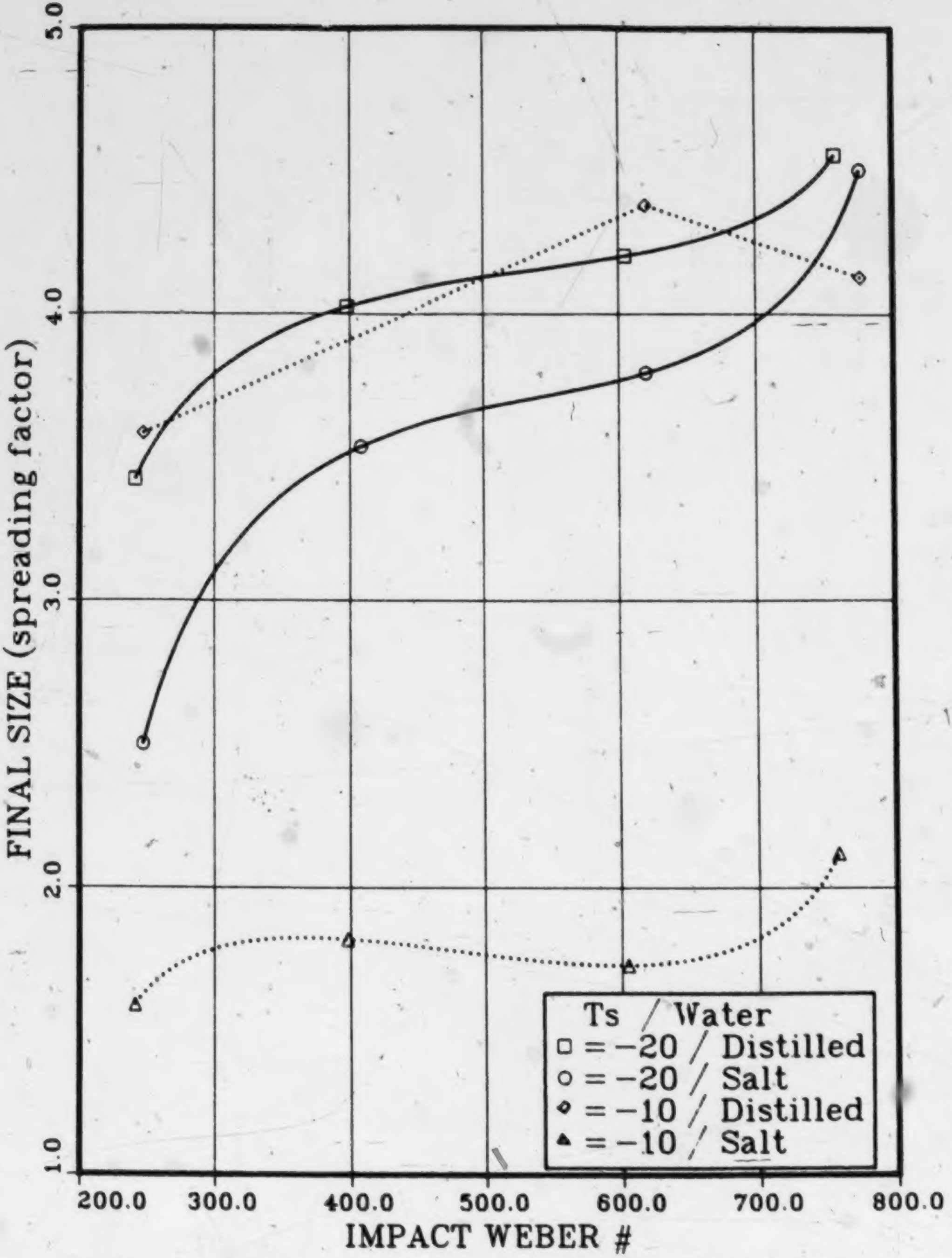

FIGURE 3.7 Final size (~~S.F.~~) verses Impact Weber # for distilled and salt waterdrops spreading on -20 and -10°C stainless steel 304 surfaces ($T_{air}=T_s=$ temp. of surface and $T_{drop}=1^{\circ}C$).

function of salinity, surface temperature and surface material (i.e. ice, copper and stainless steel surfaces).

Figure 3.5 shows the variation in final size for drops freezing on ice surfaces at temperatures of -10 and -20°C. The curves indicate that changing the surface temperature from -10 to -20°C or adding salt, have little or no effect on the final size attained by drops freezing on the ice layer. This is evidenced by the fact that for any Impact Weber Number the variation in the final size with surface temperature was never larger than 10%. The Impact Weber Numbers represent drops 1.1, 1.5, 2.0 and 2.4 mm in diameter impacting on the ice at 4.0, 4.4, 4.7 and 4.8 m/s.

The above results may be partially explained by the observations of freezing drops from the high-speed video tests. After reaching the maximum spreading factor the flattened drop with its thickened "ring" begins to contract relatively slowly. Apon reaching the final size, the outer circumference of the "ring" stops contracting while the inner circumference continues to contract as the ring flattens, this continues until the disk is completely frozen. At this point the disk has a relatively uniform thickness except for a small depression in the center (i.e. inner circumference of the "ring"). This "depression" is illustrated in Plates 3.3 and 3.4 for drops freezing on copper and ice surfaces respectively. During this time the outer diameter, representing the final size, does not change. The final size of the inner ring or depression was generally dependent on the impact surface temperature and thermal conductivity (k). Basically, if the surface temperature was increased or the thermal conductivity lowered, the inner circumference of the "ring" decreased.

In the determination of the final size of the frozen disks (drops), the depression in the center of the disk was not considered because generally the diameter of the depression was less than 1/5 th the disk diameter. This implies the depression covered less than 4 % of its area therefore, the spread-out "disk" was assumed to be of uniform thickness through its cross-section.

Similarly Figure 3.6 shows the final size attained by drops freezing on a cold dry copper surface. Once again salinity or a change in surface temperature (-10 to -20°C) had little effect on the final size of the frozen "disks". The final size in terms of spreading factors varied from 3.7 to 4.9 for distilled water and 3.5 to 4.8 for salt water over Impact Weber Numbers ranging from 240 to 780.

The curve representive of the final size attained by an unfrozen drop (on a warm copper surface) has also been shown on the figure for illustrative purposes. As illustrated, drops which spread out on warm smooth surfaces usually attain a final size (i.e. spreading factor) of approximately two, regardless of the Impact

Weber Number. It is also interesting to note that the final sizes attained by freezing drops on ice and copper were virtually the same.

Figure 3.7 shows the effect of salinity, surface temperature and roughness on the final size attained by drops spreading and freezing a cold stainless steel plate. The stainless steel plate was tested as supplied by the manufacturer, with the surface having a unidirectional series of parallel "lines" or scratches. This pattern corresponded to a centreline average roughness of 2.5 μm, compared to the copper plate with an average roughness of 1 μm (see Section 2.3). Figure 3.7 suggests that the roughness enhances the effect of salinity in terms of the final size. For a surface temperature of -20°C the addition of salt resulted in a 10 - 15% reduction in the final size attained by the frozen drops. The difference becomes more pronounced as the Impact Weber Number decreases (i.e. smaller drop diameter and impact velocity). The effect of roughness becomes even more apparent if the surface temperature is lowered to -10°C. For distilled water, freezing on a -10°C surface, the final size in terms of the spreading factor varies from 3.5 to 4.0 while the addition of the salt reduces the final size by 50 %. Indeed the salt water drops on the -10°C stainless steel surface froze in shape and size more typical of the equilibrium shape of a drop spreading on a warm surface. It appears as if the combined effect of freezing point depression and surface roughness "slowed" the freezing rate enough to allow the drop to "contract" to its final size of approximately 2. The "slowing" of the freezing rate may be explained by the poor thermal contact that can exist between a freezing drop and a conducting surface (i.e. a layer of trapped air), as a result of the roughness.

The experimental tests also showed that it was possible for the salt water drops to freeze in a spread-out shape (i.e. "disk" of uniform thickness) with spreading factors of approximately 4, even at -10^{o}C. However, the majority (≈80%) of the drops had the final sizes as indicated in Figure 3.7. Therefore, the drops with final sizes of approximately 4 were not illustrated in the figure. As well, it is interesting to note that the drops were elongated in the direction parallel to the "scratches" (surface roughness), giving the drops a somewhat elliptical final shape.

4.3 Freezing and Cooling Times

4.3.1 Introduction

Macklin (1962) examined the freezing of single supercooled drops on a cold ice layer and determined there were three stages related to the freezing and cooling of a spreading drop. The first stage is the initial freezing with a corresponding initial freezing time t_i. The time t_i

is the time required to freeze a specific portion (mass) of the spread-out drop. In Macklin's work the drops were supercooled when they arrived at the surface and the energy associated with this supercooling, the specific heat capacity of water times the degree of supercooling ($c_w (T_d - T_m)$) divided by the latent heat of fusion (L_f) determines the mass of the drop that will freeze during t_i. The time t_i is then calculated as the time required for the ice to grow in the above mass as per icing growth rates in bulk supercooled water.

The remainder of the unfrozen drop would then be at the melting temperature (T_m) of the water (i.e. 0°C for distilled water). The second stage of the freezing process corresponds to the subsequent freezing time t_f, which is the time required to remove the latent heat of fusion of the remainder of the unfrozen drop. The third stage coincides with the cooling of the drop and the surface to the initial surface temperature and is referred to as the cooling time t_c.

4.3.2 Measurement of the Freezing and Cooling Times

Figure 4.1 shows the theoretical interpretation of the temperature of a spreading drop freezing and cooling on a cold surface as a function of time. The drop arrives at the surface with a temperature of T_{impact}. In actual fact when the drop first "touches" the impact surface, the point of contact takes on a instanteous temperature

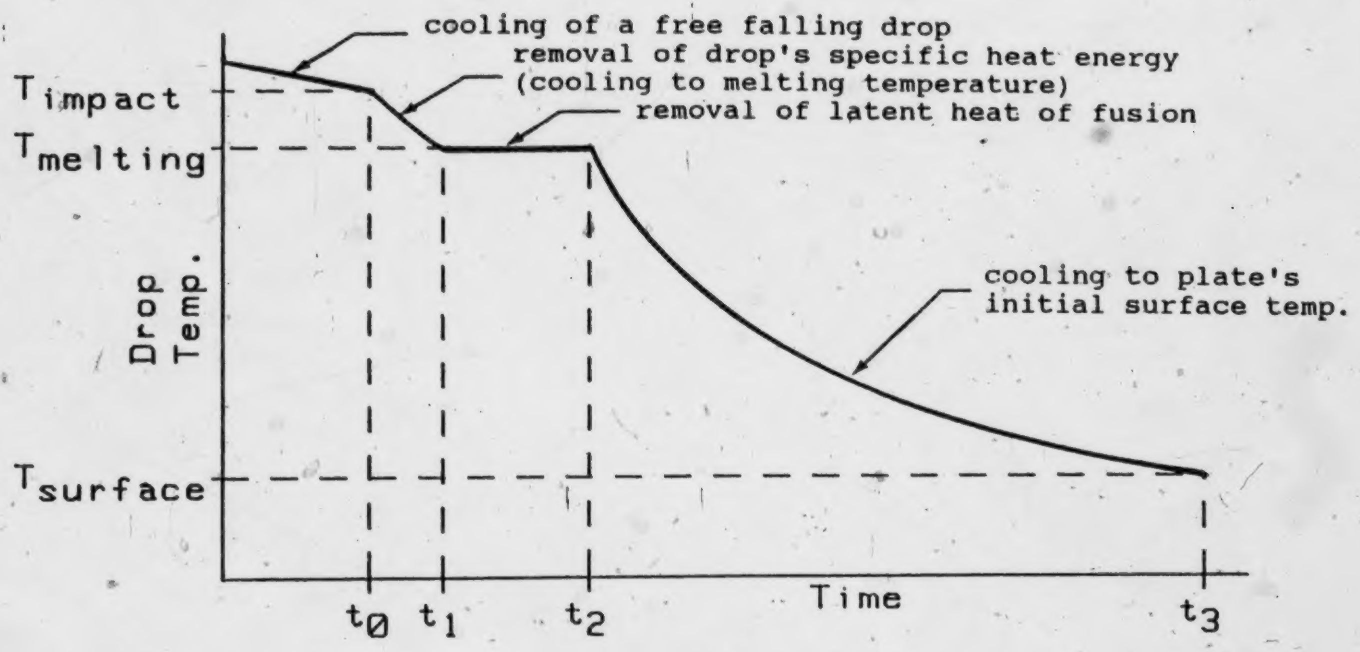

$t_i = t_1 - t_0$ = initial freezing time
$t_f = t_2 - t_1$ = subsequent freezing time
$t_c = t_3 - t_2$ = cooling time

FIGURE 4.1 Temperature of a drop (liquid layer) during freezing on a cold dry surface (theoretical).

referred to as the "contact" or "touch" temperature. The "touch" temperature is a function of the physical properties (k, ρ and c) of the drop and the impact surface. For surfaces such as copper with its large thermal conductivity, the touch temperature is essentially equal to the temperature of the copper surface (for a -20°C copper plate and a 1°C drop the touch temperature is equal to -19.963°C). However, give the relatively large size of the drops used for this study the bulk of the drop would remain at its impact temperature. Therefore, the effect of the touch temperature was ignored for the present study.

After the drop impacts on the surface it begins to cool towards its melting temperature T_m as the sensible heat is removed by conduction into the surface (or warms to T_m if the drop is supercooled). The time required to remove the sensible heat from the drop is referred to as the initial freezing time t_i. In the next stage the drop's latent heat of fusion is transferred with the drop maintained at T_m. The time required for this to take place corresponds to t_f, the subsequent freezing time. The drop is now frozen and both the drop and the impact surface are cooled to T_s, the initial surface temperature. This final stage corresponds to t_c, the cooling time.

Since it is not possible to directly measure the temperature of a drop while it is spreading and freezing on a surface, it suffices to measure the temperature of the impact surface. Figure 4.2 plots the impact surface temperature as a function of time, as a drop freezes and cools on its surface. The thicker line on the figure represents the theoretically determined surface temperature. The thinner line corresponds to the expected temperature as measured by a surface mounted thermocouple.

For the the theoretical curve, the surface starts with its initial temperature T_s, prior to the impact of the drop. As noted previously the temperature at the point of contact (i.e. "touch" temperature) is essentially equal to the temperature of the surface prior to impact. After the drop impacts on the surface, the surface temperature rises towards T_m as the drop's sensible heat flows into the surface. The drop's latent heat of fusion is then removed with the surface at T_m. Once the drop is frozen (i.e. latent heat has been removed) the drop and the surface cool to T_s, the initial surface temperature. However, partially as a result of the time lag in the thermocouple response, the measured surface temperature would be similar to the thinner line illustrated in Figure 4.2. This type of response is illustrated in Figure 3.8, for a drop freezing and cooling on a plexiglass surface.

4.3.3 Drops Freezing on Plexiglass

The surface mounted thermocouples used in the present study to measure impact surface temperatures had time constants on the order of 100 ms. In order to use the

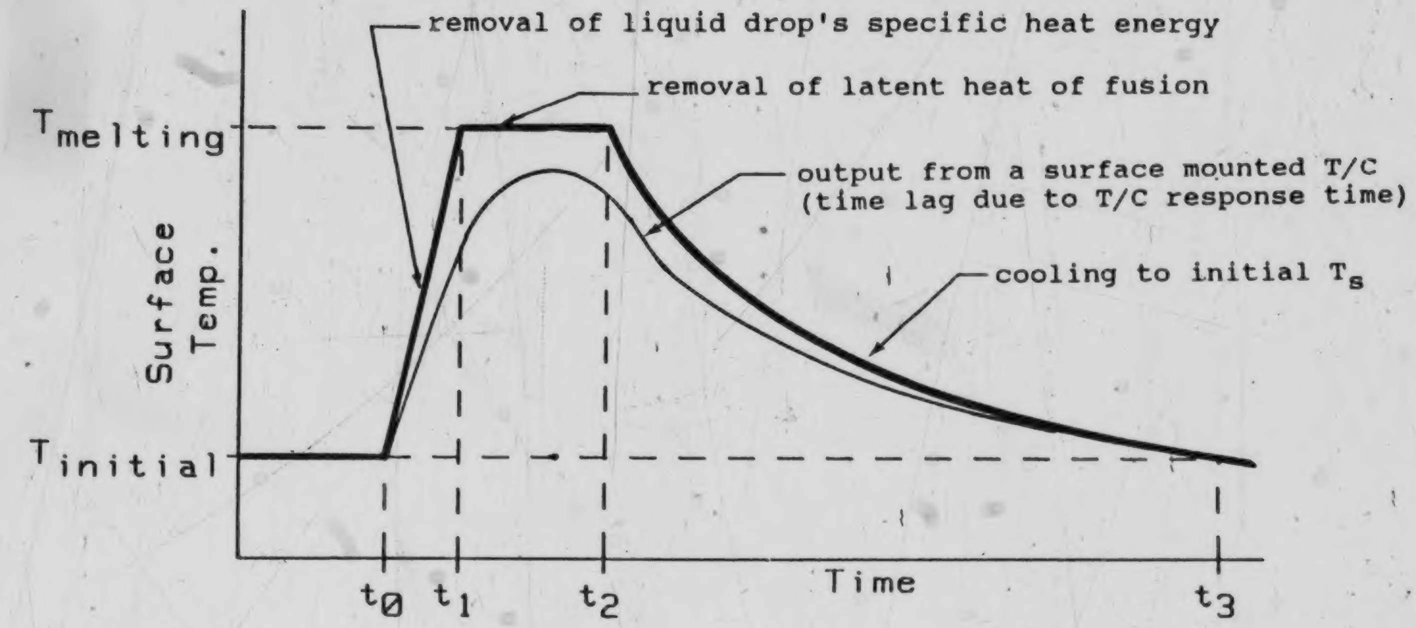
removal of liquid drop's specific heat energy
removal of latent heat of fusion
$T_{melting}$
output from a surface mounted T/C (time lag due to T/C response time)
Surface Temp.
cooling to initial T_s
$T_{initial}$
t_0
t_1
t_2
Time
t_3

FIGURE 4.2 The Surface Temperature of the impact plate as a function of time, during the freezing and cooling of a layer of water on the plate's surface (assumed profile).

previously described method to determine the time required for a drop to freeze on a surface (i.e. t_f), the freezing time would have had to be much larger than the thermocouple response time. Plexiglass's relatively low thermal conductivity ($k = 0.376$ w/m·°C) is well suited for this purpose.

Figure 3.8 shows the temperature-time curve for a single 2.55 mm diameter distilled water drop freezing on a -10 °C rough plexiglass plate. The drop impacted on the plate at 4.3 m/s and froze as a disk with a uniform thickness ($S.F._{final} = 4.5$). The figure shows the rapid rise in the surface temperature as the drop with an initial temperature of 4°C, cools to 0°C (i.e. melting temperature). This stage is followed by the subsequent freezing (removal of the latent heat of fusion), with the plexiglass at -1.4°C. As indicated in the figure it took 9.3 seconds for the drop to freeze (i.e. t_i+t_f). The drop and the surface temperature were returned to -10°C after 147 seconds (t_c). Note that this test was performed under forced convection conditions while all of the remaining experimental tests were performed under free convection conditions ($h=4.5$ W/m^2·°C; Holman, 1981).

As indicated in Table 2.9, the drops used in the present study did not arrive at the surface with any degree of supercooling. In this case, the initial freezing time t_i, as defined by Macklin (1962) cannot be determined. Therefore, the sum of the time required to

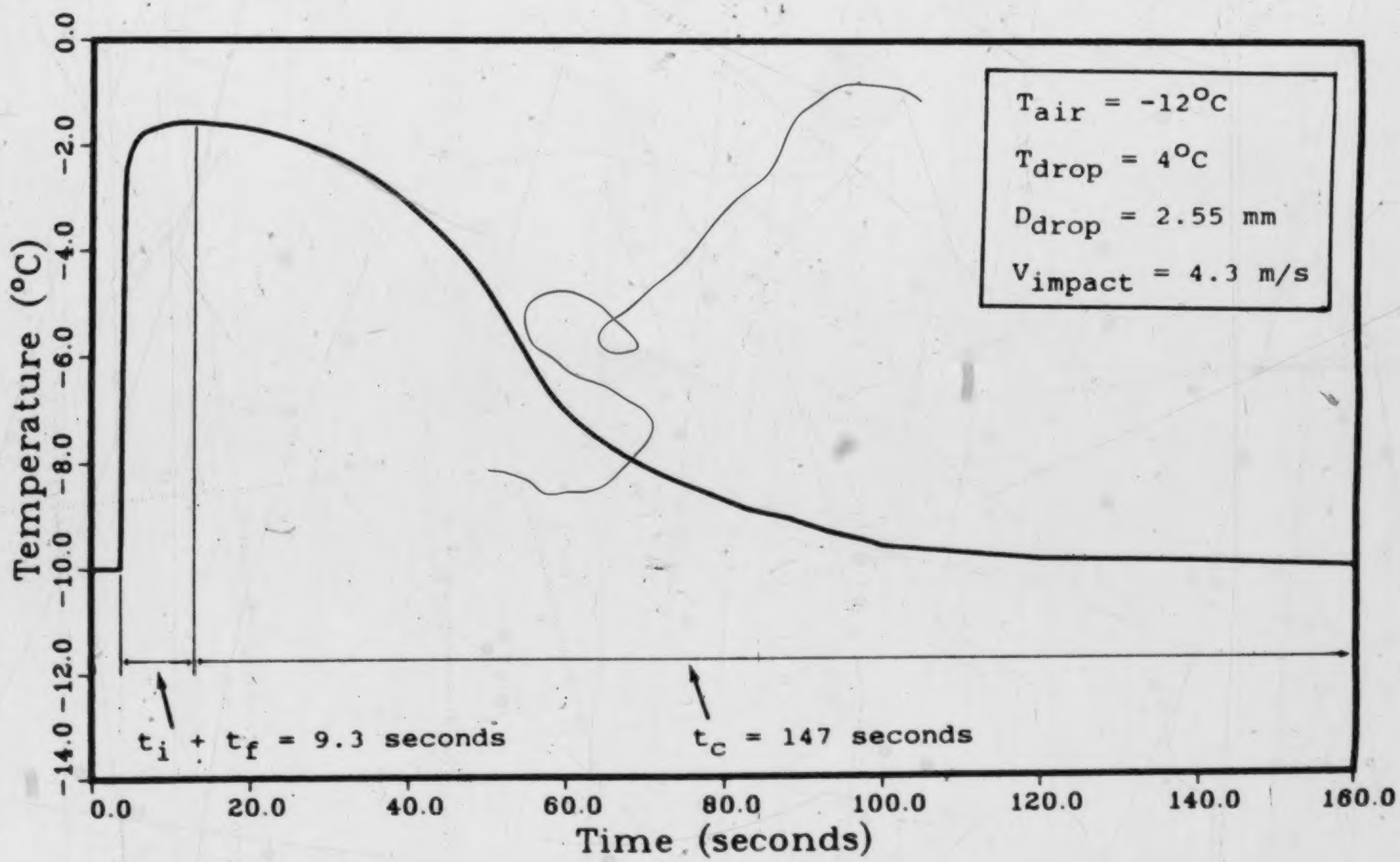

FIGURE 3.8 Freezing of a spread out (S.F. = 4.5) fresh water drop on a -10^{o}C plexiglass plate (temperature recorded from a surface mounted thermocouple).

remove the specific heat (cool drop from T_d to T_m) then freeze the disk or spread out drop (i.e. remove the latent heat of fusion) will be referred as the freezing time t_f for the remainder of this study.

4.3.4 Freezing Time

Figure 3.8 provided an illustrative perspective of the freezing of a single drop on a cold dry surface. However, as a result of the much larger thermal conductivities of most of the impact surfaces used in this study, the above method did not prove successful in determining the freezing time, although as will be shown later the method was useful in determining the total time $t_T = t_i + t_f + t_c$.

The primary purpose of this experimental study was to examine the physics of the spreading and freezing of large drops on cold dry surfaces. In particular, the freezing as a result of conduction into the surface. As a result the majority of the experimental tests were performed under free convection conditions ($h=4.5\ W/m^2 \cdot {}^oC$). Considering the relatively large thermal conductivities of the tested surfaces (i.e. copper, stainless steel), the convective heat flux was assumed insignificant. Under these conditions it is possible to estimate the freezing time t_f, by assuming one dimensional (linear) heat flow into the plane surface of a semi-infinite solid.

4.3.4.1 Freezing Time - Semi-Infinite Solid Solution

As illustrated previously, during the initial stage of the freezing and cooling process the temperature of the impact surface will rise quickly to the drop's melting temperature as the drop's sensible heat is transferred to the surface. By assuming that the surface temperature rises "instanteously" to T_m, the solution to the transient heat flow problem in a semi-infinite solid, provides an estimate of the freezing time. The solution for this transient heat flow problem in a semi-infinite solid is given by Holman (1981); in particular the surface heat flow per unit area (q_o) is given by:

$$q_o = \frac{Q_o}{A} = \frac{k_s\ (T_s - T_i)}{(\pi\ \alpha\ t)^{1/2}} \tag{4.5}$$

where

k_s = thermal conductivity of surface (W/m·°C)

T_s = initial surface temperature (°C)

T_i = temperature that surface is suddenly raised to (i.e. T_m in this case) (°C)

α = thermal diffusivity = $k_s/(\rho_s\ c_s)$

t = time (ms)

c_s = specific heat capacity of the surface (kJ/kg·°C)

ρ_s = density of the surface material (kg/m^3)

The drop was assumed to freeze as a "disk" of uniform thickness, where the thickness was based on the final size

($S.F._{final}$) of the frozen drops (i.e. Figures 3.5, 3.6 and 3.7). Table 4.2 summarizes the thickness (δR) of the "disk" as a function of drop diameters and impact speeds. The total heat (Q_d) to be removed from the freezing drop is equal to the mass of the drop times latent heat of fusion (L_f), less any heat associated with the drop's initial supercooling (i.e. $c_w (T_d - T_m)$) divided by the area of the "disk" and is given by;

$$q_d = \frac{Q_d}{A} = \rho_w \, \delta R \, [l_f + c_w (T_d - T_m)] \qquad (4.6)$$

where

δR = thickness of the disk of water (μm)

l_f = latent heat of fusion (kJ/kg)

Integrating Equation 4.5 with respect to time yields the total energy removed from the surface of the semi-infinite solid per unit time per unit area. Substituting Equation 4.6 into this result and solving for time gives the freezing time t_f:

$$t_f = \frac{\pi \rho_w^2 \, \delta R^2 \, (l_f + c_w [Td - T_m])^2}{4 \rho_s C_s V^2 k_s} \qquad (4.7)$$

where

ρ_s = density of surface material (kg/m^3)

C_s = specific heat of surface material (kJ/kg$\cdot$$^{\circ}$C)

V = temperature of surface - melting temperature

= $T_s - T_m$ ($^{\circ}$C)

TABLE 4.2 Thickness of spread out drops (i.e. disk of uniform thickness).

D_d Drop Diameter (mm)	V_d Impact Velocity (m/s)	S.F. Spreading Factor (D_s/D_d)	δR Thickness (μm)
2.4	4.8	5.0	65
2.0	4.7	4.75	59
1.5	4.4	4.6	47
1.1	4.0	4.2	42

Although this result is valid for the linear flow of heat in a semi-infinite solid, Macklin (1962) came up with the same solution for a thin layer of water freezing on a large ice sphere by assuming the flow of heat to be one dimensional towards the center of the sphere.

The freezing times estimated from Equation 4.7, correspond strictly to the time required to transfer the latent heat of fusion and any sensible heat from the drop to the surface, without any consideration for the growth of ice in the freezing disk.

4.3.4.2 Freezing Time - Kinetic Growth

Equation 4.7 estimates t_f assuming the drop is a uniformly thick disk where the heat transfer rate is based strictly on the solution of the transient heat flow in a semi-infinite solid. However, this freezing time ignores the kinetics of the ice growth. If a drop freezes on the surface of a material with a large thermal conductivity (greater than that of ice) the ice can be assumed to "grow" from the impact surface up through the "disk" of water. Under this condition the growth of ice or heat transfer rate is controlled by the conductive heat transfer rate through the growing ice layer.

In order to include the kinetics of ice growth, in estimating the freezing time, the drop was again assumed to freeze as a "disk" of uniform thickness (see Table 4.2) The drop was also assumed to freeze at T_m (i.e. 0^oC for distilled water, -1.9°C for salt water). The time required to cool the drop from T_d to T_m is first obtained using Equation 4.7. Since as noted previously the convective heat flux is insignificant with respect to conduction into the surface, the heat transfer is assumed to occur only by one dimensional conduction into the surface.

The rate of growth of the ice layer (i.e. ice is assumed to grow from cold surface up through the thickness of the "disk") is given by:

$$G_i = \rho_w \, l_f \, A \, dy/dt \tag{4.8}$$

while the rate of heat transfer through the ice layer by conduction is given by:

$$Q = k_{ice} \, (T_s - T_m)/y(t) = G_i/A \tag{4.9}$$

where

$y(t)$ = thickness of ice layer (μm)

k_{ice} = thermal conductivity of ice (W/m·°C)

A = area of disk in contact with surface (mm^2)

T_s = initial surface temperature (°C)

T_m = melting temperature (°C)

Substituting Equation 4.9 into 4.8 and integrating t from 0 to t_f and y between 0 and δR (i.e. thickness of the "disk") gives the freezing time as:

$$t_f = \frac{\rho_w \; l_f \; \delta R^2}{k_{ice} \; (T_s - T_m)} \qquad (4.10)$$

Equation 4.10 indicates that t_f is not a function of the surface properties and assumes no specific heat effects in the growing ice layer. Table 4.3 shows the freezing times calculated from Equation 4.10 and the freezing times including heat transfer by free-convection along with Equation 4.10. The freezing times including the heat transfer by free-convection reduced the freezing time by less than 0.02%, thus strengthening the assumption that the convective heat transfer was insignificant in terms of calculating the freezing time.

Table 4.4 summarizes the freezing times as calculated from equations 4.7 and 4.10. Also included in the table are the experimentally determined freezing times. The experimental freezing times were determined by observations made from the photographic and high speed video results used in recording the spreading of drops on cold dry surfaces. The freezing time was the time required for the drop to complete its spreading (i.e. no change in size for the spreading drop).

4.4 Discussion of Results - Freezing Time

As explained previously when drops spread and freeze on a cold surface they spread quickly to S.F.$_{max}$; where they are essentially a uniform thick disk with a thicker

TABLE 4.3 Comparison of freezing time t_f including the effect of convective heat transfer from the spread out drop surface as determined from Equation 4.10.

SURFACE		Thickness of spread out drop δR^1 (μm)	FREEZING TIME t_f (ms)		
Material	Temp. (^{o}C)		Eq. 4.10	Eq. 4.10 + convective heat loss to air	% Diff.
Copper	-20	65	12.8604	12.8621	0.013
	-20	47	6.7239	6.7246	0.010
	-20	42	5.3694	5.3699	0.009
	-10	65	25.7208	25.7242	0.013
	-10	47	13.4478	13.4491	0.010
	-10	42	10.7388	10.7397	0.009

1 - see Table 4.2

TABLE 4.4 Calculated and measured freezing times for salt and distilled water drops spreading on cold dry surfaces.

SURFACE Material	SURFACE Temp. (^oC)	Thickness of spread out drop δR^4 (μm)	FREEZING TIME t_f (ms) Eq. 4.7 Dis[1]	FREEZING TIME t_f (ms) Eq. 4.7 Salt[2]	FREEZING TIME t_f (ms) Eq. 4.10 Dis[1]	FREEZING TIME t_f (ms) Eq. 4.10 Salt[2]	FREEZING TIME t_f (ms) Measured Dis[1]	FREEZING TIME t_f (ms) Measured Salt[2]
Copper	-10	65	3.25	5.31	25.7	26.6	16.0	14.0
	-10	47	1.70	2.77	13.4	13.9	8.0	6.0
	-10	42	1.36	2.22	10.7	11.1	—	—
	-20	65	0.81	1.06	12.9	13.2	14.0	13.0
	-20	47	0.43	0.55	6.7	6.9	6.0	4.0
S.S. 304	-10	65	5.92	9.67	25.7	26.6	17.0	13.0
	-10	47	3.09	5.05	13.4	13.9	13.0	11.0
	-20	65	1.48	1.93	12.9	13.2	10.0	12.0
	-20	47	0.78	1.00	6.7	6.9	6.0	6.0
Ice	-10	65	829	1355	—	—	—	—
	-20	47	434	707	—	—	—	—
Plexiglass	-10	84	10380	—	—	—	9300[3]	—

1 - Distilled water (S=0 g/kg) 2 - Salinity = S =33 g/kg.
3 - determined from Figure 3.8. 4 - see Table 4.2.

layer ("ring") at the leading edge. This disk then begins to contract relatively slowly in comparison to the initial spreading. The outer edge of the disk contracts a minimal amount from $S.F._{max}$ while the thickened ring flattens as the inner diameter continues to contract. It is the contraction of this inner ring which determines the measured freezing time. The drop or disk is said to be frozen when this ring is no longer contracting.

The thickness of the spread-out drops (65, 47, 42 μm) represent 2.4, 1.5 and 1.1 mm diameter drops with S.F. of 5.0 4.6 and 4.2. In terms of calculating the freezing times the drops or disk were assumed to be of uniform thickness. The melting temperatures (T_m) were 0°C for distilled and -1.9°C for salt water.

For a 2.55 mm distilled water drop (84 μm thick disk) freezing on a -11°C plexiglass plate, Equation 4.7 indicates that the freezing time should be 10.38 seconds this compares well to a time of 9.3 seconds as obtained from the surface measurement result shown in Figure 3.8. This result suggests that Equation 4.7 could be used to calculate the freezing times for drops freezing on surfaces such as plexiglass where the thermal conductivity is less than that of ice and the freezing time is significantly larger than the response time of the measuring thermocouple.

However, for drops freezing on a copper surface, Equation 4.7 under predicts the freezing time by a significant amount. For a 2.4 mm salt water drop (65 μm thick disk) freezing on a -20^{o}C copper plate Equation 4.7 calculates the freezing time as 1.06 ms (Table 4.4) while the measured value was 13.0 ms. Certainly in consideration of the spreading results, this time of just greater than 1 ms is not probable since it takes 2.5 ms for the drop just to reach $S.F._{max}$. As summarized in Table 4.4, Equation 4.7 underpredicts the measured freezing time by as much as 90%, when the drops freeze on copper or stainless steel surfaces. This suggests that the application of Equation 4.7 should not be considered in determining the freezing time of drops on surfaces with relatively large k (in comparison to ice). This is understandable since Equation 4.7 is based strictly on the heat transfer rate in a semi-infinite solid and does not take into account the limiting kinetic growth rate of the growing ice layer (i.e. it assumes the heat is removed entirely while the drop is in the liquid phase).

The measurements in Table 4.4 indicate that the freezing times for saline drops generally appear to be 10 to 15% less than the corresponding times for distilled water drops. Based strictly on a freezing point depression it would be expected that the saline drops would take longer to freeze. However the saline drops with their larger $S.F._{max}$ have a correspondingly larger "area" through which to conduct heat.

The introduction of Equation 4.10 which accounts for the rate of heat transfer through the layer of ice growing (freezing) on the surface provides better estimates of the freezing times. For drops freezing on stainless steel or copper the calulated freezing times were 10 to 50% larger than the measured times.

The measured freezing times represent the minimal value for t_f since it was assumed that the disks were frozen when they no longer change size. As well, Equation 4.10 assumes that the heat transfer rate is controlled by the growth of the ice from the time of impact. However, the initial stage of the spreading (up until the drop reaches $S.F._{max}$) suggests that the heat transfer is occurring at the impact surface liquid water interface. Assuming that any freezing (heat transfer) occurring during this stage would be more appropriate to heat transfer in a semi-infinite solid (Eq. 4.7), the calculated t_f would be reduced by approximately 15%. These results then suggest that Equation 4.10 provides a reasonable estimate for the freezing time of drops on relatively large k surfaces such as copper and stainless steel.

4.5 Total Time

In terms of modelling the ice accretion process it is more important to determine the total time t_T required to freeze the drop and cool both the drop and the surface to the initial temperature of the surface. If the subsequent drops arrive before this process is completed the temperature of the accreting surface will rise towards T_m. If this continues, the surface will become wet as all the drops cannot be frozen.

Table 3.4 shows the total time (t_T) required to freeze a drop on a cold surface and return the surface and the drop to the air or initial surface temperature. For the results shown in Table 3.4, 2.4 mm diameter salt and distilled water drops were allowed to impact (V_{im} = 4.8 m/s) and freeze on -20°C copper and stainless steel surfaces. The drops arrived at the surface with temperatures of 1 or 20°C. Due to the relatively large thermal conductivies of copper and S.S. the energy required to freeze the drop will be transferred rapidly to the surface. This energy and the energy required to cool the frozen drop (disk) is subsequently removed by convection into the air and conduction into the impact plate. For these tests a semi-infinite solid was simulated by placing the impact plates directly on the surface of a large cooling plate which provided an essentially constant heat flux.

For the drops freezing on copper, t_T ranged from 1730 to 1990 ms. Increasing the drop temperature from 1°C to 20°C, increased t_T only 5% even though this temperature increase corresponds to a 20% increase in the total energy that must be removed. This may be partially explained by the larger S.F. of the warmer drop implying a larger

TABLE 3.4 Total time t_T ($t_i + t_f + t_c$) required to freeze 2.4 mm diameter waterdrops, impacting at 4.8 m/s, then cool the impact surface to its initial temperature (i.e. t_c = time required to cool impact surface to 99% of $T_m - T_s$).

SURFACE		Drop Temp. at Impact (^oC)	Salt or Distilled Waterdrop	Total time t_T (ms)	Standard Deviation σ	Sample Size N
Material	Initial Temp-T_s (^oC)					
Copper	-20	1	d	1730	——	1
	-20	1	s	1890	150	7
	-20	20	d	1900	100	4
	-20	20	s	1990	30	2
S.S.304	-20	1	d	1840	90	3
	-20	1	s	1900	190	2
	-20	20	d	1890	130	2
	-20	20	s	2110	130	3

conductive heat transfer area. As well, the addition of salt (S=33 g/kg) resulted in a less than 5% increase in t_T. For drops freezing on the stainless steel the trends were the same except the total time was increased by approximately 5% (i.e. ranging from 1840 to 2110 ms). This is expected since the plates were cooled using an constant heat flux source (i.e. cooling plate).

4.6 Summary

The primary purpose of the present study was to examine the physical processes related to the spreading of large distilled and saline drops on cold dry surfaces. These physical processes included the heat transfer to the icing surface, and the effect of viscous dissapation and surface tension forces on the spreading process.

Through comparison to the spreading on a warm surface it was determined that the major affect of the heat transfer was that it prevented the drop from contracting by any significant amount after reaching its maximum spreading factor (i.e. size). Thus the drops used in this study generally froze as "disks" of approximately uniform thickness. By examining the initial spreading of 2.4, 1.5 and 1.1 mm drops impacting at 4.8, 4.4 and 4.0 m/s respectively, on -10° and -20°C surfaces (copper, stainless steel and ice) it was determined that the spreading up to $S.F._{max}$ and the freezing can essentially be treated as separate processes, since it took much less time for this spreading to occur.

Of particular importance to the present study was the determination of the effect of salinity (S=0 or 33 g/kg) on the spreading and freezing processes. In terms of the maximum size of the drops, the final size of the drops, the spreading rate of the drops and time required to freeze the drops, the effect of salinity was relatively insignificant and could generally be accounted for by the freezing point depression.

From the observations of single and multiple drops impacting on an initially cold surface it was determined that the conduction into the surface dominated when the surface was bare (i.e. no previous accretion),however, the conduction soon became insignificant in terms of freezing the drops, once a layer of ice had accreted. As a result it was possible for the subsequent drops to be accreted on the layer of ice and remained unfrozen.

This condition in which all the drops (mass) accreting on the surface of an icing structure cannot be frozen is typical to marine icing and is referred to as "wet" icing. Under these wet icing conditions the mass flux (impinging drops) is large enough to prevent the heat transfer at the surface of the accretion from freezing all of the previously accreted mass and maintaining the surface at its initial temperature. As a result the accretion temperature rises towards the melting temperature of the water and the subsequent mass (drops) cannot be frozen.

Once this layer of unfrozen water has accreted, any other drops impinging on the surface can result in a "splash". As a result of this splashing on the wet accretion, it is possible that some of the previously accreted water substance may be permanently lost from the accretion surface. In terms of modelling marine icing accretions it is necessary to quantify this "mass loss" to insure the accuracy of the surface heat balance calculation and ultimately the accretion rate.

CHAPTER 5

SPLASHED DROPS

5.1 Introduction

If during the accretion process a layer of water accretes on the surface of the icing structure, the icing is said to be occurring under "wet icing" conditions. Since a typical marine icing condition is generally characterized by large saline drops which are in neither kinematic or thermodynamic equilibrium with the air (Lozowski and Gates, 1985), the accretion process usually occurs under "wet icing" conditions. Under these conditions it is possible that mass (i.e. water) will be lost from the surface as a result of splashing. In terms of modelling ice accretions, this loss of mass must be accounted for when calculating the overall heat balance at the accretion surface and ultimately the accretion rate.

List (1977) has provided experimental evidence showing that under wet icing conditions, predicted icing growth rates are far less than expected. List's wind tunnel experiments involved the icing of a 2.2 cm cylinder rotating at 2 to 4 hz, with liquid water contents ranging from 0.5 to 20 gm/m^3, air speeds from 20 to 45 m/s, air densities from 0.477 to 1.005 kg/m^3 and mean volume drop diameters of 41 to 100 μm. From this wind tunnel testing, List concluded that up to 80% of the initially accreted water can bounce off or be lost by shedding from an icing cylinder, even if the air temperature was maintained at -20°C. The 80% mass loss occurred as liquid water contents approached 20 gm/m^3 and air speeds reached 45 m/s. Joe (1975) also showed that the bouncing of supercooled water droplets from an artifically growing hailstone can reduce the collision efficiency by up to 40%. Collision efficiency is defined as the fractional mass of drops in a swept-out volume, that are accreted on a surface (List, 1977).

The main deficiency with computer modelling is its lack of ability to account for the energy associated with the shed or bounced drops. List (1977) suggests that adjustments be made to the general heat-balance equation for the steady-state icing of a cylinder, to account for the loss of accreted water from the icing surface. List accomplishes this by the introduction of a net collision efficiency term in the heat-balance equation. This net collision efficiency term is defined as the fractional mass of drops in a swept-out volume that are "permanently" accreted on a surface.

5.2 Computer Trajectory Model

This portion of the present study was undertaken in order to investigate "mass loss" associated with the splashing of drops on an unfrozen accretion. If a layer of liquid water is present on the accreting surface, impinging water drops may cause "splashed" drops to be introduced back into the air flow. The "splashed" drops may or may not re-impact on the surface of the accreting structure. To determine if the drops re-impact, a computer model was developed which was capable of tracing the trajectories of the "splashed" drops under a prescribed set of conditions (parameters).

The model's input parameters included cylinder diameter D_c, freestream air velocity V_a, air temperature T_a, and drop diameter D_d, position Ang_c, Ang_d and velocity V_d of the "splashed" drops. Ang_c corresponds to the angle measured from the stagnation line along the cylinder surface. Ang_d corresponds to the angle that the splashed drop leaves the surface of the cylinder, measured relative to the normal to the cylinder surface. These parameters are illustrated pictorially in Figure 5.1.

The basic procedure used in the trajectory model was to introduce the small "splashed" drops near ($D_d/2$) the surface of the accreting cylinder with initial position and velocity vectors then calculate their resulting trajectories. For the computer model the equations of motion for a drop were formulated utilizing the velocity components derived from the theory of potential flow around a cylinder. A Runge-Kutta numerical scheme was used to calculate the position of the drops splashed from the surface of the cylinder, as a function of time (i.e. trajectories). The details of the development of the potential flow theory, as applied to flow around a

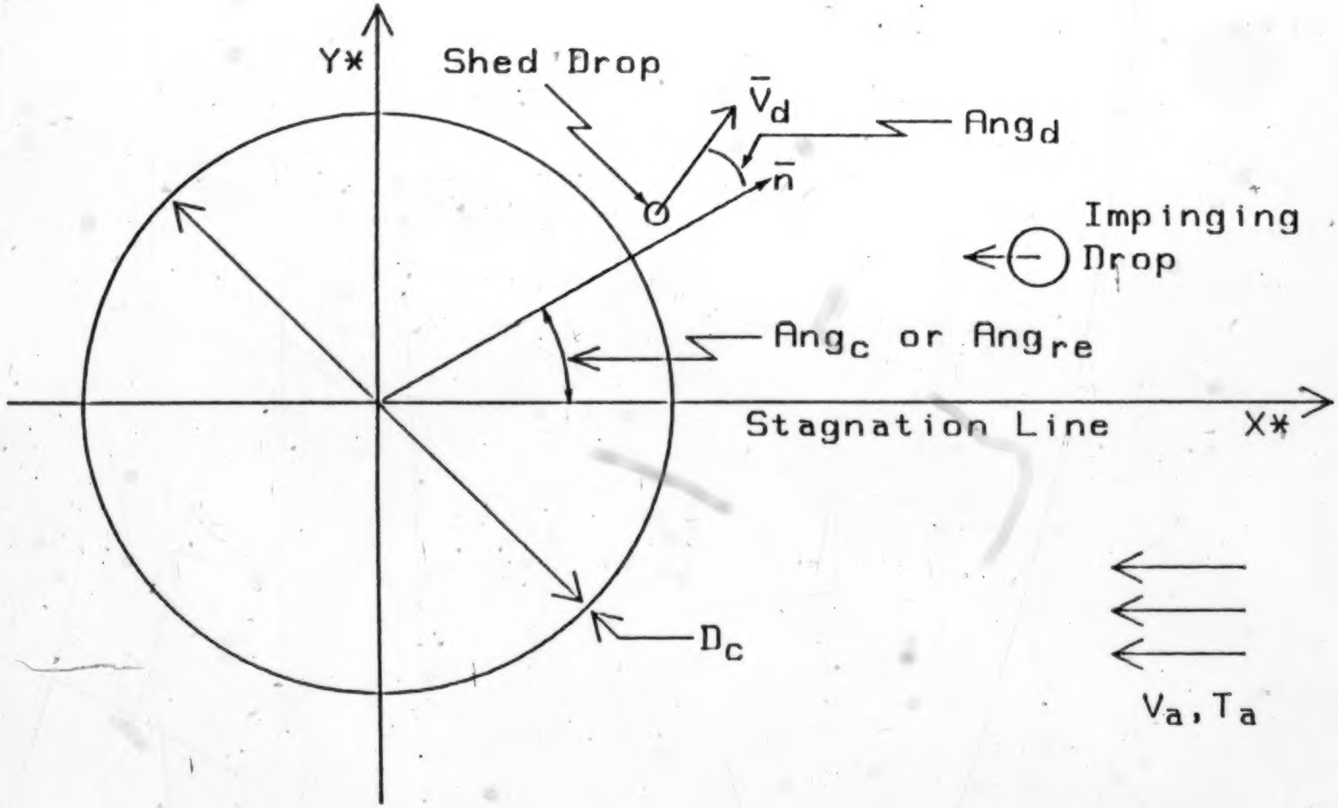
Y*
Shed Drop
$\bar{V}_d$
Ang_d
$\bar{n}$
Impinging Drop
Ang_c or Ang_{re}
Stagnation Line
X*
D_c
V_a, T_a

FIGURE 5.1 A description of the parameters used to define the trajectories of "splashed" drops.

circular cylinder, may be found in Appendix C.

The most important question to be answered through the use of the computer modelling was; Do the "splashed" drops re-impact on the accreting cylinder? In turn, what quantity of mass do the "splashed" drops which do not re-impact, represent? Knowing the temperature and the mass of the drops which do not re-impact under a given set of conditions, improvements could be made to the present icing computer models. The lost mass and its temperature would provide an additional term in formulating an overall heat transfer balance at the surface of an icing structure. However, this study was only concerned with mass represented by the "splashed" drops and not their temperature. At the present time List (Lozowski, et. al., 1983) is investigating the temperature of the mass lost from an icing cylinder under "wet" icing conditions.

5.3 Presentation of Results

In order to model the splashing on a water coated cylinder, impinging drops were assumed to produce splashed drops upon impacting on the water layer. The splashed drop trajectories were then calculated from the previously described computer model.

The range of the model parameters used was based on experimental and theoretical considerations provided by several authors. Macklin et. al (1976) and Levin et. al (1971) examined the impact of large water drops (d=2.6 mm) moving relatively slow (< 500 cm/s) on a liquid layer. Macklin determined that between 1 and 5% of the energy associated with the large drops impacting on a shallow liquid layer (depth/D_d < 0.5) may be imparted to the drops "shed" during the splashing process. From experimental tests, Levin, et. al. (1971) showed that 20 to 200% of the initial impacting drop mass may be introduced as "splashed" drops. Levin also provided experimental evidence that "splashed" drop diameters vary from 25 to 500 μm, with the majority of the shed mass represented in the 100 to 300 μm range. These results correspond to average splashed drop velocities in the 35 to 250 cm/s range.

The basic parameters use in the computer modelling and their appropriate ranges are as follows:

D_c = Cylinder Diameter = 0.1 to 1 m
V_a = Air Velocity = 5, 10, 50 m/s
T_a = Air Temperature = -15°C
D_d = Drop Diameter = 25 to 500 μm
V_d = Drop Velocity = 0.1, 1, 10 m/s
Ang_d = Drop Position from stagnation line - deg
Ang_c = Drop Velocity Vector from cylinder surface

To evaluate the effect of the basic parameters on the resulting splashed drop trajectories, each parameter was varied independently from a fixed test conditon. Namely

D_c=1 m, V_a=10 m/s, T_a= -15^oC, D_d=100 μm, Ang_c=20^o, Ang_d=90^o and V_d=2 m/s. Figures 5.2 through 5.7 show the trajectories of the "splashed" drops from their introduction at the cylinder surface until they re-impact or flow by the cylinder. The figures show half of the accreting cylinder, since the flow field is symmetrical about the stagnation line and gravitional effects were not considered. Each of the Figures 5.2 through 5.7 shows the effect of a single parameter on the drop trajectories. For each figure the parameters which are held constant and their appropriate values are noted at the top of each figure.

5.4 Discussion of Results

5.4.1 Drop Trajectories

Figure 5.2 shows the effect that Ang_c (i.e. the position angle measured from the stagnation line) has on the splashed drop trajectory. The 100 μm drops were introduced into a 10 m/s air stream with an initial velocity of 2 m/s, at angles (Ang_c) of 5, 20 and 60^o from the stagnation line. In these cases all the drops missed the cylinder, with the 5 and 20^o positioned drops missing by virtually the same distance (i.e. Y* = 0.62). Y* is the non-dimensional position of the drop measured above the cylinder's stagnation line and non-dimensionalized by the diameter of the cylinder.

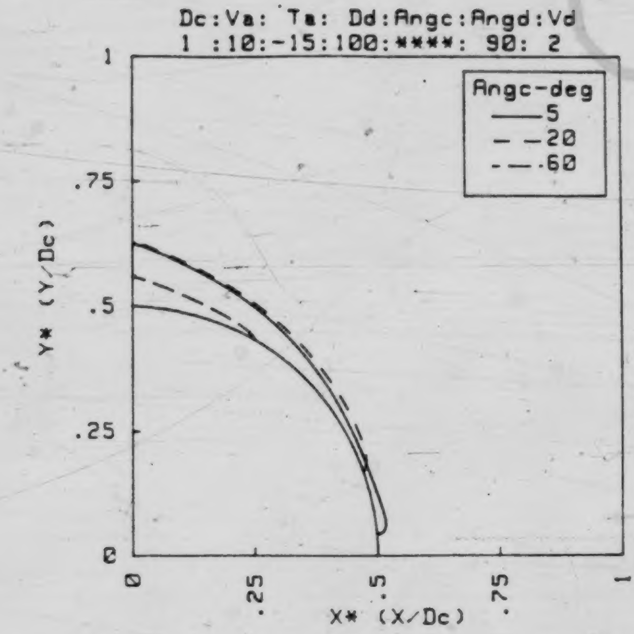

FIGURE 5.2 The effect of the initial "splashed" drop position, measured from the stagnation line on the drop trajectories (D_c=1 m, V_a=10 m/s, T_a=-15°C, D_d=100 μm, Ang_d=90°, V_d=2 m/s).

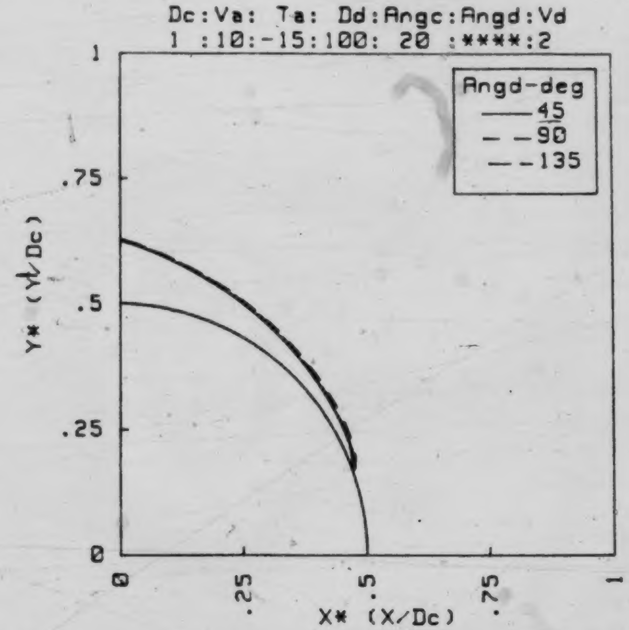

FIGURE 5.3 The effect of the initial "splashed" drop position vector (Ang_d) on the drop trajectory (D_c=1 m, V_a=10 m/s, T_a=-15°C, D_d=100 μm, Ang_c=20°, V_d=2 m/s).

For this study it was more important to determine if the drops will miss the cylinder rather than the actual distance that they miss it by. Note that a drop is said to miss the cylinder if the drop's trajectory does not carry the drop to within half its diameter from the cylinder surface, before passing the centerline of the cylinder, prescribed by $X^* = 0$ (i.e. non-dimensional X position measured from the centerline of the cylinder).

The effect of the angle at which the drop was initially shed (Ang_d) relative to the cylinder surface normal is shown in Figure 5.3. The 100 μm drops were introduced into a 10 m/s airstream with an initial velocity of 2 m/s, at 20^o from the stagnation line (Ang_c), with positions of + 45^o, -45^o and normal to the cylinder surface (Ang_d). Under these conditions all the drops failed to re-impact with the cylinder. Since all the drops follow similar trajectories, shortly after leaving the surface of the cylinder, it was determined that drop trajectories were not strongly dependent on the initial drop position vector (Ang_d).

Figure 5.4 shows the effect of the "splashed" drop diameter D_d, on its trajectory. Maintaining the initial drop velocity at 2 m/s and changing the drop diameter from 25 to 100 then 300 μm, causes the drop to miss the cylinder by increasingly larger distances. This may be expected, considering the original momentum possessed by the drops. When introduced into the flow field the larger

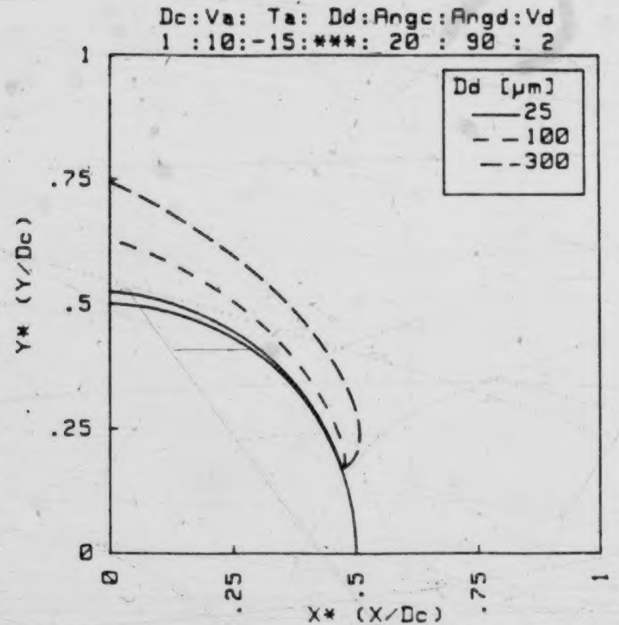

FIGURE 5.4 The effect of the "splashed" drop diameter (D_d) on the resulting drop trajectories (D_c=1 m, V_a=10 m/s, T_a=-15°C, Ang_d=90°, Ang_c=20°, V_d=2 m/s).

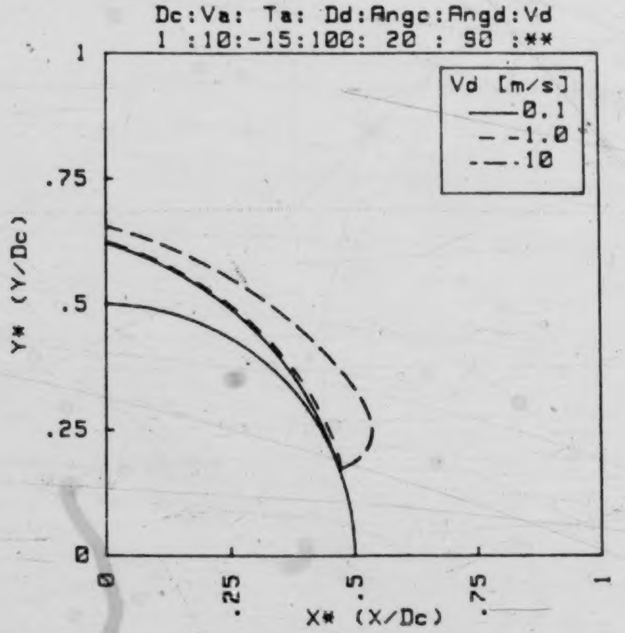

FIGURE 5.5 The effect of the initial "splashed" drop velocity (V_d) on the drop trajectories (D_c=1 m, V_a=10 m/s, T_a=-15°C, Ang_d=90°, Ang_c=20°, D_d=100 μm).

drops, having a much larger momentum, travel further away from the cylinder surface (against the flow) before their trajectories are dominated by the flow around the cylinder.

Figure 5.5 shows the effect of the drop velocity V_d (momentum) on the drop's trajectory. For $V_d = 0.1$ and 1 m/s the trajectories do not vary significantly. However, at 10 m/s the drop travels much further into the flow before the flow field can slow the outward momentum of the drop (momentum radially out from the cylinder surface). Once the drop's outward momentum has been overcome, the drop appears to follow the trajectory of a drop introduced a long way from the cylinder as predicted by the potential flow around a cylinder (Figure 5.8).

The effect of changing the cylinder diameter D_c on the trajectories of the "splashed" drops has been illustrated in Figure 5.6. Decreasing the cylinder diameter from 1 to 0.5 and then 0.1 meter causes the drops to miss the cylinder by increasingly larger non-dimensional distances ($Y^* = 0.62$, 0.66 and 0.69). Since the non-dimensional position Y^* is based on actual "Y" positions divided by the cylinder diameter, the variation in position was even more significant.

Finally, Figure 5.7 plots the trajectories of the drops under the influence of different freestream air velocities V_a. Increasing the air speed to 10 or 50 m/s causes the splashed drops, introduced with the same

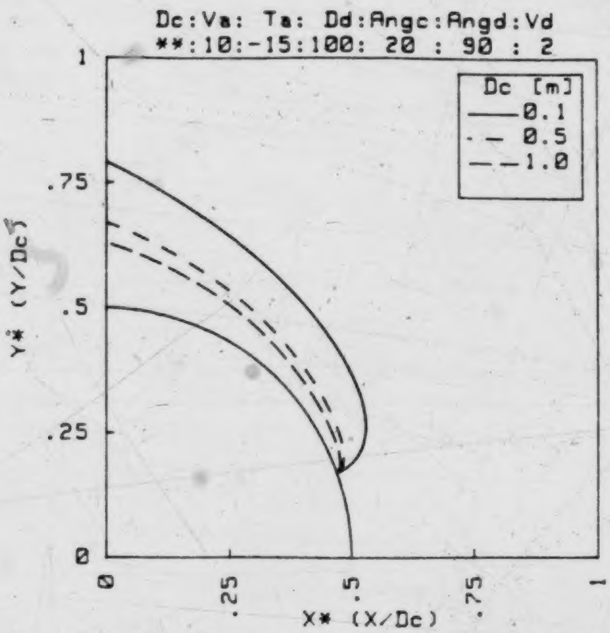

FIGURE 5.6 The effect of impact cylinder diameter (D_c) on the trajectories of "splashed" drops (V_d=2 m/s, V_a=10 m/s, T_a=-15°C, Ang_d=90°, Ang_c=20°, D_d=100 µm).

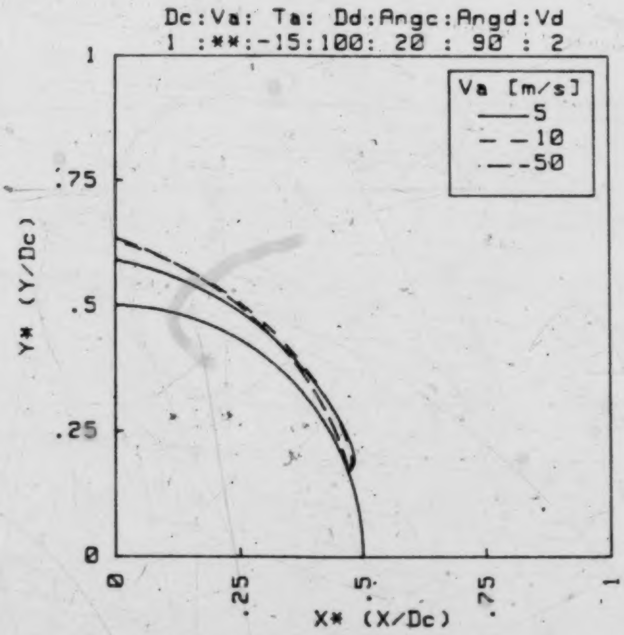

FIGURE 5.7 The effect of freestream air velocity (V_a) on the trajectories of "splashed" drops (V_d=2 m/s, D_c=1 m, T_a=-15°C, Ang_d=90°, Ang_c=20°, D_d=100 µm).

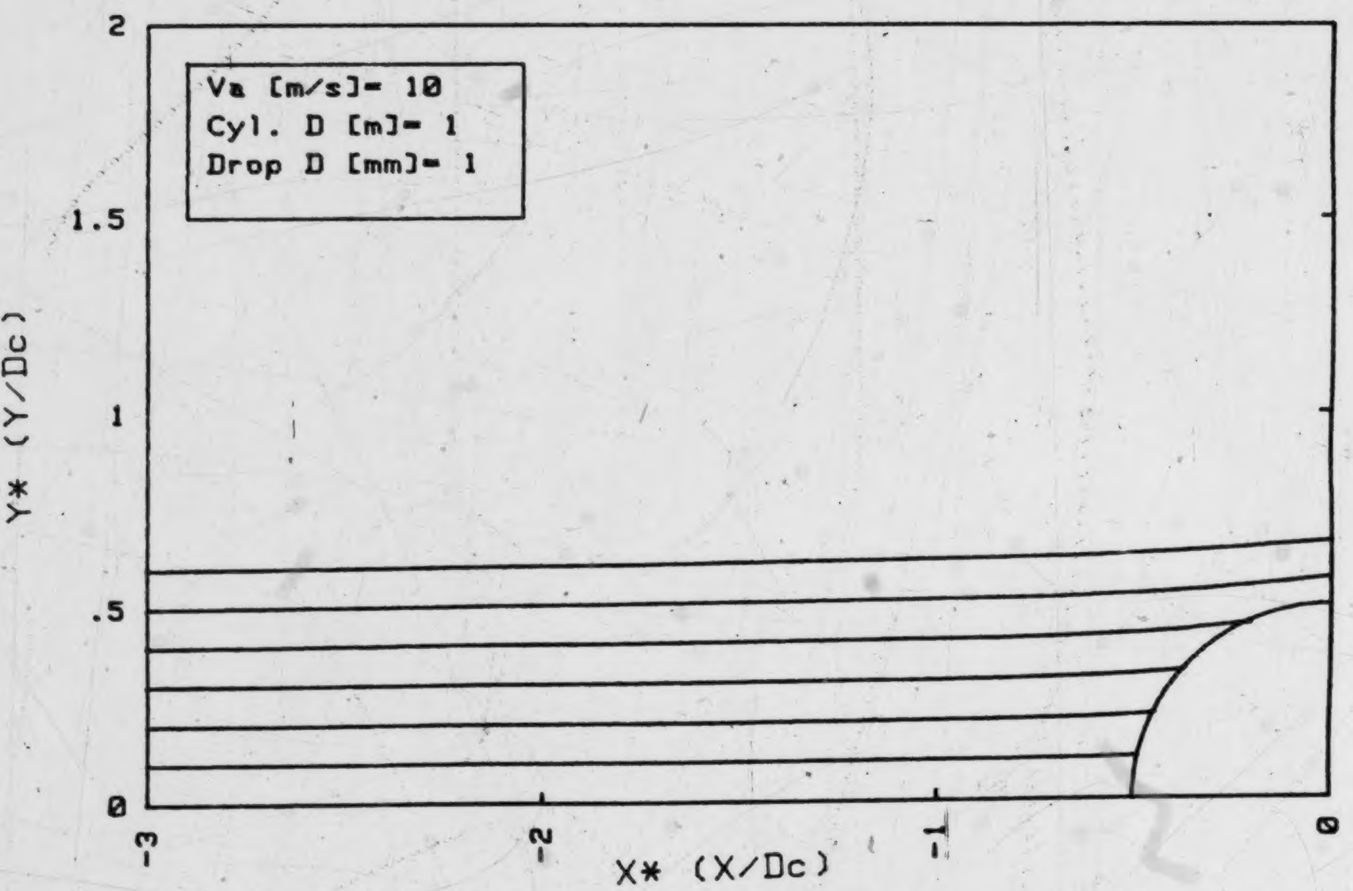

FIGURE 5.8 Predicted drop trajectories based on the theory of potential flow around a cylinder (V_d=0 m/s, D_c=1 m, T_a=-15°C, D_d=1 mm).

initial conditions, to miss the cylinder by a greater distance in comparison to an air speed of 5 m/s. However, these variations are not as large as might be expected given the large variations (5 to 50 m/s) in the air speed.

From the previous results it appears that the splashed drop diameter D_d, cylinder diameter D_c, drop velocity V_d and drop position from the stagnation line Ang_c, are the most important parameters affecting the "splashed" drop trajectories.

To get a quantitative feel for the amount of splashed mass which will pass by a cylinder, for a prescribed set of conditions, consider an angle termed Re-impact Angle (Ang_{re}, Figure 5.1). This angle represents the maximum angle, measured from the stagnation line, at which "splashed" drops can be introduced and will re-impact on the cylinder. Equivalently, this angle represents the maximum angle (position on the cylinder) that the impinging drops in the airstream can strike the cylinder and produce splashed drops that will not be permanently lost from the surface. Thus this angle can be used to determine a percentage of the incoming mass flux (liquid water content) that will not re-impact on the cylinder, given that the amount of splashed mass produced is a known quantity.

5.4.2 Re-impact Angle

As mentioned previously, Re-impact Angle (Ang_{re}) is defined as the maximum angle measured from the stagnation line (Figure 5.1) at which a "splashed" drop can be introduced and re-impact on the accreting cylinder, under a given set of conditions.

Figures 5.9 and 5.10 show the Re-impact Angle on the ordinate axis and the initial splashed drop velocity measured at the cylinder surface on the abscissa. For Figure 5.9 the cylinder diameter D_c and air temperature T_a were held constant at 1 meter and -15°C respectively, and variations were made to the air velocity and drop diameter. The figure shows that the larger the splashed drop diameter the larger the Re-impact Angle. The figure also indicates that increasing the initial drop velocity also results in a larger Ang_{re}. For example, a 300 μm drop, introduced into a 10 m/s airstream with an initial velocity of 5 m/s resulted in a Re-impact Angle of 3.5°. The same drop with an initial velocity of 1 m/s resulted in a 1.9° Re-impact Angle. If 50 and 100 μm drops are introduced at 5 m/s into the 10 m/s airstream the re-impact angles decrease to 0.1 and 1.19 ° respectively.

The change in Re-impact angle as a result of variations in the freestream air velocity were not as significant as those caused by a change in the drop diameter. Increasing the freesteam air velocity from 5 to 10 m/s results in a 15% decrease in the Re-impact Angle for the 300 μm drops and a 30-40% increase for the 100 μm drops. For the 50 μm drops the variation in Re-impact

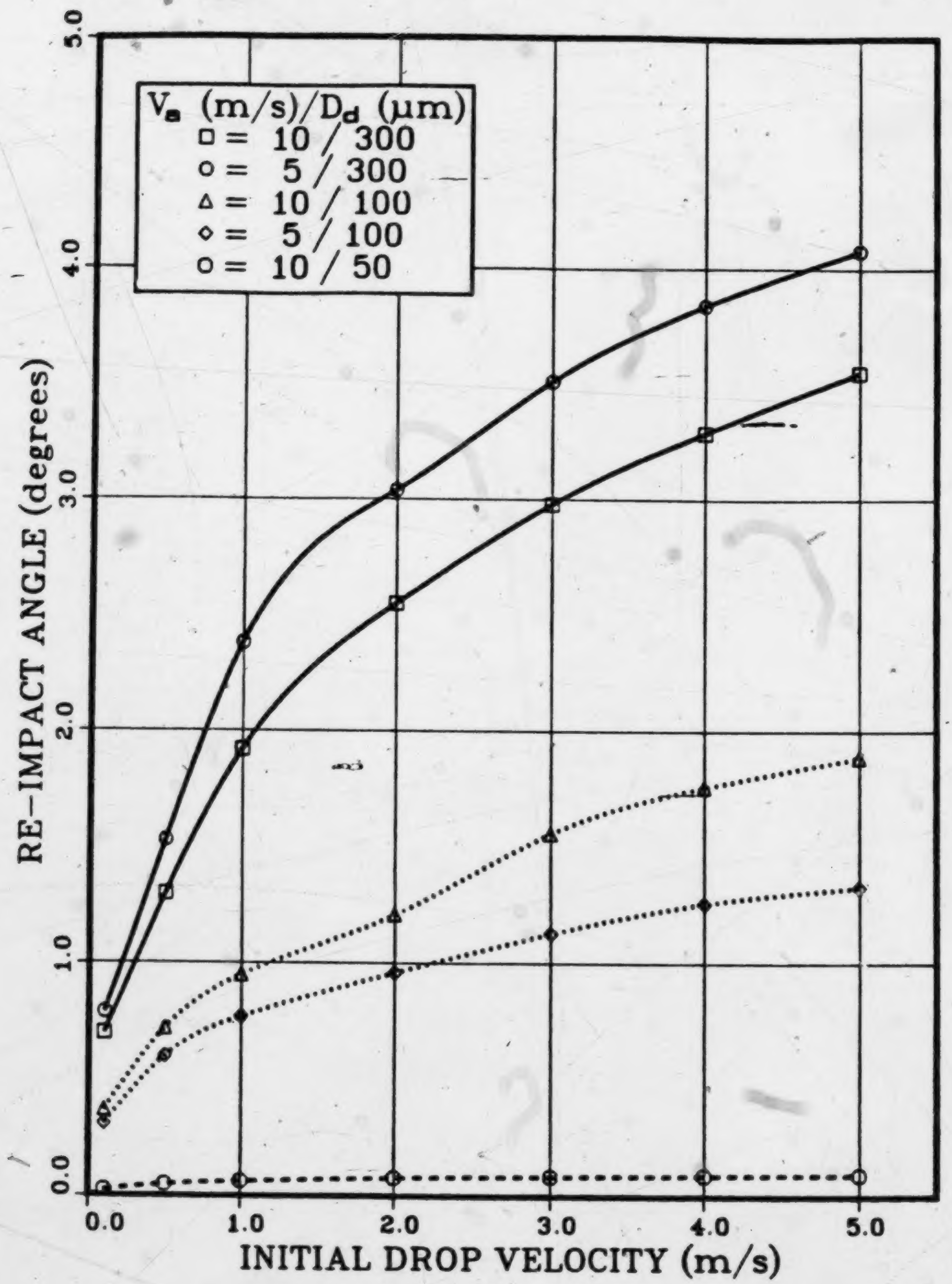

FIGURE 5.9 The effect of initial drop velocity (V_d), freestream air velocity (V_a) and drop diameter (D_d), on the Re-Impact Angle, of drops splashed from a water coated cylinder (D_c=1 m, T_a=-15°C, Ang_d=90°).

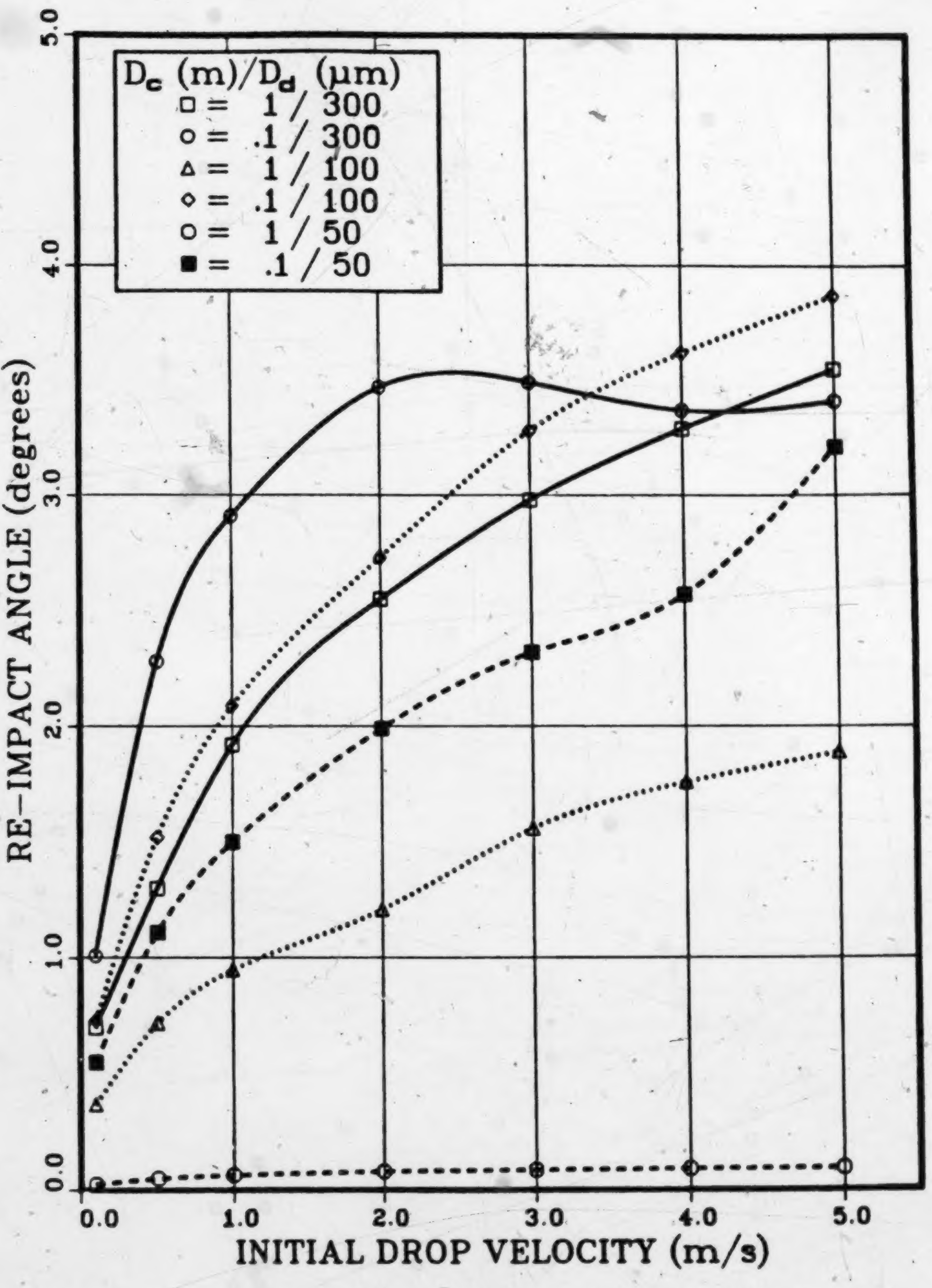

FIGURE 5.10 The effect of initial drop velocity (V_d), cylinder diameter (D_c) and drop diameter (D_d), on the Re-Impact Angle of the drops splashed from a water coated cylinder (V_a=10 m/s, T_a=-15°C, Ang_d=90°).

Angle caused by a change in the airspeed is relatively insignificant, since the Re-impact Angle was much less than 1^o for any of the choosen airspeeds. It is interesting to note that for 100 μm drops, increasing V_a from 5 to 10 m/s, resulted in an increased Re-impact Angle while producing a decrease for the 300 μm drops.

Figure 5.10 shows the effect of cylinder diameter D_c and drop diameter D_d on the Re-impact Angle. For this figure the freestream air velocity V_a and air temperature T_a, were held constant at 10 m/s and -15^oC respectively. The figure shows the Re-impact Angle verses the initial splashed drop velocity for different cylinder and drop diameter combinations. The figure indicates that a decrease in cylinder diameter by a factor of 10, from 1 to 0.1 m causes a dramatic increase (100%) in the Ang_{re} for 50 and 100 μm drops and a less dramatic increase (20-50%) for 300 μm drops. It is interesting to note that the Re-impact Angle for the 50 μm splashed drops was essentially zero if produced on a 1 meter diameter cylinder (i.e. all of the small drops flow around the cylinder).

5.4.3 Impinging Mass Loss

In terms of modelling the mass loss associated with the splashing on a wet ice accretion, it is more instructive to determine the percentage of the impinging mass flux (LWC) rather than the percentage of the splashed mass that will be permanently lost from the surface (i.e. accretion). Consider the introduction of large drops, representative of the impinging mass flux, far away from the accreting cylinder. By calculating the "position" that these drops impact on the cylinder, it is possible to determine the percentage of the impinging mass flux that impacts at angles greater than Ang_{re}. If the drops impacting at an angle greater than Ang_{re} produce a splash, the result will be a permanent loss of mass. Those impinging drops impacting at angles less than Ang_{re} will not contribute to the permanent loss of mass. In order to quantify the percentage of the impinging mass flux permanently lost as a result of splashing would require knowledge of the quantity of splashed mass produced by the impinging drops. This quantity of splashed mass was determined from experimental evidence provided by Macklin and Metaxas (1976) and Levin and Hobbs (1971).

Figure 5.11 shows the percentage of the splashed mass that re-impacts (i.e. re-impact mass) as a function of the initial velocity of the splashed drops and for different splashed drop and cylinder diameters. The re-impact mass takes into account the fact that the impinging mass, assumed to be uniformly distributed far away from the cylinder, will not accrete uniformly on the cylinder surface. In order to generate Figure 5.11 the large impinging drops were assumed to be uniformily distributed when introduced with zero initial velocity 5 cylinder

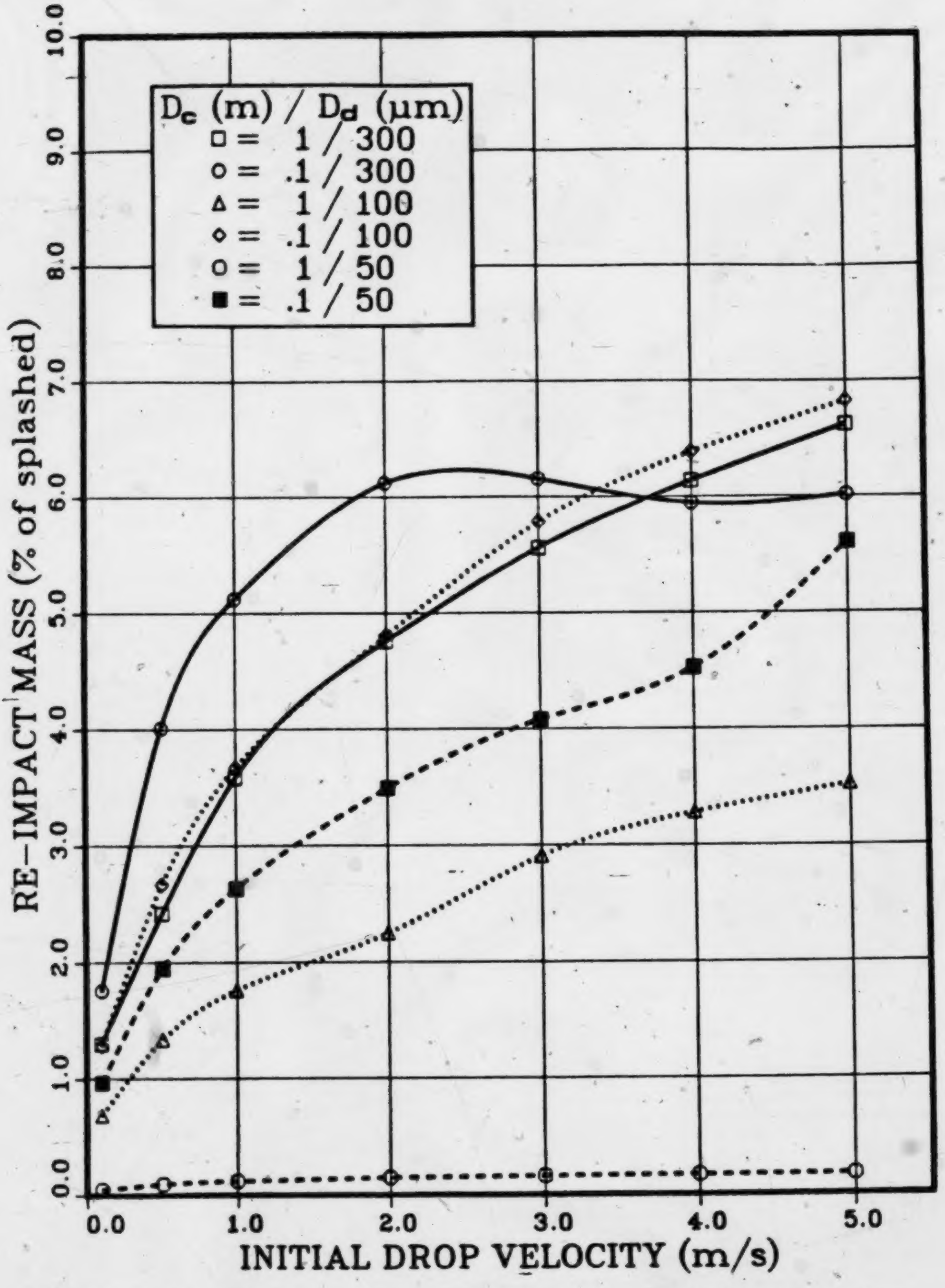

FIGURE 5.11 The percentage of the drops splashed from the surface of a water coated cylinder that re-impact on the cylinder as a function of initial drop velocity (V_d), drop diameter (D_d) and cylinder diameter (D_c) (V_a=10 m/s, T_a=-15°C, Ang_d=90°).

diameters upstream of the cylinder in a 10 m/s airstream. The major point to be drawn from this figure is that for splashed drops with diameters ranging from 50 to 300 μm, splashing from the surface of cylinders with diameters ranging from 0.1 to 1.0 m, with initial drop velocities of between 0.1 and 5 m/s, in a 10 m/s airstream, a maximum of 7% of any splashed mass will re-impact on the cylinder. In otherwords at least 93% of the splashed mass could be permanently lost from the surface.

Macklin and Metaxas (1976) and Levin and Hobbs (1971) examined the splashing of large drops (millimeter sized) on layers of water, in order to quantify the splashed mass and its size distribution. In addition these authors were interested in the physics of the splashing phonemonen. Macklin and Metaxas (1976) allowed 2.6 mm water drops to impact on a 0.52 mm liquid water layer, at speeds ranging from 1 to 5 m/s. They showed that 5% of the impacting drop's energy (surface, kinetic and potential) could be transferred to the splashed drops. Levin and Hobbs (1971) performed similiar tests allowing 2.5 mm diameter water drops to impact on a 0.5 mm water coated sphere, at speeds of 1.68 to 4.8 m/s. From photographic evidence they showed that the splashed drops ranged from 50 to 500 μm in diameter, with the majority of the splashed mass represented in the 100 to 300 μm range.

Although the previous authors work would be representative of only a small portion of the range of conditions (i.e. drop diameter and velocity, liquid layer depth, etc.) possible during splashing under "wet icing" conditions, it serves to illustrate the potential mass loss attributable to splashing. To emphasize this mass loss consider the following hypothetical example based on the typical results of Macklin and Metaxas (1976) and Levin and Hobbs (1971). A uniform distribution of 2.5 mm drops is introduced into the 10 m/s airstream around a 0.1 m diameter cylinder. The splash results in 10% of the impinging mass being introduced as 100 μm drops, with initial velocities of 2.5 m/s and 20% introduced as 300 μm drops with initial velocities of 0.3 m/s. From Figure 5.11, 6.2% of the 100 μm drops and 3.5% of the 300 μm drops will re-impact. Therefore, the percentage of the impinging mass permanently lost as a result of splashing is equal to:

$(1.0-0.062)*10\% + (1.0-0.035)*20\% = 28.7\%$.

It is important to note that this mass loss was based strictly on the probable trajectories of the splashed drops and experimental evidence as provided by Macklin, et. al. (1976) and Levin, et. al. (1971). No account has been made for the collision of "splashed" drops with each other or the larger drops making up the incoming mass flux. As well, no attempt has been made to account for the change in potential flow field resulting from a layer of accreted water on the surface of a cylinder or the presence of the cylinder wake. Determination of the flow field very near the surface of a cylinder is known to be more accurately described by viscous flow theory rather than potential flow theory (List, 1977); however, it was too involved to be undertaken for the present study. Joe (1975) also investigated viscous flow theory in considerable detail while studying the bouncing of supercooled water droplets from an artificially grown hailstones.

Certainly, as pointed out by List (1977), the loss of previously accreted water from the surface of an icing cylinder, as a result of "splashing", must be accounted for when modelling ice accretion growth rates under "wet" icing conditions. This is apparent from the previous example in which up to 29% of the incoming mass flux may be permanently lost, simply due to splashing under "wet" icing conditions. In comparison to the work of Joe (1975) which indicated that a 40% reduction in collision efficiency or equivalently a permanent loss of mass, can result from the bouncing of supercooled drops from an artificially grown hailstones, the 29% loss due to splashing certainly is significant.

Although the previous analysis is certainly a simplified approach to the modelling of the mass loss associated with splashing under wet icing conditions, it serves to emphasize the importance of this phenomenon to the marine ice accretion modeller.

CHAPTER 6

SUMMARY and CONCLUSIONS

The present study consisted of an experimental investigation into the effects of salinity, impact velocity and impact surface temperature on the spreading of large drops on cold dry surfaces, and an analytical study to determine the trajectories of droplets "splashed" from the surface of a water-coated cylinder, ultimately quantifying the permanent loss of mass from the surface. Both of these investigations were undertaken in order to determine the importance or applicability of each phenomenon to the analytical modelling of marine ice accretions.

Results from the experimental portion of this study suggest that the "spreading" of the drop up to its maximum spreading factor is essentially independent of the heat transfer rate, since it takes much longer for the freezing process to occur. However, the final size which is of more importance to the modelling of the ice accretion process is dictated by the heat transfer rate. The heat transfer causes the drops to freeze as approximately uniformly thick disks, with a size only slightly less than $S.F._{max}$. Decreasing either the thermal conductivity of the impact surface or its temperature produces a decrease in the final size of the drops, while increasing the impact velocity increases the final size, primarily because the maximum size also increases. This suggests that the final size of the spread-out drop, which is used to determine the time required to freeze the drop, is dependent on the maximum size (i.e. $S.F._{max}$) of the drop, which in turn is a function of the spreading parameters. Note that in terms of modelling the spreading of single drops, it may be more beneficial to perform the tests under forced convection conditions (experimental set-up prevented such tests in the present study) to determine if the freezing and spreading processes could still be treated separately.

The present study was also concerned with the effect of salinity (S=0 or 33 g/kg) on the spreading process. The experimental results indicated that the effect of salinity in terms of the spreading of the drops on cold dry surfaces ($S.F._{max}$ and $S.F._{final}$) was relatively insignificantly and any difference could be explained by a simple freezing point depression. Thus in terms of modelling ice accretions a simple freezing point depression would suffice in accounting for salinity during the initial stages of the an ice accretion (i.e. initially dry surface).

The experimental study also indicated that after a few drops have accreted on an initially dry surface the rate of heat transfer becomes independent of the thermal conductivity of the impact surface. This indicates that conduction into the impact surface is only important during the initial stages of an accretion. The layer of ice formed by the previously frozen drops effectively insulates the surface from the unfrozen drop.

An analytical investigation of the splashing phenomenon indicates that under typical marine icing conditions, 30% of the initially accreted mass (drops) could be lost as a result of the splashing. Although the test conditions did not encompass the entire range of marine icing conditions, it serves to illustrate the importance of the splashing phenomenon in terms of modelling the marine ice accretion process. The study suggests that more research is required to determine the quantity of mass produced by a splash to get a better handle on the splashing phenomenon.

REFERENCES

Abbott,C.E., Cannon,T.W. (1972) A Droplet Generator with Electronic Control of Size, Production Rate, and Charge. Rev. of Sci. Ins., Vol. 43, No. 9, pp. 1313-1317.

Ackley,S.F., Templeton,K. (1979) Computer Modelling of Atmospheric Ice Accretion. CRREL Report 79.4

Ahire,D.V., Kamra,A.K. (1984) Production of charged monodisperse water droplets by electrical dispersion. Mausam, Vol. 35, No. 1, pp. 27-32

Assur,A. (1960) Composition of Sea Ice and it's Tensile Strength. U.S. Army Snow Ice and Permafrost Research Establishment, Corps of Engineers. Research Report 44, 49 pp.

Auld,H.E. (1980) The Thermodynamics of Icing Sprays Masters of Science Thesis in Meteorology, Dept. of Geography, Univ. of Alberta.

Beard,K.V., Pruppacher,H.R. (1969) A Determination of the Terminal Velocity and Drag of Small Water Drops by Means of a Wind Tunnel. J. Atmos. Sci., Vol. 26, pp 1066-1072.

Beard,K.V., Pruppacher,H.R. (1971) A Wind Tunnel Investigation of the Rate of Evaporation of small water drops falling at Terminal Velocity in air. J. Atmos. Sci., Vol. 28, pp 1455-1464.

Beard,K.V. (1977) On the Acceleration of Large Water Drops to Terminal Velocity. J. App. Met., Vol. 16, pp. 1068-1071.

Brown,R.D., Roebber,P. (1985) The ice accretion problem in Canadian waters related to offshore energy and transportation. Canadian Climate Centre Report 85-13, 295 pp. unpublished manuscript.

Brownscombe,J.L., Hallett,J. (1967) Experimental and Field Studies of precipitation particles formed by the freezing of supercooled water. Q.J.R.M.S., Vol. 93, pp. 455-473.

Cannon,T.W.,Grotewold,W,W. (1980) Improved Drop Generators for Calibration of Drop Spectrometers and use in Laboratory Cloud Physics Experiments. J. of App. Meteorology, Vol. 19, pp 901-905.

Cansdale,J.T., Gent,R.W. (1983) Ice Accretion on Aerofoils in Two dimensional Compressible Flow: A Theoretical Model. RAE Tech. Report 82128.

Carslaw,H.S., Jaeger, J.C. (1959) Conduction of Heat in Solids. Oxford University Press, Glasgow, 510pp.

Cheng,L., Cross,W.G. (1975) Production of single liquid drops of controlled Size and Velocity. Rev. Sci. Ins., Vol. 46, No. 3, pp 263-265.

Comiskey,A.L., Leslie,L.D., Wise,J.L. (1984) Superstructure icing and forecasting in Alaskan waters. Unpub. draft report submitted by the Arctic Environmental Information and Data Centre to Pacific Marine Environmental Laboratory (NOAA), Seattle, 39 pp.

Eckert,R.G., Goldstein,R.J. (1976) Measurements in Heat Transfer. McGraw-Hill Book Co.,2nd ed.,New York, 642 pp.

Engel,O.G. (1955) Waterdrop Collisions with Solid Surfaces. J. Res. N.B.S., Vol. 54, No. 5, pp. 281-298.

Flannery,B.P. (1984) Energy Balance Models Incorporating Transport of Thermal and Latent Energy. J. Atmos. Sci., Vol. 41, No. 3, pp. 414-421.

Foote,G.B., DuToit,P.S. (1969) Terminal Velocity of Raindrops Aloft. J. App. Met., Vol. 8, pp. 249-253.

Gates,E.M., Lozowski,E.P., Finstad,K.J. An Approximate Method for Time-Dependent Modelling of Rime Ice Accretion. Second International Workshop on Atmospheric Icing of Structures. Trondheim, Norway, June 19-21,1984.

Gates,E.M., Lozowski,E.P. (1985) An overview of Marine icing Research. Proceedings Fourth International Symposium on Offshore Mechanics and Arctic Engineering, Dallas, 10 pp.

Gunn,R., Kinzer,G.D.,(1949) The Terminal Velocity of Fall for Water Droplets in stagnant Air. J. of Met., Vol. 6, pp.243-248.

Holman,J.P. (1981) Heat Transfer. McGraw-Hill Book Co., New York, 570 pp.

Horjen,I. (1981) Ice Accretion on ships and marine structures. Marine Structures and Ships in ice (MSSI), 103 pp.

Horjen,I., Vefsnmo,S. (1983) Offshore icing - phase 11, extended theory of sea spray icing. Offshore technology testing and research group (OTTER), Report STF88 83050, 100 pp.

Horjen,I., Vefsnmo,S. (1984) Mobile platform Stability (MOPS) Subproject 02-icing (~~MOPS~~ Report 15). Report NHL 84002, Norwegian Hydrodynamics Laboratories, 56 pp.

Horjen,I., Vefsnmo,S. (1985) Computer modelling of sea spray icing on marine structures. Paper presented at the Symposium on Automation for Safety in Offshore Operation (ASSOPO), June, 1985, Trondheim, 9 pp.

Itagaki,K. (1984) Icing rate on stationary structures under marine conditions. CRREL Report 84-12, 9pp.

Ivchenko,I.N. (1984) Condensation Growth and Evaporation of Water Droplets in Air. Sov. Phys. Dokl., Vol. 29(1), pp. 59-61.

Jessup,R.G. (1985) Forecast Techniques for ice accretion on different types of marine structures, including ships, platforms and coastal Facilities. Draft Report presented to WMO Commission for Marine Meteorology, Oct. 1984, 90 pp.

Joe,P.I. (1975) Investigation of the Bouncing of Supercooled Water Droplets from an Artificially growing Hailstone. M. Sc. Phys. , U. of Tor.

Johnson,D.A., Hallet,J. (1968) Freezing and Shattering of Supercooled Water Drops. Quarterly Journal of The Royal Meteorological Society., Vol. 94, pp. 468-482.

Johnsons Industrial Plastics (western) Limited, Winnipeg 9537-62nd Ave. Edmonton, Alberta. Ph. 435-4771, TLX 03-72626.

Kachurin,L.G., Gashin,L.I., Smirnov,I.A. (1974) Icing rate of small displacement fishing boats under various hydrometeorological conditions. Meteorologiya i Gidrologiya, 3, pp 50-60 (in Russian). Also available in English translation in Meteorology and Hydrology, 3, pp 58-71.

King,W.D. (1975) Freezing Rates of Water Droplets. J. Atmos. Sci., Vol. 32, pp. 403-408.

Lane,W.R. (1946) A Microburette for Producing Small Liquid Drops of known size. Rev. Sci. Int., Vol. 40, No. 4, pp. 98-101.

LeClair,B.P., Hamielic,A.E. (1970) A Numerical Study of the Drag on a Sphere at Low and Intermediate Reynolds Numbers. J. Atmos. Sci., Vol. 27, pp. 308-315.

Lelah,M.D., Marmur,A. (1981) Spreading Kinetics of Drops on Glass. J. Colloid and Interface Science, Vol. 82, No. 2, pp. 518-525.

Levin,Z., Hobbs,P.V. (1971) Splashing of Water Drops on Solid and Wetted Surfaces: Hydrodynamics and Charge Seperation. Phil. Tran. Roy. Soc. London, A269, pp. 555-585

List,R. (1977) Ice Accretions on Structures. J. of Glaciology, Vol. 19, No. 81, pp. 451-465.

Lopez,J., Miller,C.A., Ruckenstein,E. (1976) Spreading Kinetics of Liquid Drops on Solids. J. Colloid Computation of Saturation Vapor Pressure. J. App. Met., Vol. 16, pp. 100-103.

Lowe,P.R. (1977) An Approximating Polynomial for the Computation of Saturation Vapor Pressure. J. App. Met., Vol. 16, pp. 100-103.

Lozowski,E.P., Oleskiw,M.M. (1981) Computer Simulation of Airfoil Icing without Runback. AIAA paper No. 81-0404, 8 pp.

Lozowski,E.P.,Stallabrass,J.R., Hearty,P.F. (1983) The Icing of an Unheated Nonrotating Cylinder. Part 1: A Simulation Model. J. Climate & Applied Meteorology , Vol. 22, No. 12, pp. 2053-2062.

Lozowski,E.P., Gates,E.M. (1985) Marine Icing Models: How do they work and How good are they? Int. Conf. on offshore winds and icing., Oct. 7-11 , 1985, Nova Scotia.

Macklin,W.C. (1962) The Density and Structure of Ice formed by Accretion. Q.J.R.M.S. , Vol. 88, pp. 30-50.

Macklin,W.C., Payne,G.S. (1966) A Theoretical Study of the Ice Accretion Process. Quarterly J. Royal Met. Soc., Vol. 93, pp. 195-213.

Macklin,W.C., Payne,G,S. (1968) Some Aspects of the Ice Accretion Process. Q.J.R.M.S., Vol. 94, pp. 167-185.

Macklin,W.C., Payne,G.S. (1969) The Spreading of Accreted Droplets. Q.J.R.M.S., Vol. 95, pp. 730-742.

Macklin,W.C., Metaxas,G.J. (1976) Splashing of Drops on Liquid Layers. J. App. Phys., Vol. 47, No. 9, pp. 3963-3970.

Magarvey,R.H., Taylor,B.W. (1956) Apparatus for the Production of Large Water Drops. Rev. Sci. Ins., Vol. 27, No. 11, pp. 944-947.

Makkonen,L. (1981) Estimating Intensity of Atmospheric Ice Accretion on Stationary Structures. J. Appl. Met., Vol. 20, pp. 595-600.

Makkonen,L. (1984) Modelling of Ice Accretion on Wires. Accepted for publication in J. of Appl. Met.

Makkonen,L., Stallabrass,J.R. (1984) Ice Accretion on cylinders and wires. NRCC Report, TR-LT-005 (NRC 23649), 43 pp.

Mark's Standard Handbook for Mech., (1978) Baumeister,T., Editor in chief, 8th ed., McGraw Hill Book Co., New York.

Marmur,A., LeLah,M.D. (1980) The Dependence of Drop Spreading on the size of the Solid Surface, J. Col. Sci., Vol. 78, No. 1, pp. 262-265.

Mason,B.J., Brownscombe,J.L. (1964) Production of uniform size drops at controllable frequency and spacing from a Vibrating Capillary. J. Sci. Instr., Vol. 41, pp. 258-263.

McComber,P., Touzot,G. (1981) Calculation of the impingement of cloud droplets in a cylinder by the Finite Element Model. J. Atmos. Sci., Vol. 38, pp. 1027-1036.

Mertins,H.O. (1968) Icing on fishing vessels due to spray. Marine Observer, 38, pp 128-130.

Metals Handbook (1948) American Society for Metals. Lyman,T. Editor, The American Society for Metals. Printed in USA.

Minsk,L.D. (1977) Ice accumulation on ocean structures. U.S. Army CRREL Report 77-17, 46 pp.

Minsk,L.D. (1984) Ice observations program on the semi-submersible drilling vessel SEDCO 708. U.S. Army CRREL Special Report 84-2, 20 pp.

Murray,W.A., List,R. (1972) Freezing of Water Drops. J. of Glaciology, Vol. 11, No. 63, pp. 415-429.

Myers,G.E. (1971) Analytical Methods in Conduction Heat Transfer. McGraw-Hill Inc., New York, 508 pp.

Neogi,P., Miller,C.A. (1982) Spreading Kinetics of a Drop on a Smooth Solid Surface. J. of Colloid and Interface Science, Vol. 86, No. 2, pp. 525-538.

Neogi,P., Miller,C.A. (1983) Spreading Kinetics of a drop on a Rough Solid Surface. J. Coll. Inter. Sci., Vol. 92, No. 2, pp. 338-349.

Pease,C.H., Comiskey,A.L. (1985) Vessel Icing in Alaskan Waters - 1979 to 1984 Data Set. NOAA Data Report ERL PMEL-14, December 1985, 14 pp.

Pitter,R.L., Pruppacher,H.R. (1973) A Wind Tunnel Investigation of freezing of small Water Drops falling at Terminal Velocity in air. Q.J.R.M.S., Vol. 99, pp. 540-550.

Pfeifer,R,J. Hendricks,C.D. (1967) Charge to Mass Relationship for electrohydrodynamically Sprayed liquid Droplets. Phys. of Fluids., Vol. 10, No. 10, pp. 2149-2154.

Pruppacher,H.R., Klett,J.D. (1978) Microphysics of Clouds and Precipitation. D. Reidel Publishing Co., Dordrecht, Holland, 714 pp.

Raghupathy,B., Sample,S.B. (1970) A New Apparatus for the Production of Uniform Liquid Drops. Rev. Sci. Ins., Vol. 41, No. 5, pp. 645-647.

Reil,K. Hallet,J. (1969) An Apparatus for the Production of Uniformed Size Drops at desired Time Intervals. Rev. Sci. Ins., Vol. 41, No. 1, pp. 533-534.

Rila Marine Mix, Technical Bulletin # 343 Rila Products P.O. Box 114,Teaneck,N.J. 07666,201/836-0855.

Russo,R.E., Withnell,R., Hieftje,G.M. (1981) Simple and Inexpensive Design for an Isolated Droplet Generator useful in Studies of Atomization in Flames. Applied Spectroscopy, Vol. 35, No. 6, pp. 531-536.

Samuels,W.E., Sparks,R.E. (1973) Fluidropper - A Device for forming Highly Uniform Drops. Rev. Sci. Ins. Vol. 44, No. 2, pp. 132-134.

Schneider,J.M., Hendricks,C.D. (1964) Source of Uniformed size Liquid Droplets. Rev. Sci. Ins., Vol. 35, No. 10, pp. 1349-1350.

Savic,P., Boult,G.T. (1955) The Fluid Flow associated with the Impact of Liquid Drops with Solid Surfaces. National Research Council of Canada, Report No. MT-26 , Ottawa, 43 pp.

Stallabrass,J.R. (1980) Trawler Icing - A Compilation of Work done at Nrc. NRCC Report MD-56 (NRC 19372), 103 pp.

Stebnovskii,S.V. (1979) Characteristics in the Intial Stage of the Spreading of a Drop on a Solid Surface. Sov. Phys. Dokl., Vol. 27(2),pp. 60-69.

Stow,C.D., Hadfield,M.G. (1980) An Investigation of the Condition for splashing of Water Drops on Solid Dry Surfaces. J. of Met. Soc. Jap., Vol. 58, No. 1, pp. 59-67.

Tattelman,P. (1982) An Objective Method of Measuring Surface Ice Accretion. J. App. Met., Vol. 21, pp. 599-612.

Thomas,L.C. (1980) Fundamentals of Heat Transfer. Prentice Hall Inc., New Jersey, 702 pp.

Tsurikov,V.L. (1974) Freezing Point of Sea Water. Ocean. (USA) Vol. 14, No. 2, pp. 209-214.

Tsurikov,V.L. (1976) New Data on the freezing point of seawater of varying Salinity. Oceanology (USA) Vol. 16, No. 5, pp. 457-459.

Wise,J.L., Comiskey,A.L. (1980) Superstructure icing in Alaskan Waters. U.S. Dept. of Commerce, NOAA Special Report, April 1980.

Wolf,W.R. (1961) Study of the Vibrating Reed in the Production of Small Droplets and Solid Particles of Uniform Size. Rev. of Sci. Ins., Vol. 32, No. 10, pp. 1124-1129.

Zarling,J.P. (1980) Heat and Mass Transfer from freely falling drops at low temperature. C.R.R.E.L. Report 80-18, 14 pp.

APPENDIX A

DROP IMPACT VELOCITY

This study required that the velocity and position of a drop falling under the influence of gravity, be known as a function of time. It is well known that large drops do not remain spherical for relatively large Reynolds Numbers. This deviation of a drop from a spherical form requires corrections be made to drag coefficients used for solid spheres, before they maybe applied to non-spherical drops. Since this study used relatively large drops (1.1 to 2.4 mm in diameter) corrections to the drag coefficients were required.

A.1 Reynolds Number < 400

Towards this end an iterative numerical program was developed to determine the drop velocity and position. Auld (1980) showed that for Re < 400, water drops can be modelled as rigid spheres. Under this condition Auld used the empirical drag relationship described by Beard and Pruppacher (1969):

$$\frac{F}{F_s} = 1 + a\,Re^{b} = C_{drag} \qquad (A.1)$$

Where, a and b are experimentally determined coefficents. F the steady state drag force on the drop and F_s, Stokes drag force given by:

$$F_s = 6 \pi \mu r_d (V_a - V_d) \qquad (A.2)$$

The acceleration of the drop can then be determined from the difference between the acceleration due to gravity, less the acceleration resulting from the drag force (i.e. F/drop mass).

$$a = g - \frac{F}{m} = g - \frac{F_s}{m} (1 + a\,Re^b) \qquad (A.3)$$

Equation A.3 lends itself well to an iterative numerical solution which can be used to determine the drop's velocity and position as a function of time. The drop velocity after a time step dt is given by:

$$V_{i+1} = V_i + dt/2\,(a_{i+1} + a_i) \qquad (A.4)$$

and similarly drop position is given by:

$$X_{i+1} = X_i + dt/2\,(V_{i+1} + V_i) \qquad (A.5)$$

A.2 Reynolds Number > 400

For Re $\geq$ 400 it is no longer permissible to use the Stokes Force formulation as given in Equation A.1. Hence consider the forces acting on a drop falling under the influence of gravity in stagnant air. The gravitional force (mg) and the drag force ($1/2\ \rho_{air}\ V_d^2\ C_{drag}\ \pi\ r_d^2$). Dividing these forces by the drop's mass and making the appropriate substitutions results in an alternate expression for the drop acceleration:

$$a = g - 3\ \rho_a/\rho_w\ C_{drag}\ V^2/(8\ r_d) \qquad \text{(A.6)}$$

In this case experimentally obtained data for C_{drag}, as a function of Reynolds number (Re) must be used to account for any drop deformation. Gunn and Kinzer (1949) provide this data from a series of tests in which water drops were allowed to fall in stagnant air. The range of Re ($400 < Re < 1500$) was choosen to encompass all possible situations encountered during this study. An iterative scheme, similar to the one used for Stokes flow, was then implemented to determine the drop's velocity and position as a function of time.

The velocities obtained from this program were checked by two independent methods. The first by comparison with the experimentally obtained velocities of other authors, for freely falling drops of similiar size to those used in this study. Table 3.1 shows a comparison of the velocities obtained by Levin and Hobbs (1971), and the "Velocity" program for a 2.5 mm diameter water drop.

As well, the experimental set-up also conveniently provided a second check on the calculated drop velocity (Figure 2.1). The experimental set-up required the use of

TABLE A.1 Comparison of the velocities of a freely falling water drop (D=2.5 mm) obtained from the "Velocity" program and those measured by Levin and Hobbs (1971).

Y (cm) Distance Fallen	VELOCITY (m/s) "Velocity" Program	Levin & Hobbs	(%) Percent Difference
15.0	1.69	1.68	0.5
45.0	2.86	2.81	1.7
145.5	4.80	4.80	0

a time delay unit in order to photograph the impacting of the single drops. From Figure 2.1, the distances H1 and H2 are known quantities and the time delay can be used to determine the time required for the drop to travel the distance H2. For comparison the corresponding times and positions can also be obtained directly from the program. For the 2.4 mm diameter drops and the distances that the drops were allowed to fall (1.45 to 1.75 m.) the time differed by a maximum of only 3%. These results suggested that the program was a reliable method of determining the drop's velocity at any point during its free fall.

A.3 Drops with an Initial Velocity

In the cases in which drops less than 2.4 mm were produced by electrical means, as described in Section 2.2.3 a modification to the impact velocity calculation had to be made. In this case, the initial drop velocity apon leaving the dropping tip was not equal to zero. Figure 2.2 shows the high voltage set-up used for the production of the small drops. In this set-up the initial drop velocity becomes a function of several factors, namely the plate to tip spacing, drop size (applied voltage) and tip dimensions.

It was assumed that the acceleration of the drop resulting from the coulomb attraction was only significant when the drop is near to the charged plate and far away from the charged plate the drops fall only under the influence of gravity. These assumptions appear valid based on the fact that the attractive force varies as $1/L^2$ and during experimental testing all other grounded objects were relatively far away from the falling drop.

Of primary importance in the present study was the impact velocity of the drops. Since the Velocity program calculated both the velocity and position (distance fallen) of a falling drop as a function of time, knowing two of the three variables the third was explicitly known. Referring to Figure 2.1, the distance H2 is known and the time for the drop to travel this distance could be measured. Therefore, the impact velocity could be determined from the Velocity program. Figure 2.5 graphically illustrates the result obtained using this method. The Figure shows drop velocity as a function of distance travelled. For an uncharged 1.1 mm diameter drop the initial velocity (i.e. velocity as the drop leaves the tip) would be equal to zero, however, the same drop produced by the high voltage system would leave the tip with an initial velocity of 1.9 m/s (i.e. calculated from the "Velocity" program) and thus have a different impact velocity. Note that the impact plate was located 1.68 m from the dropping tip, which results in impact velocities of 4.8 and 4.0 m/s, for the 2.4 and 1.1 mm diameter drops respectively.

APPENDIX B

DROP TEMPERATURE AT IMPACT

One of the drop producing modes typical of marine icing is the generation of relatively large drops (1 to several millimeters in diameter) from impacting waves. The large drops are generally not in thermodynamic or kinematic equilibrium with the surrounding environment at the instant they impact on the surface of the accreting object. For the present study the temperature of the drop at the moment of impact with the surface was required to perform a proper heat transfer analysis for the freezing drops. Therefore, in addition to calculating the drop's velocity during its free fall, the temperature was determined simultaneously.

Auld (1980) calculated the velocity of small drops in a wind tunnel as well as the heat and mass transfer from the drops. For Auld's work, relatively small drops (< 100 μm) and Reynolds numbers up to a maximum of 400 were considered. For this study the drops are much larger (up to 2.4 mm) resulting in correspondingly larger Reynolds numbers (up to 1000). Thus, a need to extend the theory applied by Auld for the larger drops and Reynolds numbers. As well, modifications had to be made to account for the salinity of salt water and its effect on the various heat transfer modes.

B.1 Heat Transfer from a Stationary Drop

For a drop, stationary with respect to the surrounding air, the rate of change in internal energy of the drop must balance with the rate of heat transfer from the drop. The heat transfer away from the drop results from a combination of the conductive, radiant and mass heat transfer modes. The different heat transfer modes appropriate to a stationary drop as defined by Pruppacher and Klett (1978) are as follows:

Mass transfer rate:

$$\frac{dq_{mass}}{dt} = \frac{4 \pi l_v \, DIF \, r_d}{R_v} (Pv_{air}/T_{air} - Pv_d/T_d) \qquad (B.1)$$

Heat transfer rate by thermal diffusion:

$$\frac{dq_{cond}}{dt} = 4 \pi r_d K_{air} (T_d - T_{air}) \qquad (B.2)$$

Radiant heat transfer rate:

$$\frac{dq_{rad}}{dt} = 4 \pi r_d^2 \sigma E (T_d^4 - T_{air}^4) \qquad (B.3)$$

Drop internal energy:

$$\frac{dq_{internal}}{dt} = \frac{4}{3} \pi r_d^3 \rho_w c_w \frac{dT_d}{dt} \qquad (B.4)$$

where

l_v = latent heat of vaporization
DIF = diffusivity of water vapor in air
r = radius
R_v = specific gas constant, water vapor
Pv = partial vapor pressure
T = temperature
K = thermal conductivity
σ = Stefan-Boltzman constant
E = emissivity of water drop
ρ_w = density of water
c_w = specific heat capacity of liquid water
μ = dynamic viscosity of air

Subscripts

air = environment
d = drop

B.2 Ventilation Effects

Now in the case in which the air and drop are moving with respect to each other the ventilation effect will result in an increase in the heat and mass transfer rates. The increase in the mass transfer rate is determined by the dimensionless Sherwood Number (Sh) or the ventilation coefficient (f); where $f = Sh/2$ and $f = 1$ for a stationary drop. Pruppacher and Klett (1978) define the ventilation coefficient as follows:

$$\bar{f} = 1.00 + 0.108\,(Sc^{1/3}\,Re^{1/2})^2 \qquad (B.5)$$

$$\text{for}\quad Sc^{1/3}\,Re^{1/2} < 1.4$$

$$\bar{f} = .78 + .308\,(Sc^{1/3}\,Re^{1/2}) \qquad (B.6)$$

$$\text{for}\quad 1.4 \le Sc^{1/3}\,Re^{1/2} \le 16$$

where

Sc = Schmidt Number = $\mu/DIF\ \rho_{air}$

Re = Reynolds Number = $\rho_{air}\ V\ D_d\ /\mu$

Beard and Pruppacher (1971) also showed through comparison to experimental results that Equation B.6 could be extended to include values of $Sc^{1/3}\,Re^{1/2}$, up to 44. For the present study the maximum value of $Sc^{1/3}$ was .84, which corresponds to a maximum allowable Re of 2700. The maximum value of the Re used in this study was less than 1000, therefore Equation B.6 can be used to modify the expression for the mass heat transfer term (Equation B.1).

Similarly the effect of ventilation on the conductive heat transfer rate is accounted for by the introduction of the Nusselt Number (Nu), given by:

$$Nu/2 = 1.00 + .108\,(Pr^{1/3}\,Re^{1/2}) \qquad (B.7)$$

$$\text{for}\quad Pr^{1/3}\,Re^{1/2} < 1.4$$

$$Nu/2 = .78 + .308\,(Pr^{1/3}\,Re^{1/2}) \qquad (B.8)$$

$$\text{for}\quad 1.4 \le Pr^{1/3}\,Re^{1/2} < 16$$

where

Pr = Prandtl Number = $\mu c_{PT} / K$

c_{PT} = constant pressure specific heat capacity of moist air

By an analogy similar to the ventilation coefficient formulation, Pruppacher and Klett (1978) showed that the validity of Equation B.8 can be extended to cover the conditions relevent to the present study, namely Re up to 1000. Note that the radiant heat transfer rate is unaffected by ventilation. Equations B.1 through B.8 provided the basis to determine the temperature of a freely falling water drop as a function of time or distance fallen.

APPENDIX C

TRAJECTORIES OF DROPS "SHED" DURING A SPLASH ON A WATER COATED CYLINDER.

A computer simulation was used to determine the trajectories of the small drops, "shed" when a large drop splashes on the surface of a cylinder, with a layer of accreted water. The Theory of Potential Flow around a cylinder and the equations of motion for a drop are derived for use in an iterative computer scheme.

C.1 Equations of Motion for a Drop

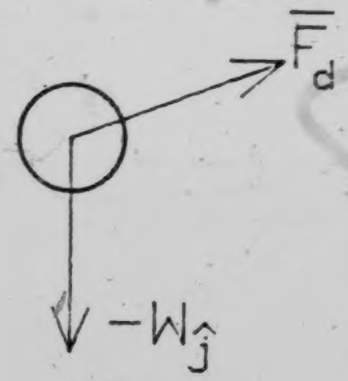

FIGURE C.1 Forces acting on a Drop.

$$m_d \frac{d\bar{V}_d}{dt} = -W_j + \frac{1}{2} \rho_a A \, C_{drag} \, (\bar{V}_a - \bar{V}_d) \, |\bar{V}_a - \bar{V}_d| \qquad (C.1)$$

Introduce the non-dimensional quantities:

$$\bar{V}^* = \bar{V}/U_o \qquad (C.2)$$

$$\overline{X}^* = \overline{X}/D_c \tag{C.3}$$

$$t^* = tU_o/D_c \tag{C.4}$$

and

$$m_d = 1/6 \, \pi \, d^3 \, \rho_w \tag{C.5}$$

where

$\overline{V}_a$ = Air Velocity Vector
$\overline{V}_d$ = Drop Velocity Vector
ρ_a = Air density
A = Drop Cross-sectional Area
C_{drag} = Coefficient of drag
t = Time
m_d = Mass of Drop

Substituting equations C.2 through C.5 in C.1 yields:

$$K \frac{d\overline{V}_d^*}{dt^*} = -H_j + \frac{Re \; C_{drag}}{24} (\overline{V}_a^* - \overline{V}_d^*) \tag{C.6}$$

where

$$K = \frac{d^2 \rho_w U_o}{18 \, D_c \, \mu_a} \qquad H = \frac{d^2 \rho_w g}{U_o \, \mu_a}$$

$$Re = \rho_a D_d U_o \, |\overline{V}_a^* - \overline{V}_d^*| \, / \, \mu_a$$

Dropping the * notation and resolving C.6 into X and Y components:

$$K \frac{dVx_d}{dt} = \frac{Re\ C_{drag}}{24} (Vx_a - Vx_d) \qquad (C.7)$$

$$K \frac{dVy_d}{dt} = \frac{Re\ C_{drag}}{24} (Vy_a - Vy_d) \qquad (C.8)$$

Where $Vx_d = dx_d/dt$ and $Vy_d = dy_d/dt$

C.2 Coefficient of Drag

The coefficient of drag due to McComber and Touzot (1981) is given by:

$$\frac{C_{drag}\ Re}{24} = 1 + 0.102\ Re^{0.995} \qquad 0.2 < Re \leq 2.0 \qquad (C.9)$$

$$= 1 + 0.115\ Re^{0.802} \qquad 2.0 < Re \leq 21.0 \qquad (C.10)$$

$$= 1 + 0.089\ Re^{0.632} \qquad 21.0 < Re \leq 200.0 \qquad (C.11)$$

$$= 1 + 0.197\ Re^{0.63} + 2.6E\text{-}4\ Re^{1.38} \qquad Re > 200 \qquad (C.12)$$

C.3 Potential Flow around a Cylinder

The Stream Function (Ψ) and its velocity components are given by:

$$\Psi = U_o\ Y - \frac{U_o\ Y\ D_c^{\ 2}}{4\ (X^2 + Y^2)} \qquad (C.13)$$

$$Vx_a = \frac{\partial \Psi}{\partial Y} = U_o + \frac{U_o\ D_c^{\ 2}\ (Y^2 - X^2)}{4\ (X^2 + Y^2)} \qquad (C.14)$$

$$Vy_a = \frac{\partial \Psi}{\partial X} = \frac{-U_o\ Y\ X\ D_c^{\ 2}}{2\ (X^2 + Y^2)^2} \qquad (C.15)$$

Non-dimensionalize using equations C.2 through C.4 and dropping the * notation gives the velocity components:

$$Vx_a = 1 + \frac{Y^2 - X^2}{4\ (X^2 + Y^2)} \tag{C.16}$$

$$Vy_a = \frac{-Y\ X}{2\ (X^2 + Y^2)^2} \tag{C.17}$$

Equations C.7 through C.12, C.16 and C.17 were used in a Runge Kutta iterative scheme to determine a drop's trajectory (position), as a result of the potential flow around a circular cylinder.

APPENDIX D

"VELOCITY" PROGRAM LISTING

```
FILENAME: VEL6

**********************************************************
*                                                        *
*  PROGRAM TO CALCULATE THE VELOCITY OF A DROPLET        *
*  FALLING UNDER THE INFLUENCE OF GRAVITY                *
*                                                        *
*  A HEAT TRANSFER BALANCE IS USED TO OBTAIN THE         *
*  DROPLET TEMPERATURE DURING IT'S FALL                  *
*                                                        *
**********************************************************


**********************************************************
*                                                        *
*    INPUT DATA REQUIRED                                 *
*                                                        *
*   SYMOBOL                                              *
*                                                        *
*   H - Time Step used in Runge-Kutta solution to        *
*       Droplet Velocity and Position    (seconds)       *
*   D - Intial Droplet Diameter    (meters)              *
*   VI   - Intial Droplet Velocity   (m/s)               *
*   HMAX- Limit for falling Time    (s)                  *
*   XMAX- Limit for Position    (m)                      *
*   TA1 - Air Temperature Outside Room  (K)              *
*   TA2 - Air Temperature in Cold Room   (K)             *
*   TD  - Droplet Temperature   (K)                      *
*   PAT - Barometric Pressure   (in. Hg -> Pascals)      *
*   RH  - Relative Humidity                              *
*   SG  - Specific Gravity of Droplet                    *
*                                                        *
*                                                        *
**********************************************************


**********************************************************
*                                                        *
*    CONSTANTS USED IN PROGRAM                           *
*                                                        *
*    Specfic Heat Capacities    (J/kg-K)                 *
*     CPD - Constant Pressure: Dry air                   *
*     CPV - Constant Pressure: Vapor                     *
*     CVD - Constant Volume: Dry air                     *
*     CVV - Constant volume: Vapor                       *
*     CPT - Constant Pressure: Moist air                 *
*   RA  - Ideal Gas Constant: Dry air   (J/kg-K)         *
*   RV  - Ideal Gas Constant: Vapor     (J/kg-K)         *
*   SIG - Stefan-Boltzman Constant  (J/m2-s-K4)          *
*   EMI - Emmisivity                                     *
*                                                        *
**********************************************************
```

```
*********************************************************
*                                                       *
*    VARIABLES USED IN PROGRAM                          *
*                                                       *
*   RE   - Reynolds #                                   *
*   K1...K4,L1..L4 - Runge-Kutta Variables              *
*   X    - Position based on average velocity  (m)     *
*   XR   - Position from Runge-Kutta       (m)          *
*   PAW - Saturation Vapor Pressure @ TA   (Pa)         *
*   PAD - Pressure of Dry air  @ TA  (Pa)               *
*   TF   - Film Temperature  (K)                        *
*   TVIRT - Virtual Temperature  (K)                    *
*   R    - Mixing Ratio                                 *
*   DFF - Mass Diffusion Coefficient    (m2/s)          *
*   LV   - Latent Heat of Vaporization  (J/Kg)          *
*   GWA - Surface Tension: Water and Air                *
*   PDW - Saturation Pressure @TD, corrected for        *
*          droplet curvature   (Pa)                     *
*   PF   - Average Saturation Pressure   (Pa)           *
*   KA   - Thermal Conductivity :Dry Air  (J/m-s-K)     *
*   VIS - Absolute Viscosity of Air @ TA (N-s/m2)       *
*   KD   - Thermal Conductivity :Vapor    (j/m-s-K)     *
*   DEND- Density of droplet   (Kg/m3)                  *
*   KF   - Thermal Conductivity :Moist air (J/m-s-K)    *
*   SC   - Schmidt #                                    *
*   PR   - Prandtl #                                    *
*   SH   - Sherwood #                                   *
*   NU   - Nusselt #                                    *
*   MASSHT - Mass Heat Transfer Term                    *
*   CONDHT - Conductive Heat Transfer Term              *
*   RADHT  - Radiant Heat Transfer Term                 *
*   DTBDT- Delta Tem. by Delta Time                     *
*   DELTAT - Change in Droplet Temperature  (K)         *
*   DMBDT  - Delta Mass/Delta Time                      *
*                                                       *
*********************************************************


REAL H,HT,D,VI,VIS,HMAX,XMAX,LV,KA,KV,KF,MDET,TVIRT
REAL K1,K2,K3,K4,L1,L2,L3,L4,CPD,CPV,CVV,CVD,CPT,GWA
REAL MASSHT,CONDHT,RADHT,DELT,SG,PAT,TF
REAL TA,TA1,TA2,VIS2,PAW2,PAD2,R2,TVIRT2,DENA2,XCOLD
READ(5,100)H,D,VI,HMAX,XMAX,TA1,TA2,TD,RH,PAT,SG,XCOLD
100   FORMAT(13F10.6)

*********************************************************
*                                                       *
*  CONSTANTS & INTIAL VALUES                            *
*                                                       *
*********************************************************
```

```
DEND=1000.*SG
CPD=1005.
CPV=1850.
CVD=718.
CVV=1390.
RA=287.05
RV=461.51
SIG=5.6687E-8
EMI=.95
X=0.0
HT=0.0
XR=0.0

***************************************************
*                                                 *
*  DROPLET & AIR PROPERTIES                       *
*                                                 *
***************************************************

PAT=PAT*3386.4
TA=TA1
VIS=1.8325E-5*416.16/(TA+120.)*(TA/296.16)**1.5
PAW=VAP(TA)*RH
PAD=PAT-PAW
R=.62198*PAW/PAD
TVIRT=TA*(1.+.6077688*R/(R+1.))
DENA=PAT/(RA*TVIRT)
VIS2=1.8325E-5*416.16/(TA2+120.)*(TA2/296.16)**1.5
PAW2=VAP(TA2)*RH
PAD2=PAT-PAW2
R2=.62198*PAW2/PAD2
TVIRT2=TA2*(1.+.6077688*R2/(R2+1.))
DENA2=PAT/(RA*TVIRT2)

***************************************************
*                                                 *
*   FORMATTED OUTPUT                              *
*                                                 *
***************************************************

WRITE(6,202) D,VIS,VIS2,RH
202 FORMAT(/'DROPLET DIAMETER=',F8.5,' m',/'VISCOSITY',
@'IN OUTSIDE ROOM=',F10.9,' Kg-m/s',/'VISCOSITY IN ',
@'COLD ROOM',F10.9,' Kg-m/s',/,'REL. HUMIDITY=',F8.3)
WRITE(6,203) TA1,TA2
203 FORMAT('AIR TEMPERATURE OUTSIDE ROOM =',F10.2,' K'/
@'AIR TEMPERATURE IN COLD ROOM =',F10.2,' K',/)
WRITE(6,200)
200  FORMAT(/6X,'TIME(S)',9X,'X(M)',5X,'XRUNGE(M)',3X,
@'VELOCITY(M/S)',6X,'RE',7X,'DROP TEMP.(K)'/)
RE=DENA*D*VI/VIS
WRITE(6,201) HT,X,XR,VI,RE,TD
```

```
**********************************************************
*                                                        *
*  DETERMINATION OF DRAG COEFFICIENTS                    *
*                                                        *
*     A) SEMI-EMPIRICAL FOR RE # < 400                   *
*     B) EXPERIMENTAL FOR RE # > 400                     *
*                                                        *
*  NUMERICAL SCHEME : RUNGE-KUTTA                        *
*                                                        *
**********************************************************

IF(RE.EQ.0.0)  GOTO 10
12   IF(RE .GE. 400.)      GOTO 11
IF(RE.GE.0.01.AND. RE.LT.1.5)  CD=1.0+0.102*RE**.995
IF(RE.GE.1.5 .AND. RE.LT.20.)  CD=1.0+0.115*RE**.802
IF(RE.GE.20.0 .AND. RE .LT.400.0) CD=1.0+0.189*RE**.632
GOTO 20
11   RE=ALOG10(RE)
CD=1.751-.2204*RE-.2225*RE**2.+.05247*RE**3.
L1=H*VI
K1=H*F2(D,CD,VI,DENA,DEND)
L2=H*(VI+K1/2.)
K2=H*F2(D,CD,VI+K1/2.,DENA,DEND)
L3=H*(VI+K2/2.)
K3=H*F2(D,CD,VI+K2/2.,DENA,DEND)
L4=H*(VI+K3)
K4=H*F2(D,CD,VI+K3,DENA,DEND)
GOTO 13
10   CD=0.
20   CONTINUE
L1=H*VI
K1=H*F(D,CD,VI,VIS,DEND)
L2=H*(VI+K1/2)
K2=H*F(D,CD,VI+K1/2.,VIS,DEND)
L3=H*(VI+K2/2)
K3=H*F(D,CD,VI+K2/2.,VIS,DEND)
L4=H*(VI+K3)
K4=H*F(D,CD,VI+K3,VIS,DEND)
13   VN=VI+(K1+2*K2+2*K3+K4)/6.
XN=X+(VN+VI)*H/2
XRN=XR+(L1+2*L2+2*L3+L4)/6.
**********************************************************
*                                                        *
*  NEW DROPLET POSITION AND VELOCITY as a f(t)           *
*                                                        *
**********************************************************

HT=HT+H
VI=VN
X=XN
XR=XRN
```

```
******************************************************
*                                                    *
*  HEAT TRANSFER BALANCE AT DROPLET'S SURFACE        *
*                                                    *
******************************************************

C1=2.0*3.14*D
TF=(TA+TD)/2.
DFF=0.211/10**4*(101325./PAT)*(TF/273.15)**1.94
LV=597.3*(273.15/TD)**(0.167+3.67/10.**4.*TD)*4186.84
GWA=1.0E-3*(76.1-.155*(TD-273.15))
PDW=VAP(TD)*EXP(4.*GWA/(DEND*D*RV*TD))
PF=(PAW+PDW)/2
KA=4.1868/10**3*(5.69+.017*(TF-273.15))
KV=4.1868/10**3*(3.78+.020*(TF-273.15))
KF=KA*(1-(1.17-1.02*KV/KA)*R/(R+1.))
SC=VIS/(DENA*DFF)
CPT=CPD*(1.+R/(R+1.)*(CPV/CPD-1.))
PR=VIS*CPT/KF
MDET=SC**(1./3.)*RE**0.5
HDET=PR**(1./3.)*RE**0.5
IF(MDET.LT.1.4) SH=1.+0.108*MDET**2
IF(MDET.GE.1.4) SH=0.78+.308*MDET
IF(HDET.LT.1.4) NU=1.+0.108*HDET**2
IF(HDET.GE.1.4) NU=0.78+.308*HDET
MASSHT=C1*LV*SH*DFF*(PAW-PDW)/(2*(1-PF/PAT)*RV*TF)
CONDHT=C1*KF*(TA-TD)*NU/2
RADHT=C1*SIG*EMI*D/2*(TA**4-TD**4)
IF(TD.GT.273.15) CW=4186.84*(.9979+3.1/10**6*(TD-308.15
@))**2+3.8/10**9*(TD-308.15)**4
IF(TD.LE.273.15) CW=4186.84*(1.0074+8.29/10**5*(TD-273.
@15)**2)
CONS=C1*D**2/12.*DEND*CW
DTBDT=(MASSHT+CONDHT+RADHT)/CONS
DELTAT=DTBDT*H

******************************************************
*                                                    *
* NEW DROP TEMPERATURE & CHANGE IN DROP SIZE         *
*                                                    *
******************************************************

TD=TD+DELTAT
DMBDT=MASSHT/LV
D=(D**2-12*DMBDT*H/(DEND*C1))**0.5
RE=DENA*D*VI/VIS
WRITE(6,201)HT,X,XR,VI,RE,TD
201    FORMAT(7F14.4)
IF(XRN .LE. XCOLD .OR. XRN .GT.(XCOLD+.1))      GOTO 14
PAW=PAW2
PAD=PAD2
R=R2
```

```
TVIRT=TVIRT2
DENA=DENA2
TA=TA2
VIS=VIS2
14   IF(HT.LT.HMAX.AND.X.LT.XMAX) GOTO 12
STOP
END
REAL FUNCTION F(A,B,C,D,E)
F=9.804-18.0*B*D*C/E/(A**2.)
RETURN
END
REAL FUNCTION F2(A,B,C,D,E)
F2=9.804-D*B*C**2.*.75/E/A
RETURN
END

********************************************************
*                                                      *
*  VAPOR PRESSURE: EMPIRICAL RELATIONSHIP              *
*                                                      *
********************************************************

REAL FUNCTION VAP(T)
REAL A0, A1, A2, A3, A4, A5, A6, T
A0=6984.505294
A1=-188.9039310
A2=2.133357675
A3=-1.2885809730D-02
A4=4.393587233D-05
A5=-8.023923082D-08
A6=6.136820929D-11
VAP=(A0+T*(A1+T*(A2+T*(A3+T*(A4+T*(A5+T*(A6)))))))*100.
RETURN
END
```